TRACTOGRAPHY-BASED DIFFUSION MRI MARKERS OF CEREBRAL SMALL VESSEL DISEASE

Graduate School of
Systemic Neurosciences
LMU Munich

Dissertation at the

Graduate School of Systemic Neurosciences

Ludwig-Maximilians-Universität München

Anna Dewenter

September 13, 2022

Date of submission: September 13, 2022
Date of defense: December 09, 2022

First supervisor and reviewer: Prof. Dr. med. Marco Düring
Institute for Stroke and Dementia Research, University Hospital, LMU Munich, Germany

Second reviewer: Prof. Dr. Michael Ewers
Institute for Stroke and Dementia Research, University Hospital, LMU Munich, Germany

CONTENTS

SUMMARY

Cerebral small vessel disease (SVD) is the second most common cause of cognitive decline and dementia in aging. Diffusion magnetic resonance imaging (MRI) has become the method of choice to quantify white matter tissue alterations in SVD. Alterations in white matter fiber tracts interconnecting brain regions has led to the notion of SVD as a disconnection syndrome, which can be assessed using diffusion MRI tractography to reconstruct structural brain networks. However, this analysis concept is complex and depends on many arbitrary design choices, starting from the requirements for data acquisition up to node and edge definitions. The advantage over simpler skeleton-based diffusion markers was unknown, which motivated Study I.

Study I systematically assessed the clinical and technical validation of structural brain network analysis compared to skeleton-based diffusion MRI markers in two independent samples of sporadic SVD, the most common form of the disease. In this pre-registered study, we reconstructed multiple brain networks with varying edge and node definition using either a simpler, established pipeline based on single-shell diffusion data or using a more advanced pipeline based on multi-shell diffusion data considering crossing fibers. The corresponding network architecture was quantified by network efficiency. For clinical validation, we assessed the added benefit of structural brain network analysis in explaining processing speed deficits, i.e., the main cognitive deficit in SVD and in detecting disease progression over time. For technical validation, we assessed the test-retest reliability in a high-frequency serial imaging longitudinal dataset. Our main findings were that: i) for clinical validation, structural brain networks provide only a small benefit in explaining processing speed over skeleton-based diffusion markers; ii) structural brain networks do not capture short-term disease progression over time; iii) multi-shell diffusion imaging does not improve the clinical validity of structural networks; iv) most structural brain networks show excellent test-retest reliability and thus a high technical validity and v) node and edge definitions have a substantial effect on brain network topology, highlighting the need for standardization to facilitate comparisons between research studies.

SVD is frequently accompanied by comorbid Alzheimer's disease. Markers that provide an understanding of specific pathological contributions in the individual patient are of great clinical need. Diffusion alterations have also been observed in Alzheimer's disease with tracts of the posterior temporal lobe being affected while SVD is considered a global brain disease. However, disease-specific diffusion markers are lacking. Recent advances in diffusion MRI

allow to assess properties specific to underlying fiber populations, i.e. on the *fi*ber population per vo*xel* (fixel) level. Using this technique, one can derive measures of microstructure reflected in fiber density and macrostructure reflected in fiber-bundle cross-section.

Study II explored the utility of tract-specific fixel metrics to disentangle effects of Alzheimer's disease and SVD on white matter in three independent samples. We assessed the fiber density and fiber-bundle cross-section of 29 tractography-based key white matter tracts and imaging hallmarks of SVD and Alzheimer's disease in addition to age and brain volume as a measure of neurodegeneration. Our main findings were that i) fiber density was substantially reduced in genetically defined SVD and showed the strongest association with SVD imaging hallmarks; ii) especially in AD, fiber-bundle cross-section was associated with brain volume; iii) both fiber density and fiber-bundle cross-section were reduced in the presence of amyloid, but this was not further exacerbated by abnormal tau deposition.

In conclusion, tractography-based diffusion MRI markers are appealing in SVD research since they allow to approach the disease as disconnection syndrome through structural brain network analysis and to derive fiber-specific properties of white matter fiber tracts through fixel-based analysis. Structural brain network analysis does not show an added benefit over skeleton-based diffusion markers in explaining cognitive deficits in SVD or detecting disease progression. Thus, these simpler markers based on diffusion tensor imaging remain the preferred choice for these purposes. Fixel-based analysis yields promise to disentangle effects of SVD and neurodegeneration in mixed disease. White matter microstructure, as captured by fiber density, is highly sensitive towards SVD-related brain alterations while neurodegeneration is associated with fiber-bundle cross-section, suggesting altered white matter macrostructure. Future research should address the sensitivity of fixel metrics to change upon disease progression and their test-retest reliability in longitudinal studies to facilitate widespread clinical use and the development of a surrogate endpoint for clinical trials.

ABBREVIATIONS OF INTRODUCTION AND GENERAL DISCUSSION

AAL	automated anatomical labelling
Aβ	amyloid-beta
CAA	cerebral amyloid angiopathy
CADASIL	cerebral autosomal dominant arteriopathy with subcortical infarcts and leukoencephalopathy
CN	cognitively normal
CSD	constrained spherical deconvolution
DKI	diffusion kurtosis imaging
DTI	diffusion tensor imaging
FA	fractional anisotropy
fixel	fiber population within a voxel
FLAIR	fluid-attenuated inversion recovery
FLASH	fast low angle shot
HARDI	high angular resolution diffusion MRI
MCI	mild cognitive impairment
MD	mean diffusivity
MRI	magnetic resonance imaging
NfL	neurofilament light chain
NODDI	Neurite orientation dispersion and density imaging
PET	positron emission tomography
ROS/MAP	Religious Orders Study and Rush Memory and Aging Project
STRIVE	STandards for ReportIng Vascular changes on nEuroimaging
SVD	cerebral small vessel disease

1. INTRODUCTION

Cerebral small vessel disease (SVD) is an age-related disorder of the small perforating arterioles, capillaries, and venules leading to damage of the brain parenchyma (Wardlaw, Smith, and Dichgans 2019; Dichgans and Leys 2017). SVD accounts for approximately 25% of all ischemic and most hemorrhagic strokes and is a key contributor to dementia, frequently co-occurring with neurodegenerative diseases such as Alzheimer's disease (Attems and Jellinger 2014; van der Flier et al. 2018). As life expectancy increases, the incidence of SVD is steadily rising, imposing a great burden on public health and affected individuals (Iadecola et al. 2019). SVD is associated with apathy, depression, cognitive decline, gait impairments and urinary disturbances (Pantoni 2010; Wardlaw, Smith, and Dichgans 2019). Cognitive symptoms include most frequently impairments in executive function and processing speed – especially in early disease stages – but also impairments in episodic memory, attention, and language (Charlton et al. 2006; Salvadori et al. 2022; Hamilton et al. 2021).

To date, no cure for SVD exists. Monitoring disease progression and treatment of vascular risk factors (especially arterial hypertension) remains the most promising therapy. Reliable biomarkers can not only support in monitoring disease progression, but can also facilitate the development of new therapies when used as surrogate endpoints in clinical trials. SVD leads to distinct brain alterations on magnetic resonance imaging (MRI), which can be quantified and used as imaging biomarkers. Conventional MRI markers of SVD are typically based on lesions, such as white matter hyperintensities (WMH), lacunes, and microbleeds (Wardlaw, Smith, and Dichgans 2019). However, white matter tissue changes long before lesion manifestation apparent on conventional MRI (Maillard et al. 2014). Diffusion MRI markers capture these subtle white matter tissue alterations of SVD and have been shown to outperform conventional MRI markers in both explaining clinical deficits and capturing disease progression (Baykara et al. 2016; Konieczny et al. 2021).

SVD induces tissue alterations in white matter tracts that interconnect remote brain regions (ter Telgte et al. 2018). These local tissue effect are accompanied by remote effects of the disease such as cortical thinning caused by lacunes and white matter hyperintensities via the disconnection of white matter tracts (Duering et al. 2012; 2015). These findings led to the notion that SVD is a disconnection syndrome which can be assessed with structural brain network analysis of diffusion MRI (ter Telgte et al. 2018; Tuladhar et al. 2016). However, network analysis is complex and the added benefit over simpler, established diffusion MRI markers for SVD characterization has so far not been evaluated. This motivated Study I, in which we

systematically assessed the value of structural brain network analysis as imaging marker for SVD.

Yet, SVD often co-occurs with Alzheimer's disease (Kapasi, DeCarli, and Schneider 2017; Kalaria 2016). Diffusion alterations in white matter fiber tracts have been observed in both SVD and Alzheimer's disease with differing spatial patterns (Duering et al. 2014; Nasrabady et al. 2018; Raghavan et al. 2022). However, disease-specific diffusion markers are lacking, and it remains unclear if and how Alzheimer's disease confounds diffusion alterations observed in SVD. In Study II, we assessed the capacity of a novel diffusion MRI model operating on the fixel level (*fi*ber population within a vo*xel*) to disentangle the effects of SVD and Alzheimer's disease on white matter integrity of major white matter fiber tracts (Raffelt et al. 2017; Dhollander et al. 2021).

In the following, types of cerebral small vessel disease and underlying pathology, the prevalence of mixed disease as well as conventional and diffusion MRI markers are introduced in more detail.

1.1. Types of cerebral small vessel disease and underlying pathology

SVD is an umbrella term of several subtypes:

Sporadic SVD is the most common form of the disease and is associated with traditional vascular risk factors (i.e., arterial hypertension, hypercholesteremia, diabetes mellitus and smoking) (Wardlaw, Smith, and Dichgans 2013). The pathophysiological mechanisms of sporadic SVD are still incompletely understood, but vessel wall stiffening and thickening, luminal narrowing, hypoperfusion and blood-brain barrier dysfunction have been proposed to play key roles (Wardlaw, Smith, and Dichgans 2013; Walsh et al. 2021). Neuroimaging manifestations of sporadic SVD are present to some degree in nearly every individual over the age of 60 (Leeuw et al. 2001) – the most prevalent lesion being white matter hyperintensities (WMH) of presumed vascular origin as seen on T2-weighted imaging (Wardlaw et al. 2013). Sporadic SVD frequently accompanies other diseases prevalent in the elderly. Both studies of this thesis included samples of sporadic SVD.

Cerebral autosomal dominant arteriopathy with subcortical infarcts and leukoencephalopathy (CADASIL) is a rare, yet the most common hereditary form of SVD. CADASIL is caused by

mutations in *NOTCH3* (Chabriat et al. 2009) and can be confirmed by skin biopsy or by molecular genetic testing (cysteine altering *NOTCH3* mutation). While most clinical and neuroimaging hallmarks are similar to sporadic SVD, CADASIL patients are much younger at disease onset, often suffer from migraine with aura and show more extensive white matter lesions extending to the anterior temporal pole (Markus et al. 2002; Singhal, Rich, and Markus 2005; Duchesnay et al. 2018). Due to young age, comorbidities are rare, rendering CADASIL a unique model of pure SVD. Study II included a sample of CADASIL patients to investigate the effects of pure SVD on fixel metrics.

Cerebral amyloid angiopathy (CAA) is characterized by progressive accumulation of amyloid-beta (Aβ) in the media and adventitia of small arteries and leptomeningeal and cortical capillaries (Biffi and Greenberg 2011; Greenberg and Charidimou 2018). The most devastating manifestation of CAA is lobar intracerebral hemorrhage. On conventional MRI, the disease furthermore presents with WMH, enlarged perivascular spaces (especially in the centrum semiovale), cortico-subcortical microbleeds and cortical superficial siderosis (Viswanathan and Greenberg 2011; Wollenweber et al. 2017). While a confirmed diagnosis of CAA requires histopathological evidence of Aβ accumulation, amyloid positron emission tomography (PET) imaging as well as the Boston criteria aid the diagnosis of possible and probable CAA *in vivo* (Charidimou, Farid, and Baron 2017; Greenberg and Charidimou 2018; Charidimou et al. 2022). CAA is highly prevalent in individuals with Alzheimer's disease (Greenberg et al. 2020), who were included in Study II.

1.2 Mixed pathology in dementia

Most patients who seek clinical care in memory clinics have both neurodegenerative and cerebrovascular disease to varying degrees (Attems and Jellinger 2014; van der Flier et al. 2018). Alzheimer's disease is the most frequent neurodegenerative disease and characterized by the cortical accumulation of Aβ plaques and neurofibrillary tau tangles leading to neurodegeneration (Jack et al. 2018). Results from the large Religious Orders Study and Rush Memory and Aging Project (ROS/MAP) study demonstrate the high prevalence of mixed disease (**Figure 1**). Specifically, 85% of individuals who were diagnosed with probable Alzheimer's disease proximate to death showed cerebrovascular comorbidity upon autopsy (Kapasi, DeCarli, and Schneider 2017). But mixed pathologies were also present in cognitively normal individuals (CN) and those with mild cognitive impairment (MCI, **Figure 1**). In all three groups, pure Alzheimer's disease was rare upon autopsy and the incidence of both pure Alzheimer's and cerebrovascular pathology decreased with increasing cognitive impairment

(Alzheimer's disease only: CN, 8.33%; MCI, 7.38%; probable Alzheimer's disease, 3.13%); cerebrovascular disease only: CN, 28.33%; MCI, 21.03%; probable Alzheimer's disease: 4.92%).

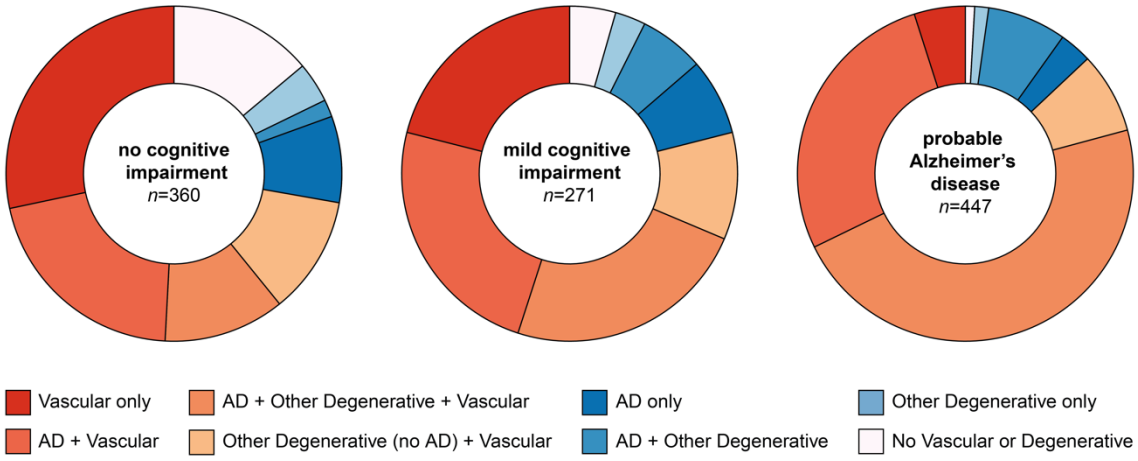

Figure 1. Prevalence of mixed pathologies in autopsied patients of the ROS/MAP study who had no cognitive impairment (left), mild cognitive impairment (middle) or were diagnosed with probable Alzheimer's disease (right) close to death. Shades of red show cerebrovascular disease, while blue shows Alzheimer's disease. Figures created with data retrieved from (Kapasi, DeCarli, and Schneider 2017).

The high prevalence of mixed pathologies warrants the development of disease-specific biomarkers to enable an understanding of the contributions of specific pathologies in the individual patient, which motivated Study II.

1.3 Conventional MRI markers of cerebral small vessel disease

Since the small vessels are difficult to visualize on magnetic resonance imaging (MRI) at conventional field strengths (i.e., 1.5 and 3 Tesla), MRI markers of SVD are typically based on parenchymal lesions (van den Brink, Doubal, and Duering 2022). Conventional MRI markers include but are not limited to (**Figure 2**): (A) white matter hyperintensities of presumed vascular origin – signal abnormalities of variable size in the white matter that appear hyperintense on T2-weighted imaging, such as fluid attenuated inversion recovery (FLAIR); (B) lacunes of presumed vascular origin – round or ovoid, subcortical fluid-filled cavities; (C) cerebral microbleeds – small areas of signal void with associated blooming seen on T2*-weighted MRI or susceptibility-weighted images and (D) brain atrophy – lower brain volume unrelated to infarctions but due to e.g. sulcal widening (in accordance with the STandards for ReportIng Vascular changes on nEuroimaging [STRIVE] criteria (Wardlaw et al. 2013)). These markers are often summarized into a semi-quantitative, global SVD score ranging from 0 to 4

(Staals et al. 2014), but some also allow the derivation of quantitative volumes through lesion segmentation (e.g., WMH volume).

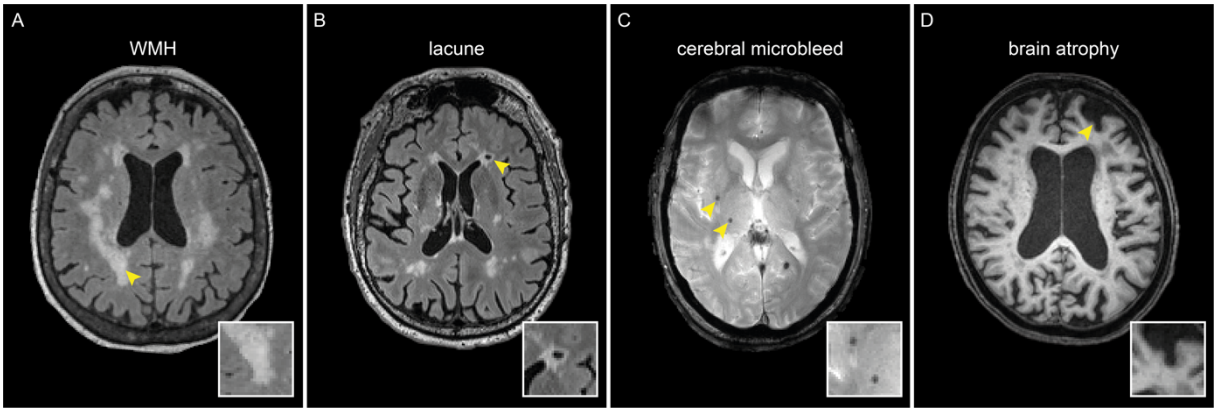

Figure 2. Conventional MRI markers (yellow arrow heads). Markers include (MRI sequence in brackets): (A) white matter hyperintensities (WMH; fluid attenuated inversion recovery [FLAIR]), **(B)** lacunes (FLAIR), **(C)** cerebral microbleeds (fast low angle shot [FLASH]), **(D)** brain atrophy (T1-weighted image).

Throughout the progression of SVD, white matter tissue changes long before symptom onset and lesion manifestation on conventional MRI (Maillard et al. 2014). These subtle white matter tissue alterations go unnoticed if employing the lesion approach since the underlying tissue is artificially binarized into lesioned and non-lesioned tissue. Quantitative markers based on advanced MRI sequences, such as diffusion MRI, yield promise since smallest alterations within the white matter are captured (van den Brink, Doubal, and Duering 2022; Vemuri, Decarli, and Duering 2022). The underlying principle of diffusion MRI and derived markers are explained in the next section.

1.4 Diffusion MRI

Diffusion MRI quantifies the extent of water diffusion *in vivo* using a (T2-weighted) spin echo sequence and the application of diffusion-sensitizing gradients in multiple directions. The mobility of water molecules depends on physical factors such as temperature and viscosity, but also obstacles and hindrances imposed by cerebral microstructure (e.g. cell membranes, myelin sheaths) (Jones, Knösche, and Turner 2013) as well as the distribution of water between intracellular and extracellular space, the latter allowing more water movement.

Diffusion MRI is prone to noise and artefacts. To go beyond signal representation – which is simple yet powerful to identify acute ischemic lesions – and to model white matter microstructure, sophisticated preprocessing techniques of multi-directional diffusion-weighted images are essential (Tax et al. 2022). Conventional diffusion MRI sequences acquire diffusion

directions typically over one shell with a diffusion weighting of e.g., b = 1000 s/mm^2 (single-shell diffusion MRI). More advanced acquisition schemes use a higher number of diffusion directions (high angular resolution diffusion MRI [HARDI]) of higher diffusion weightings (e.g., b = 3000 s/mm^2) or even multiple diffusion weightings of varying strengths (multi-shell diffusion MRI). These advanced diffusion MRI schemes have longer acquisition times but allow for more complex, potentially biologically more accurate modelling of white matter microstructure (Jeurissen et al. 2013).

1.4.1 Diffusion models

Diffusion tensor imaging (DTI) is the most common diffusion model and can be fitted on single-shell diffusion data (Nucifora et al. 2007). Estimation of tensor components is based on a linear model fit on multi-directional diffusion-weighted data. The diffusion tensor characterizes magnitude, degree of anisotropy and orientation of directional diffusion per voxel. In SVD, the typical pattern of diffusion alteration is a reduction in directionality measured by fractional anisotropy (FA) and an increase in the magnitude of diffusion measured by mean diffusivity (MD) (Raja, Rosenberg, and Caprihan 2019). Given the linear model fit, the diffusion tensor models water diffusion using a Gaussian distribution. In an unrestricted milieu, water molecule diffusion might show this distribution pattern. However, water diffusion within the brain is hindered by cerebral microstructure, leading to more skewed distributions of water movement which might violate the assumptions of the tensor model. With the aim to model cerebral microstructure more accurately, higher order diffusion models were introduced.

Diffusion kurtosis imaging (DKI) is a more complex diffusion model that quantifies the degree of water diffusion within the brain that is non-Gaussian (Jensen et al. 2005; Tabesh et al. 2011). DKI requires multi-shell diffusion MRI data acquired with specific diffusion weightings to capture non-Gaussian water diffusion. Applications of DKI in SVD are scarce, but a previous Study showed higher sensitivity of kurtosis metrics towards cognitive deficits compared to tensor metrics while showing excellent test-retest reliability (Konieczny et al. 2021). Study I included metrics of both DTI and DKI as established and advanced diffusion markers of SVD.

1.4.2 Analysis concepts of diffusion MRI

Diffusion MRI analysis concepts applied in the context of SVD research vary greatly with respect to their complexity (**Figure 3**).

Skeleton-based diffusion markers capture alterations in diffusion metrics within the main white matter tracts, the so-called white matter skeleton (**Figure 3A,** (Smith et al. 2006)). This simple and robust approach allows both regional voxel-wise analyses and the derivation of global diffusion markers (e.g. computation of the mean of a diffusion metric across the entire white matter skeleton). Using metrics derived from diffusion tensor and free water imaging, skeleton-based diffusion markers have been shown to outperform conventional MRI markers in explaining clinical deficits, capturing short-term disease progression while enabling a high grade of automation (Baykara et al. 2016; Duering, Finsterwalder, et al. 2018). Global skeleton-based diffusion markers are a surrogate endpoint candidate for clinical trials. They require substantially smaller sample sizes to assess treatment effects over time compared to conventional MRI markers (Benjamin et al. 2016; Baykara et al. 2016; Konieczny et al. 2021). The skeleton-based analysis approach was applied to DTI and DKI maps in Study I.

Network based diffusion markers require the reconstruction of streamlines using tractography and the application of an atlas-based brain parcellation (**Figure 3B**). Depending on tractography algorithm used, this analysis concept can be regarded highly complex. Tensor-based tractography follows the main direction of the diffusion tensor per voxel until a certain termination criterion is reached (Jiang et al. 2006). However, this algorithm does not take into account crossing fibers which represents a major limitation since up to 98% of the white matter contains crossing fiber orientations (Tournier, Calamante, and Connelly 2012). More advanced constrained spherical deconvolution (CSD) algorithms allow the modelling of crossing fiber orientation distributions (Tournier et al. 2019). Typically, network topology is summarized to a graph-theoretical measure, such as efficiency which is expressed as the inverse of the shortest path length between two region (Rubinov and Sporns 2010). While this approach revealed pathomechanistic insights into SVD (Tuladhar et al. 2017), derived markers and their test-retest reliability have not yet been validated for clinical use. The systematic validation of network-based diffusion markers using a deterministic and CSD-based tractography pipeline was the focus of Study I.

White matter fiber tract-based diffusion markers also rely on tractography (**Figure 3C)**. Various tools exist that allow reconstructing tracts connecting any two regions of interest by manual delineation of inclusion and exclusion masks. This approach promises flexible application but comes at cost of tractography dissection variability (Schilling et al. 2021). Fully automated tools overcome this problem by using anatomical priors to reconstruct entire white matter fiber tracts guided by subject-specific shape, location or connectivity (Wasserthal, Neher, and Maier-

Hein 2018; Warrington et al. 2020). Microstructure is probed through weighting the reconstructed fiber tract with diffusion metrics, a concept often called "tractometry". This approach was used in Study II, in which we assessed the potential of advanced fixel metrics of specific white matter fiber tracts to disentangle and describe effects of SVD and Alzheimer's disease. Fixel metrics, which were determined within tracts, will be explained in the next section.

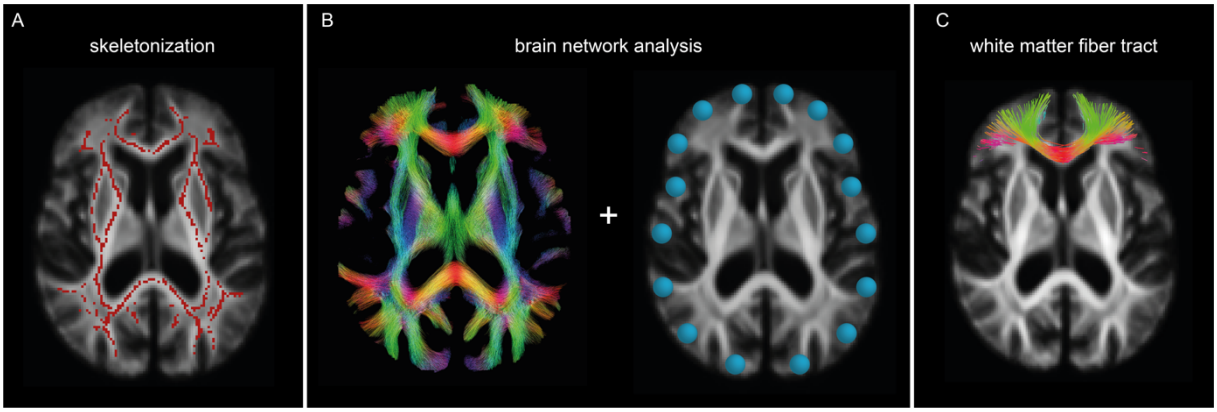

Figure 3. Diffusion MRI analysis concepts. Approaches applied in this thesis include: (**A**) skeleton-based diffusion markers, (**B**) markers based on brain network analysis include streamline reconstruction using tractography and the reconstruction of nodes using atlas-based brain parcellation and (**C**) white matter fiber tract reconstruction.

1.4.3. Beyond the voxel: fixel-based analysis

While CSD-based tractography algorithms allow to reconstruct streamlines of crossing fibers, streamlines are typically weighted by voxel-based diffusion metrics. Thus, ultimately, derived measures are not fiber-specific, but represent voxel-averages, neglecting the fact that one voxel can harbor multiple (crossing) fiber populations. Advanced tools not only model streamlines of crossing fiber orientations, but also allow assessing properties specific to each *fi*ber population within a vo*xel* – on the *fixel* level. Using this technique, one can simultaneously derive tract-specific measures of fiber density and fiber-bundle cross-section. Fiber density is a fixel-specific feature of white matter *micro*structure, approximately proportional to the total intra-axonal volume (Raffelt et al. 2012). Fiber-bundle cross-section is a fixel-specific *macro*scopic feature, presumably reflecting the accumulated axon loss (Raffelt et al. 2017; Dhollander et al. 2021). Study II investigated if these fixel metrics allow to disentangle white matter damage due to SVD and Alzheimer's disease.

1.5 Aim Study I: Systematic validation of structural brain networks in cerebral small vessel disease

Due to the unique capacity to provide insight into brain regions and their connections in health and disease, studies employing network analysis have gained much attention. In SVD, reduced network efficiency has been associated with cognitive decline, increased mortality and a high likelihood of conversion to dementia (Boot et al. 2020; Tuladhar et al. 2016; 2020). Studies on network analysis have further informed us that especially disruption of central network edges of rich club nodes (i.e., highly connected and interconnected brain regions) contributes to cognitive decline in SVD (Reijmer et al. 2016; Tuladhar et al. 2017).

While these findings have provided pathomechanistic insight into the disease, they also suggest potential of network-based markers in clinical routine by capturing disease progression and eventually as surrogate endpoints in clinical trials. However, upon closer examination, studies are highly heterogeneous in terms of tractography algorithm used for network reconstruction, node definition (i.e., atlas-based brain parcellation) and edge definition of the network. Also, the added benefit of the complex network approach on top of conventional markers and compared to established and less complex diffusion markers has not been assessed.

To address these questions, Study I investigated the potential of network-based diffusion markers by systematically assessing their clinical and technical validity in two non-overlapping samples of sporadic SVD. We reconstructed multiple structural brain networks using either a deterministic tractography pipeline based on single-shell diffusion data, which has widely been used in SVD research (Tuladhar et al. 2016; Boot et al. 2020), or a more advanced multi-shell pipeline that models crossing fibers (Tournier, Calamante, and Connelly 2012). Networks also differed with respect to the node and edge definition to find the combination most sensitive to clinical deficits and most reliable. We a priori only assessed the (global) efficiency of brain networks which has previously shown to be most sensitive to cognitive deficits in SVD (Boot et al. 2020). For clinical validation, we determined the added benefit of structural brain network analysis in explaining processing speed deficits, the main cognitive deficit in SVD, and in detecting disease progression over time. For technical validation, we assessed test-retest repeatability in a high-frequency serial imaging longitudinal dataset.

Our hypotheses and analysis approach were pre-registered at AsPredicted.org before carrying out any analyses. Our pre-specified hypotheses were that i) compared with simpler global white matter diffusion metrics, structural brain network analysis better explains processing speed

deficits and better captures short-term disease progression over time, and ii) a more elaborate brain network pipeline using multi-shell data and CSD-based tractography outperforms a simple deterministic brain network pipeline using single-shell data.

1.6 Aim Study II: Disentangling the effects of Alzheimer's and cerebral small vessel disease on white matter fiber tracts

Since Alzheimer's disease and SVD co-occur in most memory clinic patients, (Kapasi, DeCarli, and Schneider 2017), biomarkers that disentangle and describe the contribution of each pathology within the individual patient are of high clinical relevance. Diffusion alterations have been observed in both SVD and Alzheimer's disease. In severe SVD cases, white matter damage expands from the periventricular white matter to the deep white matter. In addition, focal SVD lesions induce remote effects in white matter due to secondary neurodegeneration (ter Telgte et al. 2018; Duering et al. 2012), rendering SVD a global brain disease. In Alzheimer's disease, white matter damage is increasingly recognized to be an early hallmark of the disease (Nasrabady et al. 2018; Araque Caballero et al. 2018). Diffusion alterations of temporal white matter fiber tracts (e.g., parahippocampal cingulum and inferior temporal white matter fiber tracts) have been found to be associated with tau pathology (Raghavan et al. 2022). Another study found an association between free-water corrected DTI metrics of the uncinate fasciculus and the posterior cingulum and Aβ and tau pathology (Pichet Binette et al. 2021). However, most diffusion MRI studies in Alzheimer's disease did not consider comorbid SVD, which has been shown to be the main driver of diffusion alterations in diffusion tensor and free water imaging in mixed disease (Finsterwalder et al. 2020).

To address the need for disease-specific biomarkers, Study II assessed the utility of advanced diffusion metrics operating on the fixel level to describe and disentangle alterations due to Alzheimer's disease and SVD. We included three independent samples covering genetically defined cerebral small vessel disease (CADASIL) and age-matched controls, the full spectrum of biomarker-confirmed Alzheimer's disease including Aβ and tau negative controls and a validation sample with presumed mixed pathology. The fiber density and fiber-bundle cross-section of 29 well-defined white matter fiber tracts was assessed. In this exploratory analysis, we did not have any pre-specified hypotheses in terms of associations between fixel-metrics and Alzheimer's disease vs. SVD pathology. Our main goal was to investigate whether SVD and Alzheimer's disease show distinct signatures of white matter damage as assessed by

advanced fixel metrics. We performed group comparisons between patients and controls and assessed associations between fixel metrics within main white matter tracts and imaging hallmarks of SVD (WMH volume, lacune and cerebral microbleed count) and Alzheimer's disease (amyloid- and tau-PET), age and a measure of neurodegeneration (brain volume). Main findings obtained in the SVD and Alzheimer's disease samples were independently validated in a third sample of elderly with presumed mixed pathology.

2. STUDIES

The original numbering of tables, figures, and supplementary material within each article has been retained.

2.1 Study I: Systematic validation of structural brain networks in cerebral small vessel disease

The following section includes the original research article "Systematic validation of structural brain networks in cerebral small vessel disease" which was published in *Journal of Cerebral Blood Flow & Metabolism (*Dewenter et al., 2022*).*

Systematic validation of structural brain networks in cerebral small vessel disease

Anna Dewenter[1], MSc, Benno Gesierich[1], PhD, Annemieke ter Telgte[2,3], PhD, Kim Wiegertjes[2], PhD, Mengfei Cai[2], MD, Mina A. Jacob[2], MD, José P. Marques[4], PhD, David G. Norris[4], PhD, Nicolai Franzmeier[1], PhD, Frank-Erik de Leeuw[2], MD, PhD, Anil M. Tuladhar[2], MD, PhD, Marco Duering[1,2,5], MD

[1] Institute for Stroke and Dementia Research (ISD), University Hospital, LMU Munich, Germany

[2] Department of Neurology, Donders Institute for Brain, Cognition and Behaviour, Radboud University Medical Center, Nijmegen, The Netherlands

[3] VASCage – Research Centre on Vascular Ageing and Stroke, Innsbruck, Austria

[4] Radboud University, Donders Institute for Brain, Cognition and Behavior, Nijmegen, The Netherlands

[5] Medical Image Analysis Center (MIAC) and Department of Biomedical Engineering, University of Basel, Basel, Switzerland

2.1.1 Abstract

Cerebral small vessel disease (SVD) is considered a disconnection syndrome, which can be quantified using structural brain network analysis obtained from diffusion MRI. Network analysis is a demanding analysis approach and the added benefit over simpler diffusion MRI analysis is largely unexplored in SVD. In this pre-registered study, we assessed the clinical and technical validity of network analysis in two non-overlapping samples of SVD patients from the RUN DMC study (n=52 for exploration and longitudinal analysis and n=105 for validation). We compared two connectome pipelines utilizing single-shell or multi-shell diffusion MRI,

while also systematically comparing different node and edge definitions. For clinical validation, we assessed the added benefit of network analysis in explaining processing speed and in detecting short-term disease progression. For technical validation, we determined test-retest repeatability.

Our findings in clinical validation show that structural brain networks provide only a small added benefit over simpler global white matter diffusion metrics and do not capture short-term disease progression. Test-retest reliability was excellent for most brain networks. Our findings question the added value of brain network analysis in clinical applications in SVD and highlight the utility of simpler diffusion MRI based markers.

2.1.2 Introduction

Cerebral small vessel disease (SVD) is a leading cause of vascular cognitive impairment and loss of independence in the elderly. Sporadic SVD, related to increased age and arterial hypertension, is particularly common with a prevalence up to 50% in individuals over the age of 70 (ter Telgte, Wiegertjes, et al. 2018; Wardlaw, Smith, and Dichgans 2019). While neuroimaging features currently used in clinical routine are typically based on visible lesions – such as white matter hyperintensities, lacunes, and microbleeds (Wardlaw et al. 2013) – there is a move towards quantitative markers for measuring disease burden and progression. Measures based on diffusion MRI, such as diffusion tensor imaging, have shown high potential as quantitative markers. They allow detecting subtle white matter changes, are strongly associated with clinical deficits and provide excellent reliability (Baykara et al. 2016; Konieczny et al. 2021).

Diffusion MRI analysis approaches differ substantially in their complexity, both in terms of data acquisition and subsequent processing (Tournier 2019). Because SVD is considered a disconnection syndrome (ter Telgte, van Leijsen, et al. 2018), brain networks based on tractography and graph theoretical analysis of network structure are regarded as a compelling approach for quantifying clinically relevant brain network alterations in SVD. These structural brain networks are based on fiber tractography and pre-defined regions-of-interest, i.e. the nodes, which are connected via white matter tracts, i.e. the edges. The corresponding network architecture is quantified with graph-informed measures, such as global efficiency (Rubinov and Sporns 2010), which has proven to be the most sensitive graph measure to capture brain alterations in SVD (Boot et al. 2020). Several studies suggest a high potential of structural

network analysis for characterizing SVD burden, for exploring the underpinnings of symptoms or for predicting the disease course (Reijmer et al. 2015; Tuladhar et al. 2020; Xu et al. 2018).

There are, however, several critical knowledge gaps that are considered major roadblocks for further application in research and clinical routine. Network analysis is a highly demanding diffusion MRI analysis approach, and the added benefit over simpler diffusion MRI analysis has so far not been systematically assessed. Also, connectome pipelines depend on arbitrary choices, especially in terms of tractography algorithm and the definition of nodes and edges. Of particular interest are more elaborate tractography algorithms, which better model the complex fiber architecture of the brain, but typically rely on a more demanding data acquisition, such as multi-shell diffusion imaging and high-angular resolution (Jeurissen et al. 2013). These different choices have so far not been systematically compared in SVD. Previous studies suggest that most graph metrics capturing structural network architecture show good to excellent test-retest reliability in healthy young volunteers (Welton et al. 2015). Importantly, the reliability of the network analysis approach in SVD is largely unknown, but is a crucial factor for clinical application.

The goal of this pre-registered study was a systematic clinical and technical validation of structural brain network analysis in SVD. We applied two different connectome pipelines, utilizing single-shell or multi-shell diffusion MRI data, while also systematically comparing different node and edge definitions. For exploration and independent validation, we used two non-overlapping patient samples with state-of-the-art diffusion MRI from the RUN DMC study (ter Telgte, Wiegertjes, et al. 2018; van Norden et al. 2011).

For clinical validation, we assessed the added benefit of structural brain network analysis in explaining processing speed deficits, the main cognitive deficit in SVD, and in detecting disease progression over time. Our pre-specified hypotheses were that i) compared with simpler global white matter diffusion metrics, brain network analysis better explains processing speed deficits and better captures disease progression over time, and ii) a more elaborate connectome pipeline using multi-shell data and constrained-spherical deconvolution-based tractography outperforms a simpler deterministic connectome pipeline using single-shell data. For technical validation, we assessed test-retest repeatability in a high-frequency serial imaging longitudinal dataset.

2.1.3 Methods

Our study design, analysis plan, and hypotheses were pre-registered and are available at https://aspredicted.org/382ha.pdf.

Participants

We included data from SVD patients participating in the RUN DMC study (van Norden et al. 2011). For exploration, we used data from the RUN DMC – InTENse sub-study (Radboud University Nijmegen Diffusion tensor and Magnetic resonance imaging Cohort – Investigating The origin and EvolutioN of cerebral small vessel disease, ter Telgte, Wiegertjes, et al. 2018). In this sub-study, 54 patients from the main study were invited to a baseline MRI assessment, used for the cross-sectional analysis, and a total of 9 monthly follow-up MRI scans, used for the longitudinal analysis. For the cross-sectional exploratory analysis, two patients were excluded because of confounding neuropsychological test results (Konieczny et al. 2021), which resulted in a final sample of 52 sporadic SVD patients.

For independent validation of the cross-sectional results, we used a non-overlapping sample from the 3rd follow-up visit of the RUN DMC main study (n=183). Some patients had to be excluded due to missing DWI data (n=2), non-SVD infarcts (n=6), MRI protocol violation (n=1), missing neuropsychological data (n=16), or insufficient image quality (n=5). To ensure that results were not driven by outlier observations, we excluded five patients with Trail Making Test (TMT) compound scores qualifying as outlier according to the interquartile range criterion (i.e., scores outside the range defined by the cut-points of the first and third quartile plus 1.5 times the interquartile range above and below). Since the InTENse sub-study deliberately included a subset of patients with higher lesion load, we restricted the main study sample to SVD patients above 70 years of age to keep disease severity roughly similar across both samples (**Table 1**). This resulted in a final sample of 105 SVD patients for validation.

For the longitudinal analysis, we split the sample from the RUN DMC – InTENse sub-study into an exploration (n=27) and validation group (n=26) while accounting for a similar number of visits and disease severity (i.e. WMH volume) across groups. A few visits had to be excluded from the longitudinal analysis due to insufficient data quality, of which some only became apparent during tractography (n=7). Only patients with at least 3 MRI visits were included for the longitudinal analysis, rendering the sample size to 25 patients for exploration and 26 patients for validation with a median of 9 (range 3-10) MRIs per participant.

Study protocols were in accordance with the declaration of Helsinki and approved by the medical research ethics committee (CMO Arnhem-Nijmegen). Written informed consent was obtained from all participants prior to the start of the study.

Neuropsychological testing

Neuropsychological testing was performed following identical protocols in both samples. We pre-specified to focus on the core deficit in SVD, i.e. processing speed, which was assessed by the time to complete Trail Making Test matrix A and B. We derived age- and education-corrected z-scores for matrix A and B separately as based on healthy subjects (Baykara et al. 2016; Konieczny et al. 2021; Tombaugh 2004) and next calculated the average to derive an established compound score. Patients were further characterized with respect to vascular risk factors (arterial hypertension, hypercholesterolemia, diabetes, smoking status) and activities of daily living (Barthel scale score).

MRI acquisition and conventional SVD imaging markers

MRI scans were performed on a single 3 Tesla scanner (Magnetom Prisma with 32-channel head coil; Siemens Healthineers, Erlangen, Germany). Imaging protocols in both studies were largely similar and included 3D T1-weighted, 3D fluid-attenuated inversion recovery (3D-FLAIR), and 3D gradient echo (T2*-weighted) sequences. The diffusion MRI protocol was identical in both samples and comprised a multi-band echo planar imaging multi-shell diffusion-weighted imaging sequence (repetition time 3220 ms, echo time 74 ms, diffusion-encoding directions 30 x b = 1000 s/mm^2 and 60 x b = 3000 s/mm^2, 10 x b = 0 images, multi-band factor 3). One b = 0 image with inverted phase-encoding direction was acquired for correction of susceptibility-induced distortions during preprocessing. A complete description of all sequence parameters can be found in **Table e-1**.

Conventional SVD imaging markers (white matter hyperintensity [WMH] volume, lacune count, microbleed count, brain volume) were quantified according to the STRIVE consensus criteria (Wardlaw et al. 2013). All volumes were normalized to the intracranial volume. Details on the calculation of conventional SVD imaging markers have been described previously (Telgte et al. 2019).

Diffusion MRI preprocessing

Preprocessing steps included visual quality control, Marchenko-Pastur principal component analysis-based denoising, Gibbs artefact removal, and correction for susceptibility-induced distortions, eddy current-induced distortions, as well as head motion. This was done using tools from MRtrix3 (www.mrtrix.org/, version 3.0.0, dwidenoise, (Veraart et al. 2016; Veraart, Fieremans, and Novikov 2016; Cordero-Grande et al. 2019; Tournier et al. 2019), mrdegibbs (Tournier et al. 2019; Kellner et al. 2016)) and the Functional Magnetic Resonance Imaging of the Brain (FMRIB) Software Library (FSL; version 5.0.10 [RUN DMC – InTENse], version 6.0.1 [RUN DMC main], topup (Andersson, Skare, and Ashburner 2003; Smith et al. 2004), eddy (Andersson and Sotiropoulos 2016)).

Skeleton-based, global white matter diffusion markers

To assess the added benefit of structural brain network analysis, we included measures of global white matter integrity as reference, that were based on diffusion tensor imaging (DTI) and diffusion kurtosis imaging (DKI) metrics. DTI metrics were calculated using ‘dtifit’ in FSL (using only b = 0 and b = 1000 s/mm^2 images) and DKI metrics using the Diffusional Kurtosis Estimator (www.nitrc.org/projects/dke, (Tabesh et al. 2011)).

For DTI, we included the most commonly used diffusion metrics fractional anisotropy and mean diffusivity (Smith et al. 2006). For DKI, we included mean kurtosis and radial kurtosis as reference metrics, since these showed the highest association with processing speed in a previous study (Konieczny et al. 2021).

Global white matter measures of these metrics were derived as average over a skeleton of the major white matter tracts, as implemented in the tract-based spatial statistics (TBSS) pipeline in FSL (Smith et al. 2006). The TBSS-based registration to standard space and projections onto the white matter skeleton was estimated from fractional anisotropy images and then applied to all other diffusion metrics. Prior to averaging, we applied a custom mask to remove all areas from the skeleton that are typically susceptible to cerebrospinal fluid partial volume effects in SVD patients (Baykara et al. 2016). The resulting global white matter diffusion metrics will be referred to as ‘skeleton-based’ diffusion markers.

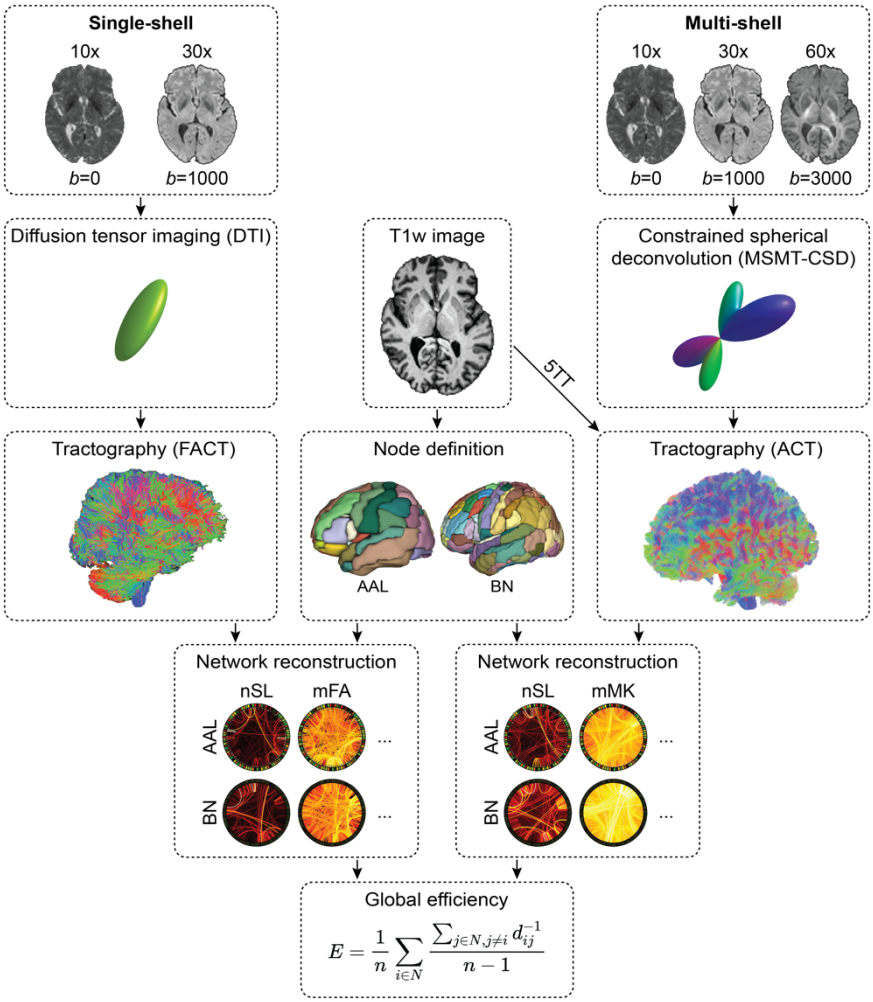

Figure 1. Overview of the two connectome pipelines (single-shell left, multi-shell right). The single-shell pipeline relies on diffusion tensor imaging and tractography using the FACT algorithm. The multi-shell pipeline relies on MSMT-CSD and anatomically constrained tractography. For both pipelines, we applied the node definition according to the AAL or Brainnetome atlas. After network reconstruction, each structural brain network was summarized by the global efficiency metric (E). N is the set of all nodes in the network, and n is the number of nodes, whereas d(i,j) is the weighted distance between nodes i and j, (i,j ∈ N). Abbreviations: AAL = automated anatomical labelling; ACT = anatomically constrained tractography; BN = Brainnetome; DTI = diffusion tensor imaging; FACT = fiber assignment through continuous tracking; mFA = mean of fractional anisotropy of streamlines; mMK = mean of mean kurtosis of streamlines; MSMT-CSD = multi-shell multi-tissue constrained spherical deconvolution; nSL = number of streamlines; T1w = T1-weighted image; 5TT = five tissue-type image.

Overview of the structural brain network analysis

We applied two brain network pipelines (described in detail in the following sections), using either single-shell or multi-shell data as starting point. The key difference between these two brain network pipelines was the tractography approach. In the single-shell pipeline (**Figure 1**, left), streamlines were tracked by following the main direction of the diffusion tensor per voxel. The multi-shell data (**Figure 1**, right) enabled a more advanced tractography approach based on constrained-spherical deconvolution (CSD), which reconstructs complex fiber orientation distributions of multiple fiber populations within a voxel. As such, CSD-based tractography allows to track crossing fibers, which occur in most white matter regions (Tournier, Calamante, and Connelly 2012). In addition to CSD, we improved the biological accuracy of the streamline reconstruction by introducing anatomical constraints (i.e. streamlines followed white matter fiber orientation distributions, were terminated when entering cortical grey matter and rejected when entering fluid-filled regions; for full algorithm details see original publication (Smith et al. 2012).

We then applied a brain parcellation to the reconstructed streamlines to form structural networks, which are defined by a set of nodes (i.e., brain regions) and edges connecting these nodes. Across both pipelines, we defined the nodes based on the AAL atlas (automated anatomical labelling, 90 ROIs in total, after excluding cerebellar regions) and the Brainnetome atlas with a higher number of smaller regions (246 ROIs in total). Several commonly used edge definitions were used to calculate edge weights (details are given below for each pipeline).

Finally, we derived the global efficiency as a well-established network marker of SVD burden from each structural network (**Figure 1**, center bottom). Efficiency between two regions is expressed as the inverse of the shortest path length between two regions (Rubinov and Sporns 2010), where the length of each possible path is equal to the sum of the lengths of all edges in that path. Global efficiency of the network is then defined as the average efficiency across all node pairs. To assess whether some nodes within the global network disconnect faster than others over time, we also calculated local efficiency for each node of the structural network that showed the highest clinical and technical validity in the longitudinal dataset (i.e. highest effect sizes in regression analyses, highest added benefit in random forest regression and highest intraclass correlation coefficient [ICC]).

Single-shell Pipeline

For single-shell networks, streamlines were reconstructed based on the diffusion tensor using the fiber assignment by continuous tracking (FACT) algorithm ('dti_tracker', Diffusion Toolkit, version 0.6.4.1). In short, the algorithm started at the center of all voxels with fractional anisotropy > 0.2 and terminated if the streamlines left the brain mask, encountered voxels with fractional anisotropy < 0.2 or when the turning angle exceeded 45°. Reconstructed streamlines were filtered and smoothed requiring a step length of 1 voxel ('spline_filter', Diffusion Toolkit). Two nodes were considered connected if the endpoints of the reconstructed streamlines lay within both nodes. Atlas parcellations were registered to diffusion space, applying a series of linear and non-linear registrations, leading from the MNI template space, through T1-weighted and FLAIR space, to the diffusion space. All registrations were estimated and concatenated with the Advanced Normalization Tools (ANTs) (Avants et al. 2011)). For the longitudinal data, as previously described in detail (Gesierich et al. 2020), baseline T1-weighted images were indirectly normalized into MNI space via an intermediate custom template, and follow-up scans were normalized by concatenating this normalization with the registration between baseline and follow-up T1-weighted images.

Five commonly used edge weights were applied in the single-shell pipeline: number of streamlines (nSL), number of streamlines weighted by the mean length (mLen), number of streamlines weighted by the inverse of the streamline length (invLen) (Hagmann et al. 2007) mean fractional anisotropy over all streamlines (mFA), number of streamlines weighted by the mean fractional anisotropy (wFA). Each edge was further normalized by the average volume of the connected nodes to correct for the different volumes of the nodes and for different brain sizes.

For each of the resulting 10 (2 node definitions x 5 edge definitions) weighted undirected networks, we calculated the global efficiency using the Brain Connectivity Toolbox (Rubinov and Sporns 2010).

Multi-shell Pipeline

For the advanced multi-shell networks, streamlines were reconstructed using a multi-shell multi-tissue constrained spherical deconvolution tractography pipeline using tools from MRtrix3 (Tournier et al. 2019). To limit false positives and improve biological accuracy (Smith et al. 2012), tractography was anatomically-constrained to white matter by using a 5-tissue-type

image generated from T1-weighted images. WMH masks were set as the fifth volume (i.e., pathological tissue) of the 5-tissue-type image to allow tracking within these regions, which are often is misclassified as grey matter, leading the tracking algorithm to terminate prematurely. Importantly, WMH segmentations were performed on each time point in the longitudinal dataset. The remaining steps were: response function estimation ('dhollander' algorithm), estimation of the fiber orientation distributions (Jeurissen et al. 2014), multi-tissue informed log-domain intensity normalization, modelling 10 million streamlines using anatomically constrained streamlines tractography, dynamic seeding and cropping at the GMWM-interface, as well as SIFT2 filtering of the streamlines (Smith et al. 2015).

Consistent with the single-shell pipeline, nodes were defined either according to the AAL atlas or Brainnetome atlas.

Seven different edges were applied in the multi-shell pipeline: number of streamlines (nSL), number of streamlines weighted by the length of each streamline (mLen), number of streamlines weighted by the inverse length of each streamline (invLen) (Hagmann et al. 2008), mean of the mean kurtosis of streamlines (mMK), number of streamlines weighted by the mean of the mean kurtosis (wMK), mean fractional anisotropy of streamlines (mFA), number of streamlines weighted by the mean fractional anistropy (wFA). While fractional anisotropy maps were calculated on single-shell diffusion data, edges based on fractional anisotropy were also included here to allow a more direct comparison of the two pipelines. Again, we calculated global efficiency for the 14 (2 node definitions x 7 edge definitions) networks.

Statistical analysis

All statistical analyses were performed in R (version 3.6.1, R Core Team 2016). The statistical significance level was set at $\alpha < 0.05$. Since we mainly focused on the effect sizes when interpreting the results, we did not correct for multiple comparisons.

To compare sample characteristics between RUN DMC – InTENse and RUN DMC main, we used chi-squared ($\chi 2$) tests (for categorical variables) and non-parametric Wilcoxon rank sum tests (for numeric variables), as appropriate.

Subsequent analyses were conducted completely independently for both samples. The processing speed compound scores were power-transformed using the Yeo-Johnson transformation to approximate a normal distribution (Yeo and Johnson 2000).

Four main analyses were conducted to examine clinical and technical validation of structural brain network analysis in SVD.

First, we performed simple linear regression analyses between global efficiency of structural brain networks (independent variable) and processing speed performance (i.e., TMT compound score, dependent variable). We used the adjusted R^2 to quantify and compare associations. Second, we assessed the added benefit for each marker on top of conventional SVD imaging markers (i.e., normalized WMH volume, lacune count, microbleeds and normalized brain volume). We used multivariable random forest regression with conditional inference trees (R package 'party', version 1.3.3) to overcome the problem of multicollinearity, which is a critical aspect since SVD imaging markers and diffusion markers are intercorrelated. We constructed one random forest regression model with conventional SVD imaging markers only (number of trees=1501, mtry=3), and additional models adding respectively one of the diffusion-based markers. Prediction accuracy was calculated for each random forest regression model as the root-mean-square error (RMSE) between observed and predicted values using leave-one-out cross-validation. The added benefit of each diffusion-based marker for prediction of processing speed was quantified by the difference of the RMSE between the model with and without that diffusion-based marker (Konieczny et al. 2021). We repeated random forest regression for each model (with cross-validation) 100 times to determine a point estimate and 95% confidence interval for the RMSE.

Third, to assess the ability of structural brain networks to capture change over time, we calculated linear mixed effects models in the split exploration and validation longitudinal samples. Brain network and skeleton-based diffusion markers were first normalized individually for each patient to the baseline score and then centered and scaled (by subtracting the mean and dividing by the standard deviation). Time of MRI visits (relative to baseline visit) was modelled as fixed effect. To account for patient-specific variation, we included a random intercept for each patient in the model architecture, but models with random slopes per patient did not converge. The fixed effect reflects the mean change in the structural brain network over time, marginal R2 reflects the explained variance by the fixed effect. The following R packages were used for estimation of linear mixed models: 'lme4' (version 1.1.21, Bates et al. 2014), 'lmerTest' (version 3.1.2) (Kuznetsova, Brockhoff, and Christensen 2017), 'boot' (version 1.3.22) (Canty 2002), 'MuMIn' (version 1.43.15) (Barton and Barton 2019).

For technical validation, we assessed the test-retest reliability of structural brain networks as our fourth analysis within the same exploration and validation sample used for the longitudinal

analysis. Intraclass correlation coefficients (1,1) (Shrout and Fleiss 1979) were calculated with the R package ‘psych’ (version 1.9.12.31) (Gesierich et al. 2020).

Deviations from the pre-registered analysis protocol

For parts of this investigation, we had to follow an unplanned path for valid reasons. First, for the independent validation sample of the cross-sectional analysis, we originally planned to randomly sample one hundred subjects from a subset of the UK Biobank with matching range of the WMH volume and age of the RUN DMC – InTENse subjects. However, when calculating the established TMT compound score, we noticed implausibly low z-scores in many UK Biobank subjects due to extremely low reaction times. This might have resulted from a key difference in task administration, since in the UK Biobank study the TMT was performed using a computer mouse, whereas the norm data was based on the paper-pencil version (Tombaugh 2004). Since the TMT data was pre-specified as the clinical endpoint for the cross-sectional analyses, we did not want to deviate from this aspect, but instead chose a different validation sample.

Second, we pre-registered to normalize global efficiency values by the global efficiency of random networks using the Brain Connectivity Toolbox. However, after revisiting the literature, we noticed that in most brain network studies in SVD – if not all – global efficiency values were not normalized. This might result in important consequences of the interpretation of these global efficiency values per se (see discussion), however, to ensure comparability with previous studies, we chose to follow the established procedure for brain networks in SVD.

Third, we planned to compare a random forest regression model with skeleton-based DTI/DKI metrics only as a comparison model, but since we were interested in the added benefit of brain networks compared with skeleton-based diffusion markers – and not in the added benefit of brain networks on top of skeleton-based diffusion markers – we revised our random forest regression approach accordingly.

Data availability

Anonymized data will be made available upon request to the corresponding author.

2.1.4 Results

Sample characteristics are presented in **Table 1**. SVD patients of the RUN DMC – InTENse sub-study were younger and presented with higher brain volumes compared to patients from the RUN DMC main study ($p < 0.0001$).

Table 1: Sample characteristics

	RUN DMC – InTENse sub-study *n*=52	RUN DMC main study *n*=105	*p-value*
Demographic characteristics			
Age [years], median (IQR)	68.50 (8.25)	77.15 (8.19)	< 0.0001
Female, *n* (%)	18 (35)	48 (46)	0.2484
Vascular risk factors, *n* (%)			
Hypertension	43 (83)	75 (72)[a]	0.2102
Hypercholesterolemia	25 (50)	62 (60)[a]	0.3318
Diabetes	6 (12)	16 (15)[a]	0.6843
Current or past smoking	37 (71)	72 (69)	0.8835
Clinical scores, median (IQR)			
Processing speed z-score	-0.15 (1.16)	-0.18 (1.55)	0.6265
Barthel scale score	100 (5)	100 (5)[a]	0.8930
SVD imaging markers, median (IQR)			
WMH volume[b] [%]	0.35 (0.59)	0.31 (0.74)	0.7984
Lacune count	0 (0)	0 (1)	0.3648
Microbleed count	0 (1)	0 (1)	0.8816
Brain volume[b] [%]	77.73 (5.35)	72.51 (4.79)	< 0.0001

Abbreviations: IQR = interquartile range; WMH = white matter hyperintensities. [a] based on *n*=104 due to missing data for one patient; [b] Normalized by intracranial volume

Clinical validation: Associations with processing speed performance

Associations with processing speed performance as assessed by simple regression greatly varied depending on node, edge, and tractography pipeline (**Figure 2A; Table e-2**).

In the exploratory sample, brain networks defined by nSL/wFA edges and AAL nodes explained the highest variance of processing speed deficits (R^2=11%) in the single-shell pipeline. Thus, this combination performed slightly better than the simple, skeleton-based diffusion marker mean diffusivity (R^2=8%). Explained variance was overall higher for the multi-shell pipeline. Brain networks defined by the wFA edge and Brainnetome nodes best explained processing speed deficits (R^2=20%), followed by skeleton-based mean kurtosis (R^2=18%) and radial kurtosis (R^2=15%).

In line with the findings in the exploration sample, brain networks defined by nSL/wFA edges and AAL nodes yielded the strongest associations with processing speed deficits (up to R^2=16%) in the validation sample, explaining more variance than the best-performing skeleton-based diffusion marker fractional anisotropy (R^2=13%). In contrast with the exploratory sample, explained variance was barely higher for the multi-shell pipeline. Only brain networks defined by the mLen edge performed as well as the skeleton-based diffusion marker radial kurtosis (R^2=14%).

To assess an added benefit in explaining processing speed deficits on top of conventional SVD imaging markers (normalized WMH volume, lacune count, microbleed count, normalized brain volume), we performed multivariable random forest regression analyses (**Figure 2B**). In the exploratory sample, brain networks based on the nSL/wFA edges and AAL nodes showed the highest added benefit (RMSE decrease 5%), whereas the skeleton-based diffusion markers only showed a small added benefit (RMSE decrease 2.5%), or even no benefit (i.e., skeleton-based fractional anisotropy). In the multi-shell pipeline, skeleton-based radial kurtosis added the highest benefit in explaining processing speed deficits (RMSE decrease 7%), followed by brain networks based on the wMK edge (RMSE decrease 6%).

In the validation sample, skeleton-based fractional anisotropy added the highest benefit on top of conventional SVD imaging markers (RMSE decrease 4%), but brain networks with the wFA/mFA edge and the Brainnetome nodes showed a similar benefit. Results from the multi-shell pipeline showed a mixed pattern in the validation sample, with no consistent difference between skeleton-based diffusion markers and most structural brain networks.

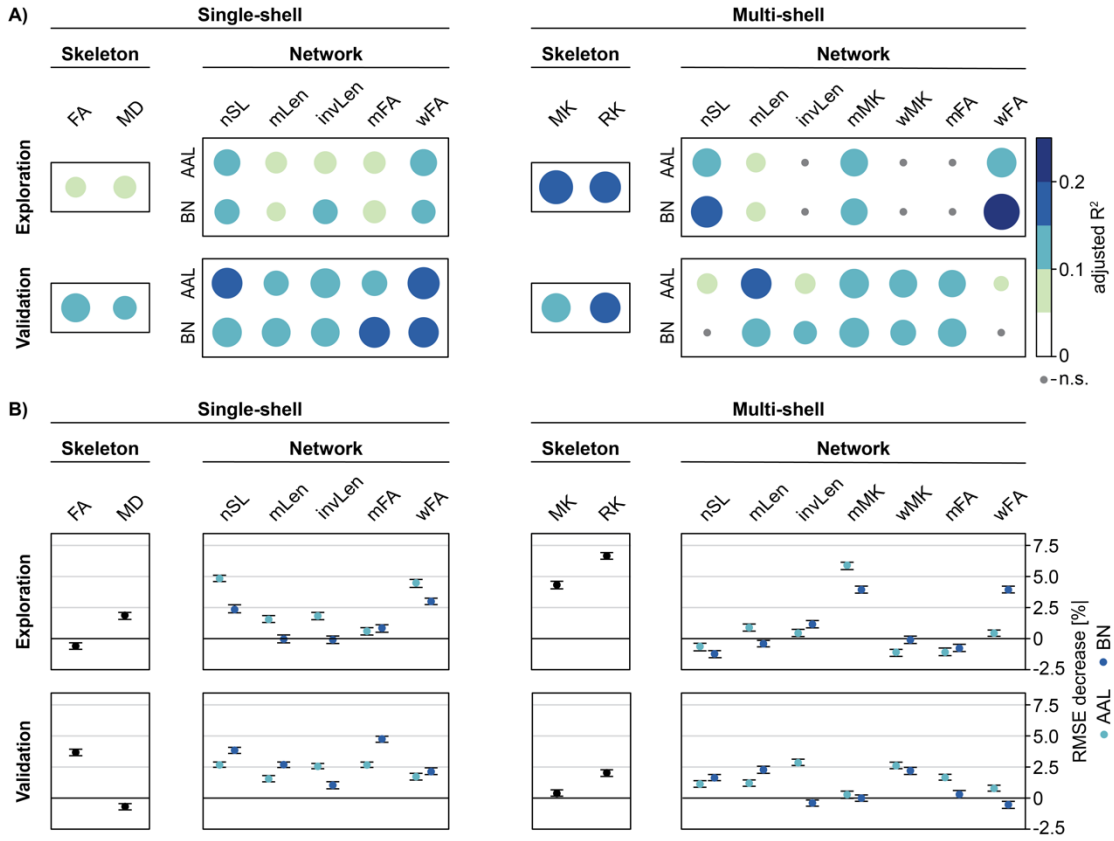

Figure 2. Associations between diffusion MRI markers (skeleton- or network-based) and processing speed. Analyses were performed in an exploration (RUN DMC – InTENse) and validation sample (RUN DMC main study). A) Simple linear regression between each diffusion marker and processing speed. Color and circle size depict explained variance (adjusted R^2). B) Multivariable random forest regression assessing the added benefit of each diffusion marker on top of conventional SVD markers. Plots indicate point estimate and 95% confidence interval for the change in model accuracy as assessed by the RMSE decrease. Abbreviations: AAL = automated anatomical labelling; BN = Brainnetome; FA = fractional anisotropy; invLen = number of streamlines weighted by the inverse length of each streamline; MD = mean diffusivity; mFA = mean of fractional anisotropy of streamlines; MK = mean kurtosis; mMK = mean of mean kurtosis of streamlines; mLen= mean length of streamlines; nSL = number of streamlines; RK = radial kurtosis; RMSE = root mean squared error; wFA= number of streamlines weighted by fractional anisotropy; wMK = number of streamlines weighted by mean kurtosis.

Clinical validation: Tracking short-term disease progression in serial MRIs

To assess the ability of brain networks to monitor short-term disease progression, we used data from high-frequency serial imaging and linear mixed effects models (**Figure 3A, B; Table e3**). In the exploratory sample and using the single-shell pipeline, the brain network based on the mFA edge was the only network parameter demonstrating a significant change over time. A change over time was more evident for skeleton-based diffusion markers (all $p < 0.05$), as indicated by substantially larger marginal R^2. Most brain networks derived from the multi-shell pipeline showed a change over time. However, also in this pipeline, the simpler, skeleton-based diffusion markers outperformed brain networks in the ability to capture short-term disease progression.

This pattern was replicated in the validation sample (**Figure 3C**).

To assess regional changes over time, we calculated local efficiency of each node of the structural brain network weighted by the mFA and defined by the AAL atlas, since this was the network with the largest change over time among global networks. Only four out of 90 nodes showed a significant change over time, but effect sizes were extremely small (fixed effects < 0.002, marginal $R^2 < 0.02$).

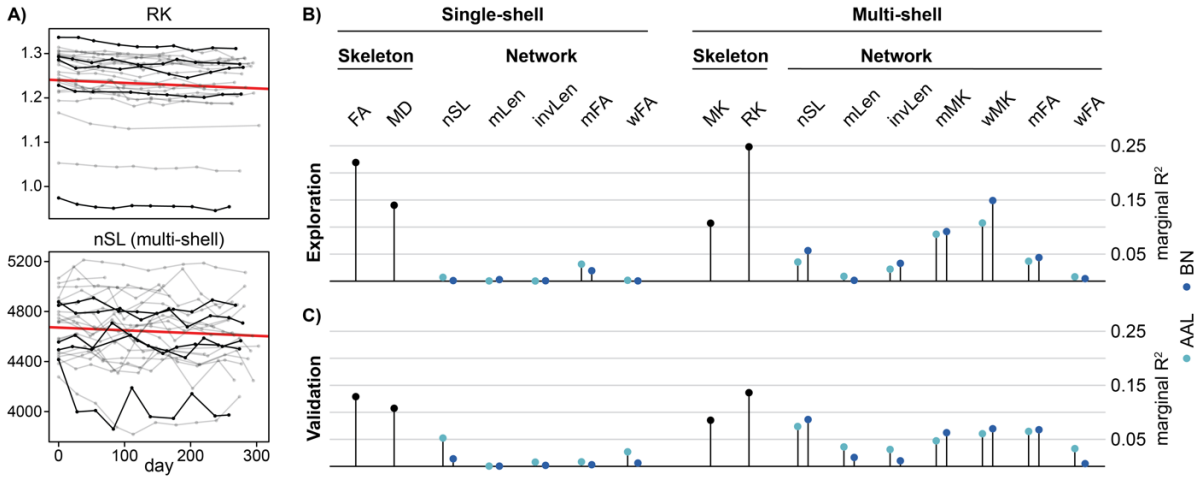

Figure 3. Short-term disease progression analysis using linear mixed effects models. A) Single subject data from the exploration sample. Skeleton-based RK (top) and structural brain networks with AAL node and nSL edge definition (bottom) plotted against time as examples. For better visibility, five subjects are depicted in black and the fixed effect of time is depicted in red. B) Marginal R^2 (variance explained by time) from the linear mixed-effects models in the exploration and C) validation sample. Abbreviations: AAL = automated anatomical labelling; BN = Brainnetome; FA = fractional anisotropy; invLen = number of streamlines weighted by the inverse length of each streamline; MD = mean diffusivity; mFA = mean of fractional anisotropy of streamlines; MK = mean kurtosis; mLen = mean length of streamlines; mMK = mean of mean kurtosis of streamlines; nSL = number of streamlines; RK = radial kurtosis; wFA= number of streamlines weighted by fractional anisotropy; wMK = number of streamlines weighted by mean kurtosis.

Technical validation: Test-retest repeatability

For technical validation, we used intraclass correlation coefficients to estimate test-retest repeatability in the serial MRI dataset. Most networks from the single-shell pipeline showed excellent test-retest repeatability with intraclass correlation coefficients higher than 93% in the exploratory sample (**Figure 4A, B; Table e4**). Only brain networks based on the AAL node and mLen edge definition were less reliable (ICC < 89%). Still, skeleton-based diffusion markers demonstrated a better test-retest repeatability (ICC > 98%). Some brain networks derived from the multi-shell pipeline showed also high test-retest repeatability, in particular those based on a mMK or mFA edge definition were in the range of the skeleton-based diffusion markers (ICC > 97%). The remaining brain networks of the multi-shell pipeline were less reliable. Especially the invLen edge showed intraclass correlation coefficients below 60%, indicating the worst technical validity of all assessed brain networks. Again, this pattern was replicated in the validation sample (**Figure 4C**).

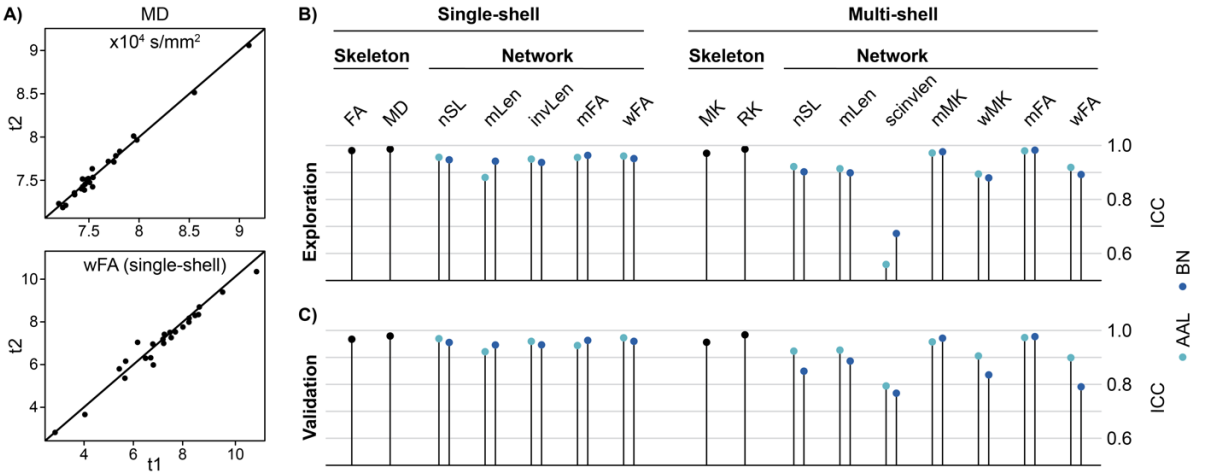

Figure 4. Test-retest repeatability of diffusion markers. A) Scatterplots showing the consistency of diffusion markers illustrated using the first two visits (time points t1 and t2) for skeleton-based MD (top) and wFA structural brain networks (bottom) as examples. In case of perfect test-retest repeatability, all points would lie on the diagonal. B) Intraclass correlation coefficients of diffusion markers assessed in the exploration and C) validation sample. Abbreviations: AAL = automated anatomical labelling; BN = Brainnetome; FA = fractional anisotropy; ICC = intraclass correlation coefficient; invLen = number of streamlines weighted by the inverse length of each streamline; MD = mean diffusivity; mFA = mean of fractional anisotropy of streamlines; MK = mean kurtosis; mMK = mean of mean kurtosis of streamlines; mLen = mean length of streamlines; nSL = number of streamlines; RK = radial kurtosis; wFA= number of streamlines weighted by fractional anisotropy; wMK = number of streamlines weighted by mean kurtosis.

2.1.5 Discussion

We systematically assessed the clinical and technical validity of brain network analysis as a marker for SVD. Our main findings are that i) for explaining processing speed, structural brain networks provide only a small added benefit over simpler, global white matter diffusion markers; ii) structural brain networks do not capture short-term disease progression over time; iii) multi-shell imaging does not improve the clinical validity of structural networks; iv) most structural brain networks show excellent test-retest reliability and thus a high technical validity and v) node and edge definitions have a substantial effect on brain network analysis results, highlighting the need for standardization to facilitate comparisons between studies.

Markers from diffusion MRI are well-established quantitative markers for SVD, both for cross-sectional and longitudinal use (Baykara et al. 2016; Konieczny et al. 2021). While global white matter markers, e.g. obtained as average over the entire fiber tract skeleton, offer a straightforward implementation, they do not account for the complex network structure of the human brain. Brain network analysis leverages this complex information for additional mechanistic insight, but its implementation is more demanding and subject to arbitrary decisions, such as node and edge definitions. In our pre-registered analysis and systematic comparison, we did not find a substantial advantage of brain network analysis over simpler, skeleton-based diffusion MRI markers. Importantly, for capturing change over time in the

longitudinal dataset, the simple markers were clearly superior. Thus, our findings question the added value of brain network analysis over simpler methods for clinical applications in SVD.

Diffusion MRI excels especially for longitudinal studies of SVD due to excellent test-retest reliability and high sensitivity to subtle white matter changes. Previous studies have shown that diffusion MRI markers (i.e. global skeleton-based markers) yield the smallest sample size estimates for assessing treatment effects over time, thus offering great potential to facilitate phase II randomized controlled trials (Baykara et al. 2016; Benjamin et al. 2016). While brain networks were also very reliable in terms of test-retest repeatability, they failed to capture short-term disease progression over time. However, brain topology changes might only become visible throughout long-term disease progression reflecting secondary degeneration (Tiedt et al. 2018). Still, tracking short-term progression is of particular interest for clinical trials with typically limited study duration. Thus, skeleton-based markers can be considered the first choice for application in clinical trials. Nonetheless, network analysis might still be useful for gaining pathomechanistic insights. As such, previous work has shown that especially connections between rich club nodes (i.e., nodes that are highly interconnected) decline in SVD (Tuladhar et al. 2017). The development of targeted intervention strategies might benefit from such mechanistic insights. Also, while global diffusion markers are mostly determined by SVD – not Alzheimer's disease pathology (Finsterwalder et al. 2020) – in memory clinical patients, regional brain network analysis might offer the possibility to disentangle the contribution of different pathologies.

Given that the brain's white matter contains more than 80% of crossing fibers (Tournier, Calamante, and Connelly 2012), we expected the more elaborate connectome pipeline with modelling of multiple fiber populations within a voxel via constrained spherical deconvolution to better depict SVD burden. Surprisingly, networks based on the multi-shell pipeline did not show an advantage over those based on the single-shell pipeline, although the latter method completely neglects the issue of crossing fibers.

Overall, we can only speculate why there was no clear added benefit of structural network analysis over simpler, skeleton-based diffusion markers. A potential explanation might be that the complex algorithms needed to construct the networks were developed on brains of young, healthy volunteers. The marked alterations of white matter microstructure (Wardlaw, Smith, and Dichgans 2019) in SVD might interfere with or violate model assumptions, e.g. of tractography algorithms. Furthermore, small vessel disease is now recognized as a global brain disease and thus, a simple global marker, such as the skeleton-based markers, might be

sufficient to capture disease burden. Similar to the tractography algorithm, the more elaborate Brainnetome atlas with a finer parcellation and better representation of the functional organization of the cortex was not superior to the AAL parcellation, which has a rather coarse, purely anatomically based parcellation. In conclusion, the simpler connectome pipeline, which was used in most previous brain network studies in SVD, performed best among the different combinations. Along the same theme that simpler measures perform better than more complex methods, and contrary to our previous study (Konieczny et al. 2021), we did not observe a benefit of the diffusion kurtosis model in the validation sample.

In line with previous work on brain networks in SVD (Reijmer et al. 2015; Tuladhar et al. 2020), we did not normalize the brain networks by the global efficiency of random networks. We also did not threshold the corresponding networks to a certain density and refer to previous work suggesting that – at least in the multi-shell pipeline – it might not be necessary to do so (Civier et al. 2019). In addition, others have already reported the effect of density thresholding and concluded that networks weighted by fractional anisotropy might be less prone to network density effects (de Brito Robalo et al. 2020). Still, global efficiency measures might be influenced by the density of the structural network and should thus not be understood as the "efficiency" of the brain network, but rather be interpreted as a global diffusion marker of the brain network. However, to not add another level of complexity, we decided a priori against trying out different arbitrary density thresholds.

Several limitations of our study need to be discussed. First, we only focused on global efficiency as the core graph metric of structural networks in SVD, even though other graph metrics might have been suitable as well. However, others have reported global efficiency to be the most sensitive graph measure of cognitive impairment in SVD (Boot et al. 2020), which is why we decided a priori on using this graph measure to reduce the complexity of the study. Also, we did not normalize the global efficiency measure against null-models. Consequently, global efficiency might be heavily influenced by the density of the structural network. However, to facilitate a comparison with previous work (Tuladhar et al. 2020), we decided against this normalization step. Second, while the exploration and validation sample were non-overlapping in terms of study participants, they were collected at the same center with identical protocols and might therefore not be considered as fully independent. Accordingly, we cannot estimate how our results would generalize to a dataset with a different acquisition protocol. On the other hand, this can also be regarded as a strength, since observed differences between results in the exploration and validation sample are unlikely to originate from technical differences. Third,

to identify the optimal imaging marker, we did not test for significance between different markers. However, since this is methodologically non-straightforward, we decided to focus on the comparison of effect sizes and included two non-overlapping samples for replication of findings and to further facilitate the interpretation of results. A main strength of the study is its pre-registration. To our knowledge, this is the first brain network study in SVD using a fully pre-specified analysis plan. As demonstrated here, results highly depend on arbitrary choices during analysis, which is why pre-specifying the analysis plan is of great importance to improve the transparency and quality of research on network analysis in SVD.

New diffusion analysis techniques are constantly emerging. Evaluating the benefit of a novel method over established techniques as well as technical validation are indispensable for evaluating the utility in research and clinical use (Smith et al. 2019). The structural network approach is compelling as it captures the complex network structure of the human brain. But when in need of disease burden or progression markers, network analysis did not show an advantage over the simpler skeletonized approach. Because skeleton-based markers are more straightforward to implement, even with fully automated processing, we conclude that skeleton-based diffusion markers are currently better suited for clinical research, trials and potentially also routine use.

2.1.6 Acknowledgements

The author(s) disclosed receipt of the following financial support for the research, authorship, and/or publication of this article: Mengfei Cai was supported by the China Scholarship Council (201706100189). Nicolai Franzmeier was supported by the Hertie Foundation for clinical neurosciences.

2.1.7 Conflict of interest

The author(s) declared no potential conflicts of interest with respect to the research, authorship, and/or publication of this article.

2.1.8 References

Andersson, Jesper L. R., Stefan Skare, and John Ashburner. 2003. ‘How to Correct Susceptibility Distortions in Spin-Echo Echo-Planar Images: Application to Diffusion Tensor Imaging’. *NeuroImage* 20 (2): 870–88. https://doi.org/10.1016/S1053-8119(03)00336-7.

Andersson, Jesper L. R., and Stamatios N. Sotiropoulos. 2016. ‘An Integrated Approach to Correction for Off-Resonance Effects and Subject Movement in Diffusion MR

Imaging'. *NeuroImage* 125 (January): 1063–78. https://doi.org/10.1016/j.neuroimage.2015.10.019.

Avants, Brian B., Nicholas J. Tustison, Gang Song, Philip A. Cook, Arno Klein, and James C. Gee. 2011. 'A Reproducible Evaluation of ANTs Similarity Metric Performance in Brain Image Registration'. *NeuroImage* 54 (3): 2033–44. https://doi.org/10.1016/j.neuroimage.2010.09.025.

Barton, K., and MK. Barton. 2019. 'Package "Mu-MIn": Multi-Model Inference Version 1.'

Bates, Douglas, Martin Mächler, Ben Bolker, and Steve Walker. 2014. 'Fitting Linear Mixed-Effects Models Using Lme4'. *ArXiv:1406.5823 [Stat]*, June. http://arxiv.org/abs/1406.5823.

Baykara, Ebru, Benno Gesierich, Ruth Adam, Anil Man Tuladhar, J. Matthijs Biesbroek, Huiberdina L. Koek, Stefan Ropele, et al. 2016. 'A Novel Imaging Marker for Small Vessel Disease Based on Skeletonization of White Matter Tracts and Diffusion Histograms'. *Annals of Neurology* 80 (4): 581–92. https://doi.org/10.1002/ana.24758.

Benjamin, Philip, Eva Zeestraten, Christian Lambert, Irina Chis Ster, Owen A. Williams, Andrew J. Lawrence, Bhavini Patel, Andrew D. MacKinnon, Thomas R. Barrick, and Hugh S. Markus. 2016. 'Progression of MRI Markers in Cerebral Small Vessel Disease: Sample Size Considerations for Clinical Trials'. *Journal of Cerebral Blood Flow and Metabolism: Official Journal of the International Society of Cerebral Blood Flow and Metabolism* 36 (1): 228–40. https://doi.org/10.1038/jcbfm.2015.113.

Boot, Esther M., Esther MC van Leijsen, Mayra I. Bergkamp, Roy P. C. Kessels, David G. Norris, Frank-Erik de Leeuw, and Anil M. Tuladhar. 2020. 'Structural Network Efficiency Predicts Cognitive Decline in Cerebral Small Vessel Disease'. *NeuroImage: Clinical* 27 (January): 102325. https://doi.org/10.1016/j.nicl.2020.102325.

Brito Robalo, Bruno M. de, Naomi Vlegels, Jil Meier, Alexander Leemans, Geert Jan Biessels, Yael D. Reijmer, on Behalf of the Utrecht VCI Study Group, et al. 2020. 'Effect of Fixed-Density Thresholding on Structural Brain Networks: A Demonstration in Cerebral Small Vessel Disease'. *Brain Connectivity* 10 (3): 121–33. https://doi.org/10.1089/brain.2019.0686.

Canty, Angelo J. 2002. 'Resampling Methods in R: The Boot Package'. *The Newsletter of the R Project Volume* 2 (3).

Civier, Oren, Robert Elton Smith, Chun-Hung Yeh, Alan Connelly, and Fernando Calamante. 2019. 'Is Removal of Weak Connections Necessary for Graph-Theoretical Analysis of Dense Weighted Structural Connectomes from Diffusion MRI?' *NeuroImage* 194 (July): 68–81. https://doi.org/10.1016/j.neuroimage.2019.02.039.

Cordero-Grande, Lucilio, Daan Christiaens, Jana Hutter, Anthony N. Price, and Jo V. Hajnal. 2019. 'Complex Diffusion-Weighted Image Estimation via Matrix Recovery under General Noise Models'. *NeuroImage* 200 (October): 391–404. https://doi.org/10.1016/j.neuroimage.2019.06.039.

Finsterwalder, Sofia, Naomi Vlegels, Benno Gesierich, Miguel Á. Araque Caballero, Nick A. Weaver, Nicolai Franzmeier, Marios K. Georgakis, et al. 2020. 'Small Vessel Disease More than Alzheimer's Disease Determines Diffusion MRI Alterations in Memory Clinic Patients'. *Alzheimer's & Dementia* 16 (11): 1504–14. https://doi.org/10.1002/alz.12150.

Gesierich, Benno, Anil Man Tuladhar, Annemieke ter Telgte, Kim Wiegertjes, Marek J. Konieczny, Sofia Finsterwalder, Mathias Hübner, et al. 2020. 'Alterations and Test–Retest Reliability of Functional Connectivity Network Measures in Cerebral Small Vessel Disease'. *Human Brain Mapping* 41 (10): 2629–41. https://doi.org/10.1002/hbm.24967.

Hagmann, Patric, Leila Cammoun, Xavier Gigandet, Reto Meuli, Christopher J. Honey, Van J. Wedeen, and Olaf Sporns. 2008. 'Mapping the Structural Core of Human Cerebral Cortex'. *PLOS Biology* 6 (7): e159. https://doi.org/10.1371/journal.pbio.0060159.

Hagmann, Patric, Maciej Kurant, Xavier Gigandet, Patrick Thiran, Van J. Wedeen, Reto Meuli, and Jean-Philippe Thiran. 2007. 'Mapping Human Whole-Brain Structural Networks with Diffusion MRI'. *PLOS ONE* 2 (7): e597. https://doi.org/10.1371/journal.pone.0000597.

Jeurissen, Ben, Alexander Leemans, Jacques-Donald Tournier, Derek K. Jones, and Jan Sijbers. 2013. 'Investigating the Prevalence of Complex Fiber Configurations in White Matter Tissue with Diffusion Magnetic Resonance Imaging'. *Human Brain Mapping* 34 (11): 2747–66.

Jeurissen, Ben, Jacques-Donald Tournier, Thijs Dhollander, Alan Connelly, and Jan Sijbers. 2014. 'Multi-Tissue Constrained Spherical Deconvolution for Improved Analysis of Multi-Shell Diffusion MRI Data'. *NeuroImage* 103 (December): 411–26. https://doi.org/10.1016/j.neuroimage.2014.07.061.

Kellner, Elias, Bibek Dhital, Valerij G. Kiselev, and Marco Reisert. 2016. 'Gibbs-Ringing Artifact Removal Based on Local Subvoxel-Shifts'. *Magnetic Resonance in Medicine* 76 (5): 1574–81. https://doi.org/10.1002/mrm.26054.

Konieczny, Marek J., Anna Dewenter, Annemieke ter Telgte, Benno Gesierich, Kim Wiegertjes, Sofia Finsterwalder, Anna Kopczak, et al. 2021. 'Multi-Shell Diffusion MRI Models for White Matter Characterization in Cerebral Small Vessel Disease'. *Neurology* 96 (5): e698–708. https://doi.org/10.1212/WNL.0000000000011213.

Kuznetsova, Alexandra, Per B. Brockhoff, and Rune H. B. Christensen. 2017. 'LmerTest Package: Tests in Linear Mixed Effects Models'. *Journal of Statistical Software* 82 (1): 1–26. https://doi.org/10.18637/jss.v082.i13.

Norden, Anouk GW van, Karlijn F. de Laat, Rob AR Gons, Inge WM van Uden, Ewoud J. van Dijk, Lucas JB van Oudheusden, Rianne AJ Esselink, et al. 2011. 'Causes and Consequences of Cerebral Small Vessel Disease. The RUN DMC Study: A Prospective Cohort Study. Study Rationale and Protocol'. *BMC Neurology* 11 (1): 29. https://doi.org/10.1186/1471-2377-11-29.

R Core Team. 2016. 'R: A Language and Environment for Statistical Computing'. *Vienna: R Foundations for Statistical Computing*.

Reijmer, Yael D., Panagiotis Fotiadis, Sergi Martinez-Ramirez, David H. Salat, Aaron Schultz, Ashkan Shoamanesh, Alison M. Ayres, et al. 2015. 'Structural Network Alterations and Neurological Dysfunction in Cerebral Amyloid Angiopathy'. *Brain* 138 (1): 179–88. https://doi.org/10.1093/brain/awu316.

Rubinov, Mikail, and Olaf Sporns. 2010. 'Complex Network Measures of Brain Connectivity: Uses and Interpretations'. *NeuroImage*, Computational Models of the Brain, 52 (3): 1059–69. https://doi.org/10.1016/j.neuroimage.2009.10.003.

Shrout, Patrick E., and Joseph L. Fleiss. 1979. 'Intraclass Correlations: Uses in Assessing Rater Reliability'. *Psychological Bulletin* 86 (2): 420–28. https://doi.org/10.1037/0033-2909.86.2.420.

Smith, Eric E., Geert Jan Biessels, François De Guio, Frank Erik de Leeuw, Simon Duchesne, Marco Düring, Richard Frayne, et al. 2019. 'Harmonizing Brain Magnetic Resonance Imaging Methods for Vascular Contributions to Neurodegeneration'. *Alzheimer's & Dementia: Diagnosis, Assessment & Disease Monitoring* 11 (December): 191–204. https://doi.org/10.1016/j.dadm.2019.01.002.

Smith, Robert E., Jacques-Donald Tournier, Fernando Calamante, and Alan Connelly. 2012. 'Anatomically-Constrained Tractography: Improved Diffusion MRI Streamlines Tractography through Effective Use of Anatomical Information'. *NeuroImage* 62 (3): 1924–38. https://doi.org/10.1016/j.neuroimage.2012.06.005.

Smith, Robert E., Jacques-Donald Tournier, Fernando Calamante, and Alan Connelly. 2015. 'SIFT2: Enabling Dense Quantitative Assessment of Brain White Matter Connectivity Using Streamlines Tractography'. *NeuroImage* 119 (October): 338–51. https://doi.org/10.1016/j.neuroimage.2015.06.092.

Smith, Stephen M., Mark Jenkinson, Heidi Johansen-Berg, Daniel Rueckert, Thomas E. Nichols, Clare E. Mackay, Kate E. Watkins, et al. 2006. 'Tract-Based Spatial Statistics: Voxelwise Analysis of Multi-Subject Diffusion Data'. *NeuroImage* 31 (4): 1487–1505. https://doi.org/10.1016/j.neuroimage.2006.02.024.

Smith, Stephen M., Mark Jenkinson, Mark W. Woolrich, Christian F. Beckmann, Timothy E.J. Behrens, Heidi Johansen-Berg, Peter R. Bannister, et al. 2004. 'Advances in Functional and Structural MR Image Analysis and Implementation as FSL'. *NeuroImage* 23 (January): S208–19. https://doi.org/10.1016/j.neuroimage.2004.07.051.

Tabesh, Ali, Jens H. Jensen, Babak A. Ardekani, and Joseph A. Helpern. 2011. 'Estimation of Tensors and Tensor-Derived Measures in Diffusional Kurtosis Imaging'. *Magnetic Resonance in Medicine* 65 (3): 823–36. https://doi.org/10.1002/mrm.22655.

Telgte, Annemieke ter, Esther M. C. van Leijsen, Kim Wiegertjes, Catharina J. M. Klijn, Anil M. Tuladhar, and Frank-Erik de Leeuw. 2018. 'Cerebral Small Vessel Disease: From a Focal to a Global Perspective'. *Nature Reviews Neurology* 14 (7): 387–98. https://doi.org/10.1038/s41582-018-0014-y.

Telgte, Annemieke ter, Kim Wiegertjes, Benno Gesierich, José P. Marques, Mathias Huebner, Jabke J. de Klerk, Floris H. B. M. Schreuder, et al. 2019. 'The Contribution of Acute Infarcts to Cerebral Small Vessel Disease Progression'. *Annals of Neurology* 86 (4): 582–92. https://doi.org/10.1002/ana.25556.

Telgte, Annemieke ter, Kim Wiegertjes, Anil M Tuladhar, Marlies P Noz, José P Marques, Benno Gesierich, Mathias Huebner, et al. 2018. 'Investigating the Origin and Evolution of Cerebral Small Vessel Disease: The RUN DMC – InTENse Study'. *European Stroke Journal* 3 (4): 369–78. https://doi.org/10.1177/2396987318776088.

Tiedt, Steffen, Marco Duering, Christian Barro, Asli Gizem Kaya, Julia Boeck, Felix J. Bode, Matthias Klein, et al. 2018. 'Serum Neurofilament Light: A Biomarker of Neuroaxonal Injury after Ischemic Stroke'. *Neurology* 91 (14): e1338–47. https://doi.org/10.1212/WNL.0000000000006282.

Tombaugh, Tom N. 2004. 'Trail Making Test A and B: Normative Data Stratified by Age and Education'. *Archives of Clinical Neuropsychology* 19 (2): 203–14. https://doi.org/10.1016/S0887-6177(03)00039-8.

Tournier, J-Donald. 2019. 'Diffusion MRI in the Brain – Theory and Concepts'. *Progress in Nuclear Magnetic Resonance Spectroscopy* 112–113 (June): 1–16. https://doi.org/10.1016/j.pnmrs.2019.03.001.

Tournier, J.-Donald, Fernando Calamante, and Alan Connelly. 2012. 'MRtrix: Diffusion Tractography in Crossing Fiber Regions'. *International Journal of Imaging Systems and Technology* 22 (1): 53–66. https://doi.org/10.1002/ima.22005.

Tournier, J-Donald, Robert Smith, David Raffelt, Rami Tabbara, Thijs Dhollander, Maximilian Pietsch, Daan Christiaens, Ben Jeurissen, Chun-Hung Yeh, and Alan Connelly. 2019. 'MRtrix3: A Fast, Flexible and Open Software Framework for Medical Image Processing and Visualisation'. *NeuroImage* 202 (November): 116137. https://doi.org/10.1016/j.neuroimage.2019.116137.

Tuladhar, Anil M., Andrew Lawrence, David G. Norris, Thomas R. Barrick, Hugh S. Markus, and Frank-Erik de Leeuw. 2017. 'Disruption of Rich Club Organisation in Cerebral Small Vessel Disease'. *Human Brain Mapping* 38 (4): 1751–66. https://doi.org/10.1002/hbm.23479.

Tuladhar, Anil M., Jonathan Tay, Esther van Leijsen, Andrew J. Lawrence, Ingeborg Wilhelmina Maria van Uden, Mayra Bergkamp, Ellen van der Holst, et al. 2020.

'Structural Network Changes in Cerebral Small Vessel Disease'. *Journal of Neurology, Neurosurgery & Psychiatry* 91 (2): 196–203. https://doi.org/10.1136/jnnp-2019-321767.

Veraart, Jelle, Els Fieremans, and Dmitry S. Novikov. 2016. 'Diffusion MRI Noise Mapping Using Random Matrix Theory'. *Magnetic Resonance in Medicine* 76 (5): 1582–93. https://doi.org/10.1002/mrm.26059.

Veraart, Jelle, Dmitry S. Novikov, Daan Christiaens, Benjamin Ades-aron, Jan Sijbers, and Els Fieremans. 2016. 'Denoising of Diffusion MRI Using Random Matrix Theory'. *NeuroImage* 142 (November): 394–406. https://doi.org/10.1016/j.neuroimage.2016.08.016.

Wardlaw, Joanna M, Colin Smith, and Martin Dichgans. 2019. 'Small Vessel Disease: Mechanisms and Clinical Implications'. *The Lancet Neurology* 18 (7): 684–96. https://doi.org/10.1016/S1474-4422(19)30079-1.

Wardlaw, Joanna M, Eric E Smith, Geert J Biessels, Charlotte Cordonnier, Franz Fazekas, Richard Frayne, Richard I Lindley, et al. 2013. 'Neuroimaging Standards for Research into Small Vessel Disease and Its Contribution to Ageing and Neurodegeneration'. *The Lancet Neurology* 12 (8): 822–38. https://doi.org/10.1016/S1474-4422(13)70124-8.

Welton, Thomas, Daniel A. Kent, Dorothee P. Auer, and Robert A. Dineen. 2015. 'Reproducibility of Graph-Theoretic Brain Network Metrics: A Systematic Review'. *Brain Connectivity* 5 (4): 193–202. https://doi.org/10.1089/brain.2014.0313.

Xu, Xiaopei, Kui Kai Lau, Yuen Kwun Wong, Henry K. F. Mak, and Edward S. Hui. 2018. 'The Effect of the Total Small Vessel Disease Burden on the Structural Brain Network'. *Scientific Reports* 8 (1): 7442. https://doi.org/10.1038/s41598-018-25917-4.

Yeo, In-Kwon, and Richard A. Johnson. 2000. 'A New Family of Power Transformations to Improve Normality or Symmetry'. *Biometrika* 87 (4): 954–59. https://doi.org/10.1093/biomet/87.4.954.

2.1.9 Supplementary material

Table e-1: MRI acquisition parameters

Sequence	Feature	RUN DMC – InTENse sub-study	RUN DMC main study
	Scanner	Magnetom Prisma	
	Coil channels	32 (head)	
MP2RAGE	Type	Conventional	Compressed sensing
	TR [ms]	5500	5000
	TE [ms]	3.8	2.98
	TI [ms]	700, 2500[a]	732, 2500[a]
	Flip angle [˚]	7, 4[a]	4, 5[a]
	Voxel size [mm]	0.85 isotropic	
3D-FLAIR	TR [ms]	5000	
	TE [ms]	394	
	TI [ms]	1800	
	Voxel size [mm]	0.85 isotropic	
3D-GRE	TR [ms]	35	44
	TE [ms]	29.5	6.14, 10.1, 14.1, 18.1, 22.1, 26.1, 30.1, 34.1, 38.1
	Flip angle [˚]	15	20
	Voxel size [mm]	0.8 x 0.8 x 2	0.8 isotropic
MS-DWI	TR [ms]	3220	
	TE [ms]	74	
	Flip angle [˚]	90	
	In-plane resolution [mm]	1.7 x 1.7	
	Slice thickness [mm]	1.7	
	Base resolution (matrix)	130	
	Number of slices	87	
	b-values [s/mm^2]	1000, 3000	
	Directions (per b-value)	30, 60	
	b=0 [images]	10	
	Receiver bandwidth [Hz/px]	1924	
	Parallel acceleration	2	
	Multi-band acceleration	3	

[a] Double inversion

Abbreviations: FLAIR = fluid-attenuated inversion recovery; GRE = gradient echo; inTENse = Radboud University Nijmegen Diffusion tensor and Magnetic resonance imaging Cohort – Investigating The origin and EvolutioN of cerebral small vessel disease; MP2RAGE = magnetization prepared 2 rapid acquisition gradient echoes; MS-DWI = multi-shell diffusion-weighted imaging; RUN DMC = Radboud University Nijmegen Diffusion tensor and Magnetic resonance imaging Cohort; TE = echo time; TI = inversion time; TR = repetition time.

Table e-2: Simple linear regression models

		Single-shell								Multi-shell								
		Skeleton			Network					Skeleton			Network					
		FA	MD	Atlas	nSL	mLen	invLen	mFA	wFA	MK	RK	Atlas	nSL	mLen	invLen	mMK	wMK	mFA	wFA
Exploration	adj. R^2	0.066	0.080	AAL	0.109	0.073	0.079	0.077	0.111	0.176	0.151	AAL	0.125	0.059	0.027	0.117	0.025	0.011	0.134
	P	0.037	0.024		0.010	0.030	0.025	0.026	0.009	0.001	0.003		0.006	0.046	0.127	0.007	0.136	0.219	0.004
	adj. R^2	-	-	BN	0.098	0.056	0.095	0.082	0.088	-	-	BN	0.153	0.058	0.019	0.111	0.040	0.020	0.199
	P	-	-		0.014	0.050	0.015	0.023	0.019	-	-		0.002	0.046	0.167	0.009	0.084	0.158	0.001
Validation	adj. R^2	0.128	0.086	AAL	0.145	0.097	0.136	0.100	0.158	0.130	0.143	AAL	0.066	0.145	0.066	0.135	0.121	0.114	0.036
	P	0.000	0.001		0.000	0.001	0.000	0.001	0.000	0.000	0.000		0.005	0.000	0.005	0.000	0.000	0.000	0.030
	adj. R^2	-	-	BN	0.133	0.127	0.126	0.146	0.141	-	-	BN	0.003	0.125	0.084	0.136	0.102	0.124	0.001
	P	-	-		0.000	0.000	0.000	0.000	0.000	-	-		0.259	0.000	0.002	0.000	0.001	0.000	0.296

Abbreviations: adj. = adjusted; AAL = automated anatomical labelling; BN = Brainnetome; FA = fractional anisotropy; invLen = number of streamlines weighted by the inverse length of each streamline; MD = mean diffusivity; mFA = mean of fractional anisotropy of streamlines; MK = mean kurtosis; mLen= mean length of streamlines; mMK = mean of mean kurtosis of streamlines; nSL = number of streamlines; RK = radial kurtosis; wFA= number of streamlines weighted by fractional anisotropy; wMK = number of streamlines weighted by mean kurtosis.

Table e-3: Linear mixed effects models

		Single-shell								Multi-shell								
		Skeleton			Network					Skeleton			Network					
		FA	MD	Atlas	nSL	mLen	invLen	mFA	wFA	MK	RK	Atlas	nSL	mLen	invLen	mMK	wMK	mFA	wFA
Exploration	fix. ef.	0.005	0.004	AAL	0.000	0.000	0.000	0.002	0.001	0.004	0.006	AAL	0.002	0.002	0.001	0.003	0.002	0.004	0.001
	P	0.000	0.000		0.470	0.663	0.751	0.001	0.136	0.000	0.000		0.000	0.000	0.095	0.000	0.000	0.000	0.038
	m. R^2	0.219	0.140		0.002	0.000	0.000	0.031	0.007	0.107	0.248		0.022	0.035	0.009	0.087	0.037	0.108	0.008
	fix. ef.	-	-	BN	0.000	0.001	0.000	0.002	0.001	-	-	BN	0.002	0.003	0.000	0.003	0.002	0.004	0.001
	P	-	-		0.831	0.254	0.713	0.003	0.384	-	-		0.000	0.000	0.570	0.000	0.000	0.000	0.150
	m. R^2	-	-		0.000	0.003	0.000	0.019	0.002	-	-		0.033	0.056	0.001	0.091	0.043	0.149	0.004
Validation	fix. ef.	0.004	0.004	AAL	0.002	0.000	0.001	0.001	0.002	0.003	0.004	AAL	0.002	0.003	0.002	0.002	0.003	0.003	0.002
	P	0.000	0.000		0.003	0.701	0.093	0.095	0.000	0.000	0.000		0.001	0.000	0.000	0.000	0.000	0.000	0.000
	m. R^2	0.129	0.107		0.027	0.000	0.008	0.008	0.046	0.085	0.136		0.031	0.074	0.036	0.047	0.065	0.060	0.033
	fix. ef.	-	-	BN	0.001	0.000	0.000	0.001	0.001	-	-	BN	0.002	0.003	0.002	0.002	0.003	0.003	0.002
	P	-	-		0.086	0.697	0.357	0.240	0.011	-	-		0.001	0.000	0.000	0.000	0.000	0.000	0.000
	m. R^2	-	-		0.007	0.000	0.002	0.003	0.015	-	-		0.031	0.074	0.036	0.047	0.065	0.060	0.033

Abbreviations: adj. = adjusted; AAL = automated anatomical labelling; BN = Brainnetome; FA = fractional anisotropy; fix. ef. = fixed effect; invLen = number of streamlines weighted by the inverse length of each streamline; MD = mean diffusivity; mFA = mean of fractional anisotropy of streamlines; MK = mean kurtosis; mLen= mean length of streamlines; mMK = mean of mean kurtosis of streamlines; m. R^2 = marginal R^2; nSL = number of streamlines; RK = radial kurtosis; wFA= number of streamlines weighted by fractional anisotropy; wMK = number of streamlines weighted by mean kurtosis.

Table e4: Intraclass correlation coefficients

	Single-shell										Multi-shell						
	Skeleton			Network					Skeleton			Network					
	FA	MD	Atlas	nSL	mLen	invLen	mFA	wFA	MK	RK	Atlas	nSL	mLen	invLen	mMK	wMK	mFA	wFA
Exploration	0.981	0.989	**AAL**	0.958	0.883	0.951	0.958	0.963	0.973	0.988	**AAL**	0.923	0.916	0.560	0.974	0.896	0.982	0.921
	-	-	**BN**	0.949	0.944	0.939	0.965	0.953	-	-	**BN**	0.900	0.900	0.675	0.979	0.882	0.985	0.894
Validation	0.967	0.979	**AAL**	0.969	0.921	0.960	0.944	0.973	0.956	0.984	**AAL**	0.923	0.927	0.794	0.958	0.906	0.974	0.899
	-	-	**BN**	0.955	0.946	0.947	0.963	0.960	-	-	**BN**	0.849	0.886	0.767	0.971	0.835	0.977	0.791

Abbreviations: AAL = automated anatomical labelling; BN = Brainnetome; FA = fractional anisotropy; invLen = number of streamlines weighted by the inverse length of each streamline; MD = mean diffusivity; mFA = mean of fractional anisotropy of streamlines; MK = mean kurtosis; mLen= mean length of streamlines; mMK = mean of mean kurtosis of streamlines; nSL = number of streamlines; RK = radial kurtosis; wFA= number of streamlines weighted by fractional anisotropy; wMK = number of streamlines weighted by mean kurtosis.

2.2 Study II: Disentangling the effects of Alzheimer's and cerebral small vessel disease on white matter fiber tracts

The following section includes the original research article "Disentangling the effects of Alzheimer's and cerebral small vessel disease on white matter fiber tracts" which was published in *Brain* (Dewenter et al., 2022).

Disentangling the effects of Alzheimer's and small vessel disease on white matter fiber tracts

Anna Dewenter,[1] MSc, Mina A. Jacob,[2] MD, Mengfei Cai,[2] MD, Benno Gesierich,[1,3] PhD, Paul Hager,[1,4] MSc, Anna Kopczak,[1] MD, Davina Biel,[1] PhD, Michael Ewers,[1,5] PhD, Anil M. Tuladhar,[2] MD, PhD, Frank-Erik de Leeuw,[2] MD, PhD, Martin Dichgans,[1,5,6] MD, Nicolai Franzmeier[1,*], PhD, and Marco Duering[1,3,*], MD, for the SVDs@target Consortium and Alzheimer's Disease Neuroimaging Initiative (ADNI)†

* These authors contributed equally to this work.

† Data used in preparation of this article were obtained from the Alzheimer's Disease Neuroimaging Initiative (ADNI) database (adni.loni.usc.edu). As such, the investigators within the ADNI contributed to the design and implementation of ADNI and/or provided data but did not participate in analysis or writing of this report. A complete listing of ADNI investigators can be found at: http://adni.loni.usc.edu/wp-content/uploads/how_to_apply/ADNI_Acknowledgement_List.pdf

[1] Institute for Stroke and Dementia Research (ISD), University Hospital, LMU Munich, Germany

[2] Department of Neurology, Donders Institute for Brain, Cognition and Behaviour, Radboud University Medical Center, Nijmegen, The Netherlands

[3] Medical Image Analysis Center (MIAC) and Department of Biomedical Engineering, University of Basel, Basel, Switzerland

[4] Institute for AI and Informatics in Medicine, Klinikum rechts der Isar, Technical University of Munich, Munich, Germany

[5] German Center for Neurodegenerative Disease (DZNE), Munich, Germany

[6] Munich Cluster for Systems Neurology (SyNergy), Munich, Germany

2.2.1 Abstract

Alzheimer's disease and cerebral small vessel disease are the two leading causes of cognitive decline and dementia and co-exist in most memory clinic patients. White matter damage as assessed by diffusion MRI is a key feature in both Alzheimer's and cerebral small vessel disease. However, disease-specific biomarkers of white matter alterations are missing. Recent advances in diffusion MRI operating on the fixel level (*fi*ber population within a vo*xel*) promise to advance our understanding of disease-related white matter alterations. Fixel-based analysis allows to derive measures of both white matter microstructure, measured by fiber density, and macrostructure, measured by fiber-bundle cross-section. Here, we evaluated the capacity of these state-of-the-art fixel metrics to disentangle the effects of cerebral small vessel disease and Alzheimer's disease on white matter integrity.

We included three independent samples (total *n*=387) covering genetically defined cerebral small vessel disease and age-matched controls, the full spectrum of biomarker-confirmed Alzheimer's disease including amyloid- and tau-PET negative controls and a validation sample with presumed mixed pathology. In this cross-sectional analysis, we performed group comparisons between patients and controls and assessed associations between fixel metrics within main white matter tracts and imaging hallmarks of cerebral small vessel disease (white matter hyperintensity volume, lacune and cerebral microbleed count) and Alzheimer's disease (amyloid- and tau-PET), age and a measure of neurodegeneration (brain volume).

Our results showed that i) fiber density was reduced in genetically defined cerebral small vessel disease and strongly associated with cerebral small vessel disease imaging hallmarks, ii) fiber-bundle cross-section was mainly associated with brain volume, and iii) both fiber density and fiber-bundle cross-section were reduced in the presence of amyloid, but not further exacerbated by abnormal tau deposition. Fixel metrics were only weakly associated with amyloid- and tau-PET.

Taken together, our results in three independent samples suggest that fiber density captures the effect of cerebral small vessel disease, while fiber-bundle cross-section is largely determined by neurodegeneration. The ability of fixel-based imaging markers to capture distinct effects on white matter integrity can propel future applications in the context of precision medicine.

2.2.2 Introduction

Alzheimer's disease (AD) and cerebral small vessel disease (SVD) are the two most frequent causes of dementia (van der Flier et al. 2018; Dichgans and Leys 2017). AD is a proteinopathy characterized by the cortical accumulation of amyloid-beta (Aβ) plaques and neurofibrillary tau tangles that lead to neurodegeneration, which can be assessed using PET and MRI (Jack et al. 2018). In contrast, SVD is associated with pathologic alterations of small penetrating vessels that manifest on MRI mainly as white matter hyperintensities, lacunes and cerebral microbleeds (J. M. Wardlaw et al. 2013; J. M. Wardlaw, Smith, and Dichgans 2019). While AD and SVD are distinct diseases with different etiologies and pathomechanisms, the majority of patients who seek clinical care in memory clinics present with both AD- and SVD-related brain alterations to varying degrees. Histopathology studies have shown that up to 80% of patients with prodromal AD show cerebrovascular alterations upon autopsy (Kapasi, DeCarli, and Schneider 2017). This suggests substantial overlap between both disease entities in clinical populations, probably due to shared risk factors (Attems and Jellinger 2014b; Beach and Malek-Ahmadi 2021; Kapasi, DeCarli, and Schneider 2017). Hence, there is a great need for biomarkers that capture both AD and SVD and describe the extent and contribution of each disease within the individual patient.

In recent years, diffusion MRI has evolved as the method of choice to quantify white matter alterations in SVD, with most studies relying on diffusion tensor imaging (Raja, Rosenberg, and Caprihan 2019; Baykara et al. 2016). Diffusion alterations in the white matter are also frequently observed across the AD continuum (Pichet Binette et al. 2021b; Nasrabady et al. 2018). Global white matter diffusion metrics seem largely determined by SVD-related white matter damage, masking any white matter damage that might occur due to AD pathology (Finsterwalder et al. 2020). Studies using regions-of-interest or tract-based analysis suggest different spatial patterns of diffusion MRI alterations in AD and SVD, which warrants to study regional effects on white matter fiber tracts (Vemuri et al. 2019; Raghavan et al. 2022). However, specific biomarkers for AD-related and SVD-related white matter damage are still missing.

A potential reason why previous diffusion models failed to disentangle white matter alterations due to different pathologies is their incapacity to account for the complex anatomy of brain white matter (Jones, Knösche, and Turner 2013). Histology studies show that the brain's white matter architecture is highly complex with up to 98% of the white matter consisting of multiple fibers with crossing fiber orientations (Tournier, Calamante, and Connelly 2012; Jeurissen et

al. 2013). State-of-the-art constrained spherical deconvolution algorithms yield promise since they allow to derive diffusion measures specific to underlying fiber populations, i.e. on the *fixel* level (*fi*ber population within a vo*xel*) instead of the voxel level (**Figure 1**, Raffelt et al. 2017). Using this framework, one can simultaneously derive tract-specific measures of fiber density and fiber-bundle cross-section. Fiber density is a fixel-specific feature of white matter *micro*structure, approximately proportional to the total intra-axonal volume (Raffelt et al. 2012). Fiber-bundle cross-section is a fixel-specific *macro*scopic feature, presumably reflecting the accumulated axon loss (Raffelt et al. 2017; Dhollander et al. 2021).

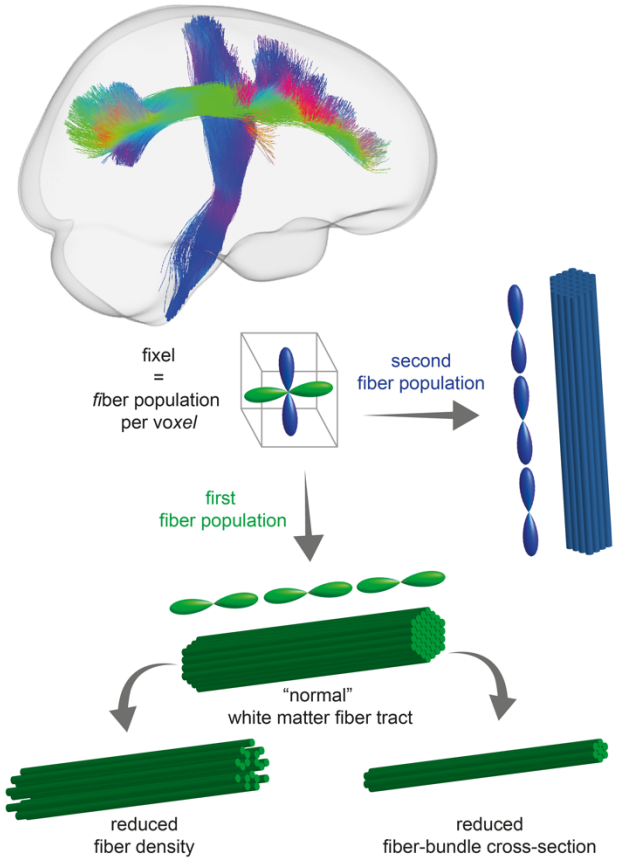

Figure 1: Illustration of fixel-based analysis of two exemplary crossing white matter fiber tracts (superior longitudinal fasciculus II in green, cortico-spinal tract in blue). A fixel corresponds to a specific fiber population per voxel. The depicted voxel harbors two fiber populations (color-coded per tract). A reduction in fiber density (with preserved fiber-bundle cross-section) is depicted on the left, while a reduction in fiber-bundle cross-section (with preserved fiber density) is depicted on the right.

The first fixel-based study in clinical AD and mild cognitive impairment reported reductions in both fiber density and fiber-bundle cross-section of main fiber tracts compared with cognitively healthy controls (Mito et al. 2018a). However, it remains elusive, 1) whether amyloid and tau pathology is associated with fiber density or fiber-bundle cross-section and 2) whether this association is altered in sporadic AD with comorbid SVD. Eventually, the ability of fiber

density and fiber-bundle cross-section to describe and disentangle the effects of SVD and AD pathology on white matter integrity within the same patient has not been explored so far.

To address the need for disease-specific markers, the first aim of this study was to assess the effects of both SVD and biomarker-confirmed AD on both fiber density and fiber-bundle cross-section of major white matter fiber tracts compared with age-matched controls. Our second aim was to explore the relationship between well-established SVD MRI and AD PET imaging hallmarks with tract-specific measures of fiber density and fiber-bundle cross-section. We addressed these aims using three independent samples (total *n*=387) covering genetically defined SVD (cerebral autosomal dominant arteriopathy with subcortical infarcts and leukoencephalopathy [CADASIL]) and age-matched controls, sporadic AD with full amyloid- and tau-PET-based biomarker characterization including controls without amyloid and tau pathology as well as a validation sample with mixed pathology. We combined conventional MRI markers and PET data with state-of-the-art fixel-based analyses of advanced diffusion MRI data. Our main goal was to disentangle white matter damage due to AD and SVD using fixel-based metrics, opening the road for disease-specific white matter characterization towards precision medicine.

2.2.3 Methods

Participants

We included three independent samples with 3 Tesla multi-shell diffusion MRI (**Figure 2**). First, to study the effect of SVD in isolation, we included patients with genetically defined SVD and age-matched controls. Second, the effect of AD was studied across the full spectrum of sporadic AD pathology, ranging from age-matched controls without evidence of amyloid or tau pathology (Aβ–T–), to patients with amyloid pathology only (Aβ+T–), and patients with both amyloid and tau pathology (Aβ+T+). Lastly, we used a third study sample with presumed mixed pathology for independent validation.

Study protocols were in accordance with the declaration of Helsinki and approved by local ethics committees. Written informed consent was obtained from all participants.

Small vessel disease sample

We included in total 95 participants with identical MRI acquisition on the same scanner from a single-center cohort in Munich (*n*=79) ((Baykara et al. 2016) and the ZOOM@SVDs study

(*n*=16) (van den Brink et al. 2021) of which 73 were patients with genetically defined SVD (CADASIL), and 22 were healthy controls matched for age and sex on the group level. CADASIL patients were symptomatic, but in an early disease stage (i.e., functionally independent).

Alzheimer's disease sample

Participants from the Alzheimer's Disease Neuroimaging Initiative 3 (ADNI) database were selected based on availability of multi-shell diffusion MRI and structural MRI, as well as ^{18}F-florbetapir or ^{18}F-florbetaben amyloid-PET and ^{18}F-flortaucipir tau-PET within 6 months of the MRI visit (*n*=106) (Weiner et al. 2017). 17 participants were excluded due to relevant diffusion MRI protocol deviations (*n*=16) or a cropped field of view (*n*=1). Controls were matched for age and sex on the group level.

We used a biological definition of AD following NIA-AA guidelines (Jack et al. 2018) and assigned participants as Aβ+ when surpassing a global pre-established Aβ positivity standardized uptake value ratio (SUVR) threshold of 1.11 for ^{18}F-florbetapir and 1.08 for ^{18}F-florbetaben amyloid-PET (Landau et al. 2012). Tau positivity was assigned when surpassing a pre-established ^{18}F-flortaucipir SUVR threshold of 1.3 in any of the pre-defined Braak stage regions (Braak1, Braak3, Braak3/4, Braak4, Braak5, Braak5/6, Braak6) (Biel et al. 2021; Schöll et al. 2016). Of note, the hippocampus (i.e. Braak2) was excluded from all analyses, due to relevant off-target binding of the ^{18}F-flortaucipir tracer in the medial temporal lobe. Since our main interest was in the neuropathological effects of amyloid and tau pathology on white matter tissue integrity, we used exclusively the biological definition of Alzheimer's disease and did not take clinical status into account. We included 71 participants, of which 34 controls had no biomarker evidence for AD pathology (Aβ–T–) and 37 Aβ+ individuals across the AD spectrum (19 Aβ+T–, 18 Aβ+T+).

Validation sample

We selected participants from the 3rd follow-up visit (approx. 14 years after baseline) of the RUN DMC study (Radboud University Nijmegen Diffusion tensor and Magnetic resonance imaging Cohort) (van Norden et al. 2011), based on the availability of multi-shell diffusion MRI (*n*=228). We excluded 6 participants with infarcts of non-SVD etiology and 1 participant due to an MRI protocol deviation, resulting in a final sample of 221 participants. While the cohort recruited non-demented elderly with SVD, neurodegenerative pathologies were not

excluded and during the long-term follow-up, some participants were in fact diagnosed with AD dementia (**Figure 2**) (Tuladhar et al. 2016). Therefore, we refer to this sample as validation sample with presumed mixed pathology. However, data on amyloid or tau, either PET or fluid biomarkers, were not available for these participants.

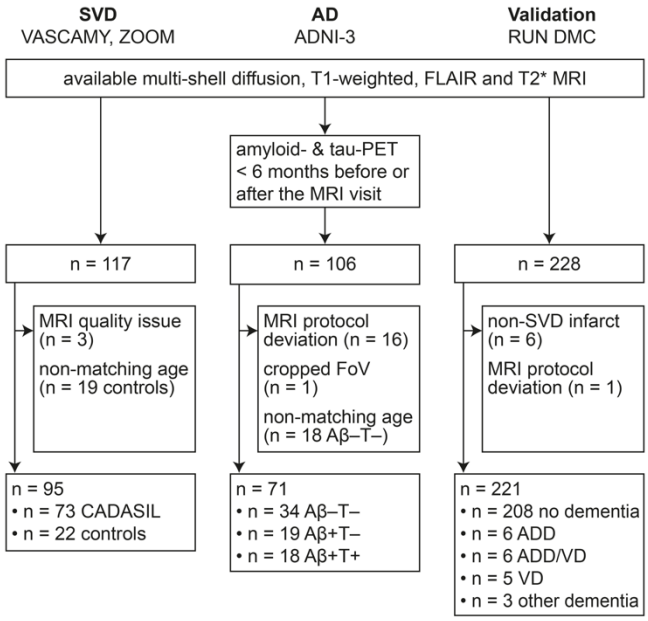

Figure 2: Participant selection flowchart. Samples included genetically defined cerebral small vessel disease (CADASIL) and matched healthy controls (SVD sample), the full spectrum of Alzheimer's disease (AD) and a validation sample with presumed mixed pathology. ADD = Alzheimer's disease dementia, FoV = field of view, VD = vascular dementia.

MRI acquisition and conventional MRI markers

Full sequence parameters are shown in **Supplementary Table e-1**. Sequence parameters varied per study, but included 3D T1-weighted, 3D fluid-attenuated inversion recovery (FLAIR) and 3D gradient echo (T2*-weighted) sequences to assess conventional MRI markers (white matter hyperintensity volume [WMHV], lacune and cerebral microbleed count, brain volume [BrainV]) as well as a multi-shell diffusion MRI sequence. Conventional MRI markers were quantified according to consensus criteria (J. M. Wardlaw et al. 2013). All volumes were normalized to the intracranial volume (e.g. WMHV/intracranial volume).

Small vessel disease sample

MRI scans were performed on a single 3 Tesla scanner (Magnetom Skyra with 64-channel head/neck coil; Siemens Healthineers, Erlangen, Germany). The diffusion MRI protocol comprised a multi-band echo planar imaging multi-shell diffusion-weighted imaging sequence (repetition time 3800 ms, echo time 105 ms, diffusion-encoding directions: 30 x b = 1000 s/mm^2 and 60 x b = 2000 s/mm^2, 10 b = 0 images, multi-band factor 3). One b = 0 image with inverted

phase-encoding direction was acquired for correction of susceptibility-induced distortions during processing (Andersson, Skare, and Ashburner 2003; Smith et al. 2004). Details on the calculation of conventional MRI markers have been described previously (Baykara et al. 2016).

Alzheimer's disease sample

MRI scans were performed on different (in total 13) 3 Tesla scanners (Magnetom Prisma or Magnetom Prisma Fit with 20-, 32- or 64-channel coils; Siemens Healthineers). The diffusion MRI protocol comprised a multi-band echo planar imaging multi-shell diffusion-weighted sequence (repetition time 3400 ms, echo time 71 ms, diffusion-encoding directions 48 x b = 1000 s/mm^2 and 60 x b = 2000 s/mm^2, 13 b = 0 images, multi-band factor 3).

White matter hyperintensities were segmented using a deep-learning algorithm based on multi-dimensional gated recurrent units (https://github.com/zubata88/mdgru, Andermatt, Pezold, and Cattin 2018). An expert rater blinded to biomarker status determined the number of lacunes on FLAIR and T1-weighted images and the number of cerebral microbleeds on T2*-weighted images. Brain and intracranial volumes were estimated from the T1-weighted image with the cross-sectional Sequence Adaptive Multimodal SEGmentation (SAMSEG) Pipeline (FreeSurfer software suite, version 7.1, Puonti, Iglesias, and Van Leemput 2016).

Validation sample

MRI scans were performed on a single 3 Tesla scanner (Magnetom Prisma with 32-channel head coil; Siemens Healthineers). The diffusion MRI protocol comprised a multi-band echo planar imaging multi-shell diffusion-weighted imaging sequence (repetition time 3220 ms, echo time 74 ms, diffusion-encoding directions 30 x b = 1000 s/mm^2 and 60 x b = 3000 s/mm^2, 10 b = 0 images, multi-band factor 3). One b = 0 image with inverted phase-encoding direction was acquired for correction of susceptibility-induced distortions during processing. Details on the calculation of conventional MRI markers have been described previously (ter Telgte, Wiegertjes, et al. 2018; Dewenter et al. 2021).

Diffusion MRI preprocessing

Preprocessing steps included visual quality control, Marchenko-Pastur principal component analysis-based denoising, Gibbs artefact removal, and dynamic correction for susceptibility-induced distortions, eddy current-induced distortions, as well as head motion using tools from MRtrix3 (www.mrtrix.org/, version 3.0.0, dwidenoise, (Veraart et al. 2016; Veraart, Fieremans,

and Novikov 2016; Cordero-Grande et al. 2019; Tournier et al. 2019) mrdegibbs (Tournier et al. 2019; Kellner et al. 2016)) and the Functional Magnetic Resonance Imaging of the Brain Software Library (FSL, version 6.0.1, topup (Andersson, Skare, and Ashburner 2003; Smith et al. 2004), eddy (Andersson and Sotiropoulos 2016) including state-of-the art replacement of outliers (Andersson et al. 2016), usage of the slice-to-volume motion model (Andersson et al. 2017) and susceptibility-by-movement correction (Andersson et al. 2018)). Due to unavailability of an unweighted diffusion image with reversed phase-encoding in the AD sample, we used Synb0-DISCO to synthesize an unweighted diffusion image without susceptibility-induced distortion from the T1-weighted image (Schilling et al. 2020; 2019). Other than this single step, preprocessing was kept identical across the three samples.

Tract-specific fixel-based analysis

We followed the fixel-based analysis pipeline recommended by the developers using multi-tissue constrained spherical deconvolution to compute fiber orientation distributions (FODs) (Dhollander et al. 2021; Jeurissen et al. 2014). Fixel-based analyses were computed independently for each sample. Diffusion data was corrected for bias fields followed by a global DWI intensity normalization between subjects of each sample, yielding diffusion weighted images with identical b=0 white matter median intensity value. Response functions were estimated for each participant using the 'dhollander' algorithm (Dhollander et al. 2019), based on which the mean response functions were computed. Remaining steps included upsampling to 1.25 mm voxel size, estimation of the fiber-orientation distributions using the group response functions ('msmt_csd' algorithm) and intensity normalization. Next, study-specific FOD templates were calculated by randomly selecting representative participants, i.e. 15 controls & 15 CADASIL patients for the SVD sample, 15 Aβ–T– & 7 Aβ+T– & 8 Aβ+T+ for the AD sample and 30 study participants from the validation sample. Subject-specific FOD images were registered to the FOD template, whereafter fixels were segmented and corresponding metrics of apparent fiber density, fiber-bundle cross-section and a combined measure of fiber density and cross-section were derived. Since our main interest was to find disease-specific metrics for white matter damage, we focused on the primary metrics fiber density and fiber-bundle cross-section (but conducted supplementary analyses on the combined metric fiber density and bundle cross-section).

Next, we used TractSeg, a deep learning-based framework for automated white matter bundle segmentation, to segment the FOD template into 72 anatomically well-established white matter fiber tracts (Wasserthal, Neher, and Maier-Hein 2018). To reduce the number of comparisons,

we averaged tract measures for left and right hemispheres. Also, to further reduce the number of regions-of-interest, we excluded the tracts located in the cerebellum – since it is up to date unclear how SVD and AD manifest in this brain area – as well as the fornix due to unavoidable CSF partial-volume effects. In addition, we excluded striatal projections from our analyses, due to a high anatomical overlap with thalamic projections. This resulted in 29 white matter fiber tracts (**Figure 3**, from top left): arcuate fasciculus (AF), uncinate fasciculus (UF), inferior fronto-occipital fasciculus (IFOF), middle longitudinal fasciculus (MLF), inferior longitudinal fasciculus (ILF), superior longitudinal fasciculus I to III (SLF-I, SLF-II, SLF-III), thalamo-prefrontal (T-PREF), thalamo-premotor (T-PREM), thalamo-precentral (T-PREC), thalamo-postcentral (T-POSTC), thalamo-parietal (T-PAR), thalamo-occipital (T-OCC), anterior thalamic radiation (ATR), superior thalamic radiation (STR), optic radiation (OR), fronto-pontine tract (FPT), cortico-spinal tract (CST), parieto-occipital pontine (POPT), corpus callosum I to VII (CC-I to CC-VII), anterior commissure (AC), cingulum (CG). We then assessed per study participant the fixel metrics per fiber tract by averaging the fiber density, fiber-bundle cross-section and fiber density cross-section of all fixels belonging to the respective fiber tract.

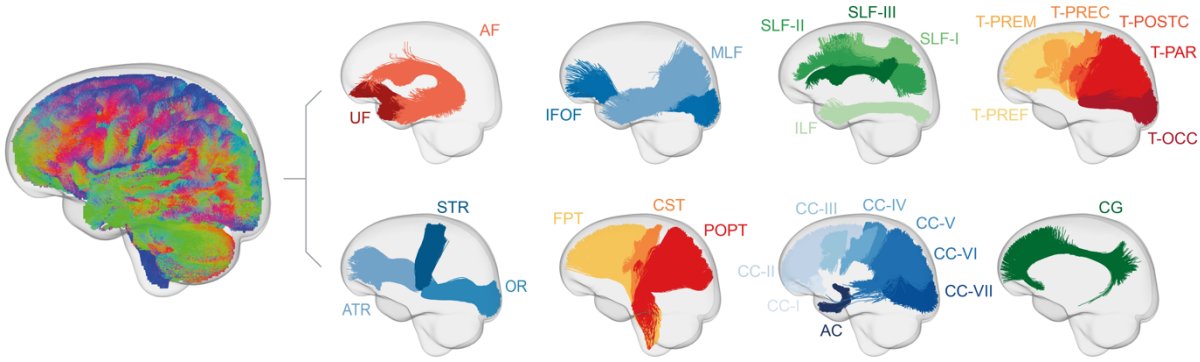

Figure 3: Sagittal view of investigated white matter fiber tracts. Tracts generated in fiber orientation distribution template space are shown for illustration. We analyzed 29 white matter fiber tracts (only left hemisphere shown): AF = arcuate fasciculus, UF = uncinate fasciculus, IFOF = inferior fronto-occipital fasciculus, MLF = middle longitudinal fasciculus, ILF = inferior longitudinal fasciculus, SLF-I to SLF-III = superior longitudinal fasciculus I to III, T-PREF = thalamo-prefrontal, T-PREM = thalamo-premotor, T-PREC = thalamo-precentral, T-POSTC = thalamo-postcentral, T-PAR = thalamo-parietal, T-OCC = thalamo-occipital, ATR = anterior thalamic radiation, STR = superior thalamic radiation, OR = optic radiation, FPT = fronto-pontine tract, CST = cortico-spinal tract, POPT = parieto-occipital pontine, CC-I to CC-VII = corpus callosum I to VII (CC-I: Rostrum, CC-II: Genu, CC-III: Rostral body [premotor], CC-IV: Anterior midbody [primary motor], CC-V: Posterior midbody [primary somatosensory], CC-VI = Isthmus, CC-VII: Splenium), AC = anterior commissure, CG = cingulum.

To assess regional associations between regional tau pathology and tract-specific fixel metrics in the AD sample, we determined regional tau-PET SUVRs in cortical projections of fiber tracts. To this end, we used masks from the beginning and ending of the fiber tracts, as obtained with TractSeg, intersected with a cortical gray matter mask. The regions of interest in FOD

template space were brought to tau-PET images in MNI space by non-linear registration with Advanced Normalization Tools (ANTs) (Avants et al. 2011) to determine regional tau-PET SUVRs.

PET acquisition and processing

Amyloid-PET was recorded in 4x5min frames 50-70min after ^{18}F-florbetapir injection or 90-110min after ^{18}F-florbetaben injection (Landau et al. 2012). Tau-PET was acquired 75-105min after injection of ^{18}F-flortaucipir in 6x5min frames. All time frames were motion corrected and averaged to obtain mean images (for details see http://adni.loni.usc.edu/methods/pet-analysis-method/pet-analysis/). Structural T1-weighted MRI images were processed using the ANTs cortical thickness pipeline and parcellated with the Desikan-Killiany Atlas (Desikan et al. 2006) and non-linearly registered to MNI-space (Tustison et al. 2014). Amyloid-PET and tau-PET images were co-registered via native-space T1-weighted images to MNI standard space using ANTs-derived normalization parameters. Global amyloid-PET SUVRs were intensity normalized to the whole cerebellum and transformed to centiloid (Klunk et al. 2015). Partial volume corrected global tau-PET SUVRs were obtained from the ADNI database, which were calculated using the inferior cerebellum as reference region and averaged across neocortical Desikan-Killiany atlas ROIs (see here for details: https://ida.loni.usc.edu/login.jsp). Partial volume correction was performed by ADNI PET Core at UC Berkeley, using the geometric transfer method. For regional tau-PET SUVRs, we employed a congruent approach, applying geometric transfer method-based partial volume correction for cortical projections of white matter fiber tracts (PETPVC toolbox: https://github.com/UCL/PETPVC (Thomas et al. 2016)). Specifically, we used the geometric transfer matrix approach to correct the ROI-based tau-PET data for grey matter density using the segmented T1-weighted image that was obtained in closest proximity to the tau-PET scan.

Statistical Analyses

All statistical analyses were performed in R (version 3.6.1) (R Core Team 2016). The statistical significance level was set at $\alpha < 0.05$.

To compare between controls and patients with respect to demographic characteristics, vascular risk factors, conventional MRI and PET markers, we used chi-squared (χ^2) tests (for categorical variables) and non-parametric Wilcoxon rank sum tests and Kruskal-Wallis tests (for continuous variables), as appropriate.

Next, we were interested in group differences in tract-specific fixel metrics between SVD and matched controls, and between groups with different biomarker status for AD (Aβ+T– vs. Aβ–T–; Aβ+T+ vs. Aβ–T– and Aβ+T+ vs. Aβ+T–). Since fixel metrics have been shown to be significantly influenced by head size (Smith, Dhollander, and Connelly 2019), we first regressed out the effect of intracranial volume and conducted subsequent analysis on residuals, i.e., fixel metrics corrected for head size ('stats' package). We then calculated the effect size for group comparisons in all predefined fiber tracts using Cohen's d ('psych' package).

Next, we performed simple linear regression analyses to explore associations between SVD and AD typical imaging hallmarks (independent variable) and fiber density and fiber-bundle cross-section of the respective fiber tract (dependent variable, 'stats' package). For SVD hallmarks, we included white matter hyperintensity volume, lacune and cerebral microbleed count. For AD hallmarks, we included global amyloid-PET (centiloid), global tau-PET, regional tau-PET (i.e. tau-PET SUVR in cortical projections of the respective fiber tract). We also included normalized global brain volume indicative of neurodegeneration as an independent variable, which is associated with both AD (Jack et al. 2018) and SVD (Smith et al. 2019). Additionally, we assessed associations with age to ensure that potential associations were not driven by aging alone. In these regression analyses, we used the full extent of the SVD and AD sample by also including the controls (but report sub-sequent sensitivity analyses in the CADASIL only and the Aβ+ only group in the Supplement). Effect sizes were determined by the adjusted R^2. *P*-values were adjusted with the false discovery rate (FDR) per sample and fixel metric resulting in a maximum of 5% of false positives.

To assess the relative variable importance of disease markers in explaining fixel metrics, we performed multivariable random forest regression analyses with conditional inference trees in the AD sample (R package 'party'). This machine-learning method overcomes the problem of multicollinearity within the disease markers. We focused on four variables of interest: WMHV as a marker for SVD, amyloid- and global tau-PET as a marker for AD and brain volume as a marker for neurodegeneration. We repeated random forest regression 100 times to determine the point estimate and a 95% confidence interval.

All analyses were conducted independently in each of the three samples.

Data availability

Anonymized data of the SVD and validation samples will be made available upon reasonable request to the corresponding author and only after permission of the regulatory bodies. ADNI data is freely available and can be retrieved from adni.loni.usc.edu upon registration to the ADNI database.

2.2.4 Results

Sample characteristics and demographics are shown in **Table 1**. As expected, SVD patients had higher WMH volumes, more lacunes and microbleeds compared to controls ($p < 0.001$). SVD patients further had higher rates of hypercholesterolemia than age-matched controls ($p < 0.05$). WMH volume increased with progressing amyloid and tau pathology in the AD sample ($p < 0.001$).

Table 1: Sample characteristics

	SVD			AD				Validation
	Control (*n*=22)	CADASIL (*n*=73)	*p-value*	Aβ–T– (*n*=34)	Aβ+T– (*n*=19)	Aβ+T+ (*n*=18)	*p-value*	(*n*=221)
Demographic characteristics								
Age [years], median (IQR)	60 (21.5)	55 (14)	0.2084	72.50 (9.5)	78.70 (7.8)	75.05 (6.85)	0.1359	73.64 (9.67)
Female, *n* (%)	9 (41)	44 (60)	0.1744	19 (56)	10 (53)	8 (44)	0.7335	98 (44)
Vascular risk factors, *n* (%)								
Hypertension	5 (23)	17 (23)	1.0	10 (29)	9 (47)	10 (56)	0.1506	146 (66)
Hypercholesterolemia	5 (23)	37 (51)	0.0471	9 (26)	3 (16)	8 (44)	0.1463	116 (52)
Diabetes	0 (0)	1 (0.01)	1.0	3 (9)	2 (11)	4 (22)	0.3647	33 (15)
Current or past smoking	9 (41)	44 (60)	0.2425	2 (6)	3 (16)	2 (11)	0.4994	143 (65)
PET markers, median (IQR)								
Amyloid-PET centiloid	-	-	-	-7.25 (11.91)	51.53 (38.26)	87.53 (46.41)	< 0.0001	-
Global Tau-PET SUVR	-	-	-	1.03 (0.12)	1.08 (0.10)	1.18 (0.30)	< 0.0001	-
MRI markers, median (IQR)								
WMH volume[a] [%]	0.03 (0.08)	4.58 (5.23)	< 0.0001	0.24 (0.33)	0.53 (0.73)	0.69 (0.74)	0.0043	0.30 (0.69)
Lacune count	0 (0)	2 (7)	< 0.0001	0 (0)	0 (0)	0 (0)	0.8763	0 (0)
Microbleed count	0 (0)	2 (7)	< 0.0001	0 (0)	0 (0)	0 (0)	0.0160	0 (1)
Brain volume[a] [%]	75.72 (7.64)	76.22 (8.46)	0.2024	70.79 (1.27)	70.00 (2.55)	70.31 (3.26)	0.4158	74.34 (5.65)

Abbreviations: IQR = interquartile range; n = number; WMH = white matter hyperintensity.

[a] Normalized to the intracranial volume

Fixel metric group comparisons

Genetically defined SVD predominantly leads to reduced fiber density

The fiber density of all white matter fiber tracts was reduced in SVD compared to controls (range of Cohen's d[0.33;0.57], **Figure 4A&B**, **Supplementary Table e-2**). Results for the fiber-bundle cross-section were less consistent. While the fiber-bundle cross-section of most fiber tracts was reduced in SVD compared to controls (Cohen's d[0.19;0.35], 11 tracts showed no group difference and the fiber-bundle cross-section of the anterior thalamic radiation and the first segment of the corpus callosum (rostrum) was even higher in SVD compared to controls (Cohen's d=–0.33, both tracts).

Both fiber density and fiber-bundle cross-section are reduced across the AD spectrum

In the AD sample, the Aβ+T– group showed consistently lower fiber density in most fiber tracts compared to the Aβ–T– control group (Cohen's d[0.27;0.49], **Figure 4C&D**, **Supplementary Table e-3**). The fiber-bundle cross-section was also reduced in the Aβ+T– group (Cohen's d[0.27;0.51]). Similarly, the Aβ+T+ group showed lower fiber density (Cohen's d[0.30;0.43]) and lower fiber-bundle cross-section (Cohen's d[0.27;0.40]) compared to the Aβ–T– control group.

To determine the extent to which these effects were driven by differences in SVD burden between groups, we included WMH volume as covariate in a sensitivity analysis. This reduced effect sizes on average by 42% for fiber density and 8% for fiber-bundle cross-section (Aβ+T– vs. Aβ–T–), and by 21% for fiber density and 7% for fiber-bundle-cross section (Aβ+T+ vs. Aβ–T–, **Supplementary Table e-3**).

The Aβ+T+ group did not show any additional white matter damage regarding fiber density or fiber-bundle cross-section compared to Aβ+T–. In summary, both fiber density and fiber-bundle cross-section were reduced in the presence of amyloid pathology, but not further altered by additional tau pathology.

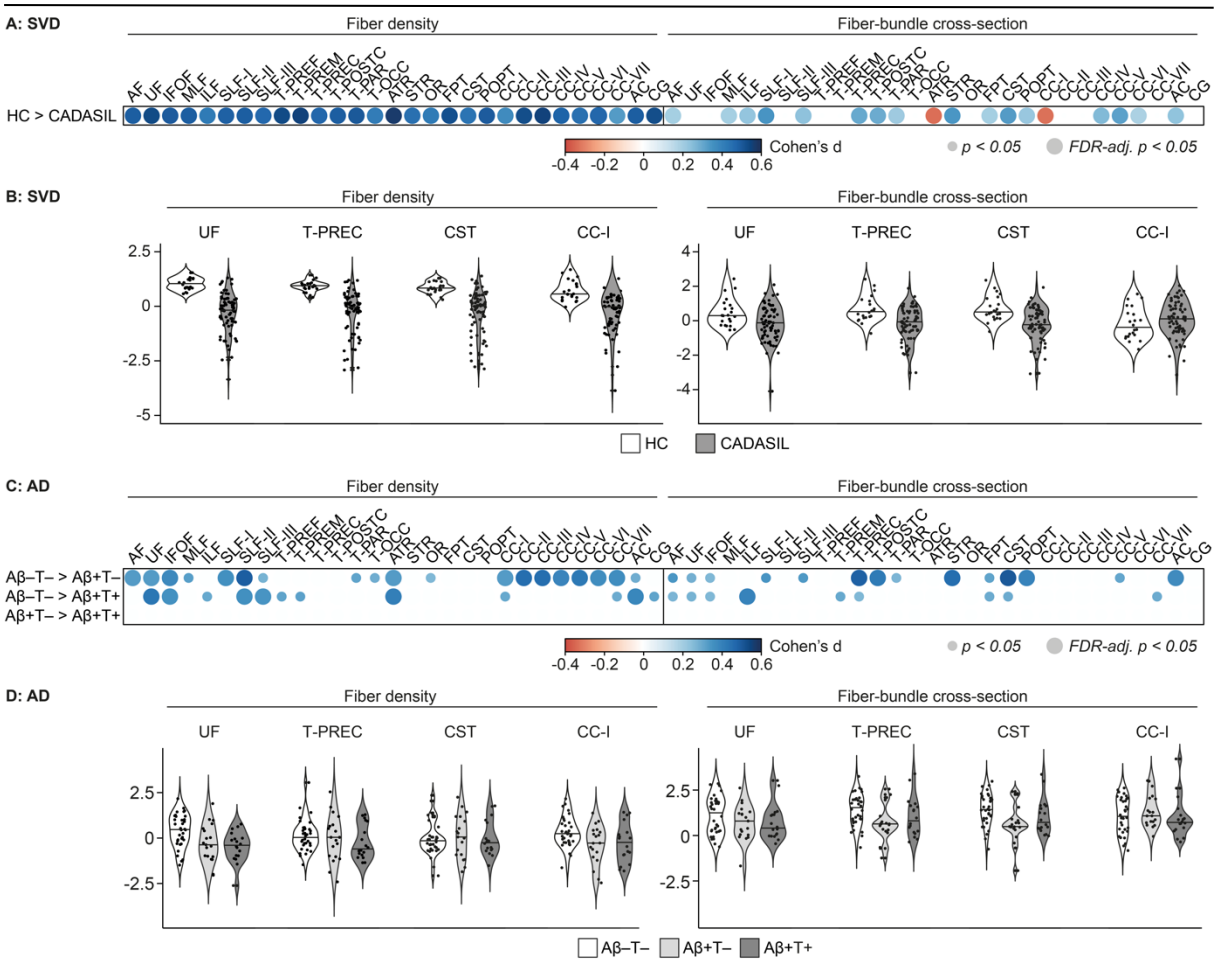

Figure 4: Group comparisons of fixel metrics. (**A**) Difference in fixel metrics between age-matched healthy controls (HC) and CADASIL patients in the SVD sample quantified with Cohen's d represented by color. Circle size depicts statistical significance level. (**B**) Violin plots of fixel metrics of four representative fiber tracts in the SVD sample for exemplary illustration. (**C**) Difference in fixel metrics between age-matched Aβ–T– and Aβ+T– ; Aβ–T– and Aβ+T+; Aβ+T– and Aβ+T+ quantified with Cohen's d represented by color. Circle size depicts statistical significance level. (**D**) Violin plots of fixel metrics of the same four tracts in the AD sample. Please refer to **Figure 3** for abbreviations of the fiber tracts.

Associations with disease markers

Reduced fiber density is mainly associated with higher SVD burden

In simple linear regression in the SVD sample, fiber density of all fiber tracts was strongly associated with WMH volume (range of R^2_{adj}[0.29;0.79]), lacunes ($R^2_{adj.}$[0.12;0.48]), and microbleeds (R^2_{adj}[0.16;0.43], **Figure 5A**, **Supplementary Table e-4**). In contrast, effect sizes were small for associations with age (R^2_{adj}[0.03;0.13]) and brain volume (R^2_{adj}[0.05;0.16]) .

Fiber-bundle cross-section was also associated with WMH volume, but with smaller effect sizes (R^2_{adj}[0.06;0.43]), as well as with lacune count (R^2_{adj}[0.06;0.52]), microbleed count

($R^2_{adj.}$[0.07;0.38]) and brain volume ($R^2_{adj.}$[0.05;0.29]). Effect sizes were small for associations with age (age: $R^2_{adj.}$[0.04;0.13]).

Findings could be replicated when assessing associations in CADASIL patients only (**Supplementary Figure e-1A**).

Reduced fiber-bundle cross-section is mainly associated with cerebral atrophy in the AD sample

In simple linear regression analyses, fiber density in the AD sample was likewise associated with WMH volume ($R^2_{adj.}$[0.04;0.20], **Figure 5B**, **Supplementary Table e-5**) and to some extent with microbleed count ($R^2_{adj.}$[0.05;0.08]) but not with lacune count, which was expected given the low number of lacunes and microbleeds in this sample (**Table 1**). Fiber density was not associated with brain volume and with age only in selected fiber tracts ($R^2_{adj.}$[0.05;0.17]). Effect sizes for associations with AD PET markers were substantially smaller than with SVD MRI markers (amyloid-PET: $R^2_{adj.}$[0.04;0.11]) and tau-PET ($R^2_{adj.}$[0.04]).

Compared to fiber density, fiber-bundle cross-section was less associated with SVD imaging markers (WMHV: $R^2_{adj.}$[0.04;0.06]; no significant associations with lacunes or microbleeds). In contrast, fiber-bundle cross-section of all fiber tracts was strongly associated with brain volume ($R^2_{adj.}$[0.06;0.35]) and to some extent with age ($R^2_{adj.}$[0.04;0.20]). Associations with AD PET markers were mostly absent or showed only small effect sizes (amyloid-PET: $R^2_{adj.}$[0.04;0.05]; tau-PET: $R^2_{adj.}$[0.05;0.06]).

All findings could be replicated when assessing associations in Aβ+ study participants only, except for associations with AD PET markers, which were even weaker (**Supplementary Figure e-1B**).

In multivariable random forest regression analyses (**Figure 6**), WMH volume showed the highest variable importance for fiber density in most fiber tracts, while brain volume showed the highest variable importance for fiber bundle cross-section in all tracts.

Fiber density is associated with SVD markers and fiber-bundle cross-section with brain volume in presumed mixed pathology

Also in the validation sample, fiber density of all tracts was highly associated with WMH volume ($R^2_{adj.}$[0.08;0.48], **Figure 5C**, **Supplementary Table e-6**). Fiber density of all tracts

was also (with smaller effect sizes) associated with lacune count ($R^2_{adj.}$[0.03;0.26]), microbleed count ($R^2_{adj.}$[0.04;0.15]), brain volume ($R^2_{adj.}$[0.01;0.19]) and age ($R^2_{adj.}$[0.03;0.23]).

Effect sizes were small for associations between fiber-bundle cross-section was only weakly associated with WMH volume ($R^2_{adj.}$[0.02;0.09]; lacune count ($R^2_{adj.}$[0.02;0.13]) and microbleed count ($R^2_{adj.}$[0.02;0.09]). Effect sizes were largest for brain volume ($R^2_{adj.}$[0.06;0.42]).

Results of group comparisons and associations with disease markers of the combined metric fiber density and bundle cross-section can be found in the Supplement as well as scatterplots of the most important findings (**Supplementary Figure e-2 to e-5).**

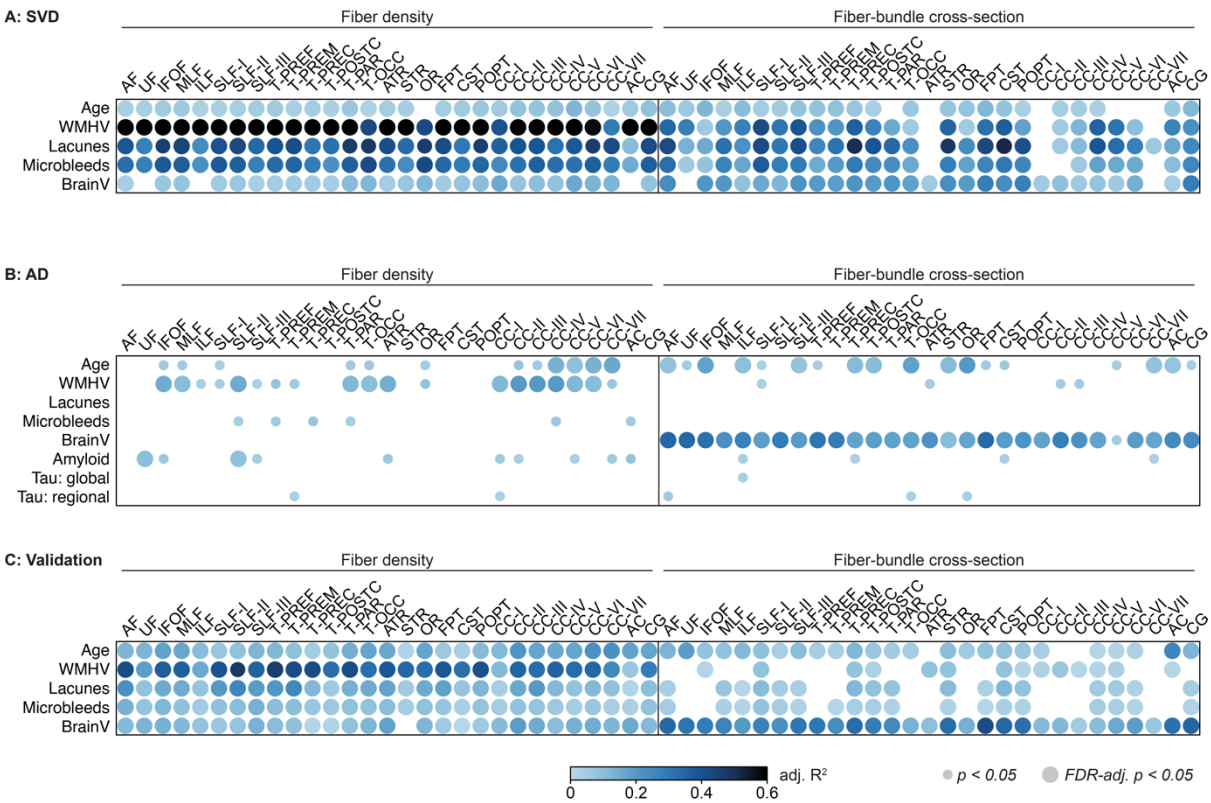

Figure 5: Associations with disease markers. Effect sizes (adj. R^2) obtained from simple linear regression analyses are represented by color. Circle size depicts statistical significance level. Associations between fixel metrics of white matter fiber tracts and disease markers were assessed in (**A**) the SVD sample, (**B**) the AD sample – including in addition amyloid-PET and tau-PET markers – and (**C**) the validation sample. Please refer to **Figure 3** for abbreviations of the fiber tracts. WMHV = white matter hyperintensity volume, BrainV = brain volume.

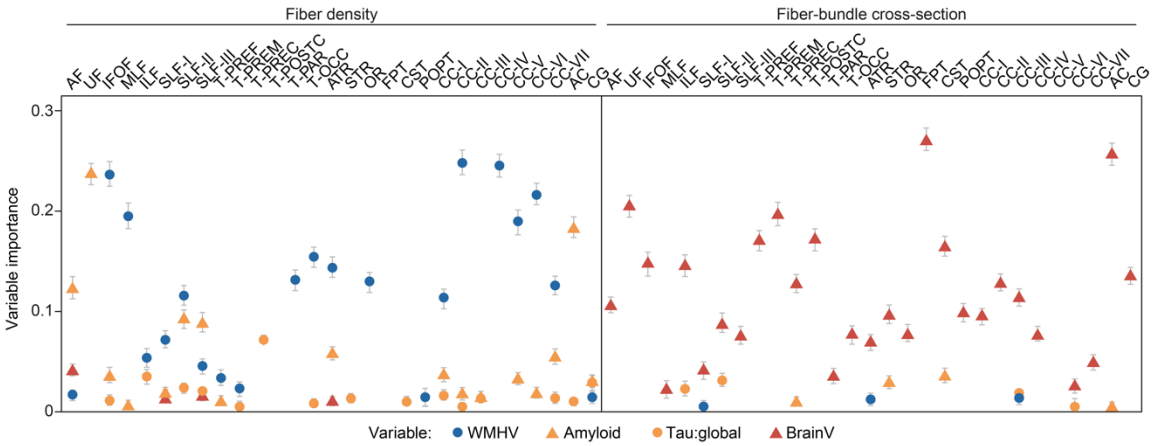

Figure 6: Multivariable random forest regression analyses for estimating the relative variable importance for the SVD marker white matter hyperintensity volume (WMHV, blue), markers of primary Alzheimer's disease pathology (orange) and brain volume (BrainV, red) with regard to tract-specific fixel metrics in the AD sample. Plots indicate point estimate and 95% confidence interval for the conditional variable importance. Please refer to **Figure 3** for abbreviations of the fiber tracts.

2.2.5 Discussion

Our multi-modal neuroimaging study systematically assessed the utility of fixel-based, tract-specific diffusion metrics to disentangle the effects of AD and SVD on white matter. Our main findings are that i) fiber density was markedly reduced in genetically defined SVD and showed the strongest association with SVD imaging hallmarks. ii) Fiber-bundle cross-section was mainly associated with brain volume, especially in the AD sample. iii) Both fiber density and fiber-bundle cross-section were reduced in the presence of amyloid, but this was not further exacerbated by abnormal tau deposition. Taken together, our results suggest that the white matter microstructure metric fiber density is primarily determined by SVD, while the macrostructure metric fiber-bundle cross-section is strongly associated with neurodegeneration. Importantly, the capability of fixel metrics to capture distinct effects of SVD and neurodegeneration was validated in an independent sample.

The marked reduction of the microscopic feature fiber density with increasing SVD burden might result from increased extracellular water moving axons further apart (Dhollander et al. 2021). In line with this, we previously demonstrated that diffusion tensor imaging alterations in SVD are mainly determined by increases in extracellular free water (Duering et al. 2018). In addition, a reduction in apparent fiber density (although not assessed using fixel-based analysis) has been suggested to accompany an increase in extracellular water within white matter hyperintensities of CADASIL patients (Yu et al. 2021). Vascular edema, e.g. resulting from blood-brain-barrier leakage in SVD, might be a main driver of this fluid shift (J. M. Wardlaw, Smith, and Dichgans 2019; De Guio et al. 2015). Interestingly, while the fiber density decreased, we observed in the genetically defined SVD sample a simultaneous increase in the

fiber-bundle cross-section of two tracts, the anterior thalamic radiation and the first segment of the corpus callosum (rostrum, harboring parts of the forceps minor). Strikingly, the anterior thalamic radiation and forceps minor were previously identified as strategic locations for processing speed performance in SVD (Duering et al. 2014; 2011), the core cognitive deficit of the disease. One might speculate that the expansion of the extracellular space following vascular edema led to a swelling of these fiber tracts which is captured by an increase in fiber-bundle cross-section (Dhollander et al. 2021; De Guio et al. 2015).

The macroscopic feature fiber-bundle cross-section was most prominently reduced with increasing amyloid pathology in group comparisons and strongly associated with cerebral atrophy as a proxy of neurodegeneration in the AD and validation sample. Together with the finding that brain volume was not or only weakly associated with fiber density, this suggests that in fixel-based analysis, neurodegeneration predominantly manifests in alterations of white matter macrostructure, but not microstructure. Thus, fiber-bundle cross-section indeed seems to be reflective of the accumulated axon loss as previously postulated (Raffelt et al. 2017).
While associations in the SVD sample were strongest for fiber density, and in the AD sample for fiber-bundle cross-section, both associations were found in the validation sample with mixed pathologies, supporting the concept that both SVD and AD contribute to white matter damage in mixed disease.

In the AD sample, both fiber density and fiber-bundle cross-section were reduced upon amyloid pathology in group comparisons, which might seem counterintuitive at first. As expected from epidemiological and histopathology studies (Kapasi, DeCarli, and Schneider 2017; Attems and Jellinger 2014b), concomitant SVD was found in the AD sample, with the largest difference in WMH burden between the A+T– group and matched A–T– controls. Controlling for this group difference in WMH volume attenuated the observed effects of amyloid, especially on fiber density. Thus, the effect of amyloid on fiber density can at least partly be explained by concomitant SVD, which is plausible given the likely presence of cerebral amyloid angiopathy, which is also captured by amyloid-PET (Charidimou, Farid, and Baron 2017; Gurol et al. 2016).

Brain atrophy clearly showed the strongest associations with fixel metrics, i.e. fiber-bund cross-section, in the AD sample. But in contrast to a previously postulated hypothesis,[44] we did not find that cortical tau pathology is a main driver of alterations in fixel metrics.

While many studies investigated white matter alterations in SVD or AD using models operating on the voxel level (Raja, Rosenberg, and Caprihan 2019), such as diffusion tensor imaging and more advanced diffusion models (Konieczny et al. 2021), only very few studies have so far utilized fixel-based analysis. Importantly, none of the prior fixel-based studies considered mixed disease, but studied either SVD or AD in isolation, thus ignoring the crucial aspect of concomitant pathologies. Despite technical limitations (Dhollander et al. 2021; Genc et al. 2020), it was recently shown that fiber density obtained from fixel-based analysis is highly sensitive towards processing speeds deficits in sporadic SVD (Petersen et al. 2022), confirming previous findings from voxel-based analysis. The aforementioned fixel-based analysis study in AD reported a reduction in both fiber density and fiber-bundle cross-section in MCI and AD patients (Mito et al. 2018a). However, besides not considering concomitant SVD, a full AD biomarker characterization was not possible due to prematurity of tau-PET tracers upon data collection of that study (Mito et al. 2018b). By considering both pathologies and by including data from both amyloid- and tau-PET, we were able to substantially extend previous results, close crucial knowledge gaps and to derive insights highly relevant for both future research studies and potentially also clinical applications.

Our study has some potential limitations. First, in the mixed pathology sample AD biomarkers were not available, precluding an independent validation of results for the direct effects of amyloid and tau pathology. Second, while all samples had diffusion MRI data suitable for fixel-based analysis, the acquisition was not harmonized across the three samples. However, this can also be regarded as a strength in terms of generalizability and independent validation of findings, because despite differences in the MRI acquisition, we found consistent results across all three samples. MRI data in the AD sample was acquired across 13 different scanners. Scanner effects were mitigated by selecting only acquisitions with identical parameters and an intensity normalization step. Eventually, excellent inter-site reproducibility of fixel metrics (**Supplementary Analysis**) enabled pooling of data from different scanners. Lastly, amyloid-PET data was not partial volume corrected due to centiloid transformation (La Joie et al. 2020), hence our results warrant further replication using a large single tracer dataset.

A main strength of this study is the extensive biomarker characterization, including multiple markers for SVD as well as amyloid- and tau-PET data in the AD sample. This enabled a multi-modal approach, which was deemed essential in further validation of fixel-based metrics by the developers of the method (Dhollander et al. 2021). Unlike in the AD field, truly SVD-specific biomarkers are still lacking. To overcome this limitation, we included the sample of genetically

defined SVD patients. Since these patients were relatively young, concomitant AD and other age-related neurodegenerative pathology can be regarded as rare, thus enabling the unique opportunity to study pure SVD without the need for biomarker characterization. While data from autosomal dominant AD would have perfectly complemented our analysis in this regard, we are not aware of any familial AD studies with diffusion MRI data suitable for fixel-based analysis.

The ability of the fixel-based analysis to identify distinct effects of SVD and neurodegeneration on white matter opens a path towards personalized medicine. Future work should address the ability of fixel-derived diffusion markers to explain the extent to which SVD and neurodegeneration contribute to cognitive impairment in mixed disease. This would enable disease-specific interventions targeting AD- or SVD-related brain alterations rather than managing disease-shared risk factors. Our results illustrate once more that it is mandatory to consider SVD when assessing white matter integrity in the context of dementia studies and trials. Furthermore, longitudinal studies are required to capture temporal dynamics of fiber density and fiber-bundle cross-section. Given recent indications for SVD lesion regression (van Leijsen, de Leeuw, and Tuladhar 2017), it remains to be assessed whether the reduction in fiber density observed in SVD is irreversible and how it changes upon disease intervention, e.g., intensified risk factor treatment. Technical validation studies, assessing test-retest reliability and inter-site reproducibility of these novel markers in patients, will be essential for developing a surrogate endpoint for clinical trials.

In conclusion, our results show that fiber density and fiber-bundle cross-section, obtained from fixel-based analysis of diffusion MRI data, allow to identify distinct effects of SVD and neurodegeneration on white matter integrity. While white matter microstructure is predominantly determined by SVD, neurodegeneration leads to alterations in white matter macrostructure. Leveraging these distinct effects, fixel-based white matter analysis can propel future research, clinical trials targeting disease-specific mechanisms and clinical applications in the context of precision medicine.

2.2.6 Acknowledgements

Data used in preparation of this article were obtained from the Munich cohort of the ZOOM@SVDs study, which is part of the SVDs@target project. As such, the investigators within the ZOOM@SVDs study contributed to the design but did not participate in analysis or writing of this report.

This project has received funding from the European Union's Horizon 2020 research and innovation programme No 666881, SVDs@target (to M Dichgans), the DFG as part of the Munich Cluster for Systems Neurology (EXC 2145 SyNergy – ID 390857198), and the Vascular Dementia Research Foundation.

Data collection and sharing for this project was funded by the Alzheimer's Disease Neuroimaging Initiative (ADNI) (National Institutes of Health Grant U01 AG024904) and DOD ADNI (Department of Defense award number W81XWH-12-2-0012). ADNI is funded by the National Institute on Aging, the National Institute of Biomedical Imaging and Bioengineering, and through generous contributions from the following: AbbVie, Alzheimer's Association; Alzheimer's Drug Discovery Foundation; Araclon Biotech; BioClinica, Inc.; Biogen; Bristol-Myers Squibb Company; CereSpir, Inc.; Cogstate; Eisai Inc.; Elan Pharmaceuticals, Inc.; Eli Lilly and Company; EuroImmun; F. Hoffmann-La Roche Ltd and its affiliated company Genentech, Inc.; Fujirebio; GE Healthcare; IXICO Ltd.; Janssen Alzheimer Immunotherapy Research & Development, LLC.; Johnson & Johnson Pharmaceutical Research & Development LLC.; Lumosity; Lundbeck; Merck & Co., Inc.; Meso Scale Diagnostics, LLC.; NeuroRx Research; Neurotrack Technologies; Novartis Pharmaceuticals Corporation; Pfizer Inc.; Piramal Imaging; Servier; Takeda Pharmaceutical Company; and Transition Therapeutics. The Canadian Institutes of Health Research is providing funds to support ADNI clinical sites in Canada. Private sector contributions are facilitated by the Foundation for the National Institutes of Health (www.fnih.org). The grantee organization is the Northern California Institute for Research and Education, and the study is coordinated by the Alzheimer's Therapeutic Research Institute at the University of Southern California. ADNI data are disseminated by the Laboratory for Neuro Imaging at the University of Southern California.

2.2.7 Conflict of interest

The author(s) declared no potential conflicts of interest with respect to the research, authorship, and/or publication of this article.

2.2.8 References

Andermatt, Simon, Simon Pezold, and Philippe C. Cattin. 2018. 'Automated Segmentation of Multiple Sclerosis Lesions Using Multi-Dimensional Gated Recurrent Units'. In *Brainlesion: Glioma, Multiple Sclerosis, Stroke and Traumatic Brain Injuries*, edited by Alessandro Crimi, Spyridon Bakas, Hugo Kuijf, Bjoern Menze, and Mauricio Reyes, 31–42. Lecture Notes in Computer Science. Cham: Springer International Publishing. https://doi.org/10.1007/978-3-319-75238-9_3.

Andersson, Jesper L. R., Mark S. Graham, Ivana Drobnjak, Hui Zhang, and Jon Campbell. 2018. 'Susceptibility-Induced Distortion That Varies Due to Motion: Correction in Diffusion MR without Acquiring Additional Data'. *NeuroImage* 171 (May): 277–95. https://doi.org/10.1016/j.neuroimage.2017.12.040.

Andersson, Jesper L. R., Mark S. Graham, Ivana Drobnjak, Hui Zhang, Nicola Filippini, and Matteo Bastiani. 2017. 'Towards a Comprehensive Framework for Movement and Distortion Correction of Diffusion MR Images: Within Volume Movement'. *NeuroImage* 152 (May): 450–66. https://doi.org/10.1016/j.neuroimage.2017.02.085.

Andersson, Jesper L. R, Mark S. Graham, Enikő Zsoldos, and Stamatios N. Sotiropoulos. 2016. 'Incorporating Outlier Detection and Replacement into a Non-Parametric Framework for Movement and Distortion Correction of Diffusion MR Images'. *NeuroImage* 141 (November): 556–72. https://doi.org/10.1016/j.neuroimage.2016.06.058.

Andersson, Jesper L. R., Stefan Skare, and John Ashburner. 2003. 'How to Correct Susceptibility Distortions in Spin-Echo Echo-Planar Images: Application to Diffusion Tensor Imaging'. *NeuroImage* 20 (2): 870–88. https://doi.org/10.1016/S1053-8119(03)00336-7.

Andersson, Jesper L. R., and Stamatios N. Sotiropoulos. 2016. 'An Integrated Approach to Correction for Off-Resonance Effects and Subject Movement in Diffusion MR Imaging'. *NeuroImage* 125 (January): 1063–78. https://doi.org/10.1016/j.neuroimage.2015.10.019.

Attems, Johannes, and Kurt A. Jellinger. 2014. 'The Overlap between Vascular Disease and Alzheimer's Disease - Lessons from Pathology'. *BMC Medicine* 12 (1): 1–12. https://doi.org/10.1186/s12916-014-0206-2.

Avants, Brian B., Nicholas J. Tustison, Gang Song, Philip A. Cook, Arno Klein, and James C. Gee. 2011. 'A Reproducible Evaluation of ANTs Similarity Metric Performance in Brain Image Registration'. *NeuroImage* 54 (3): 2033–44. https://doi.org/10.1016/j.neuroimage.2010.09.025.

Baykara, Ebru, Benno Gesierich, Ruth Adam, Anil Man Tuladhar, J. Matthijs Biesbroek, Huiberdina L. Koek, Stefan Ropele, et al. 2016. 'A Novel Imaging Marker for Small Vessel Disease Based on Skeletonization of White Matter Tracts and Diffusion Histograms'. *Annals of Neurology* 80 (4): 581–92. https://doi.org/10.1002/ana.24758.

Beach, Thomas G., and Michael Malek-Ahmadi. 2021. 'Alzheimer's Disease Neuropathological Comorbidities Are Common in the Younger-Old'. *Journal of Alzheimer's Disease* 79 (1): 389–400. https://doi.org/10.3233/JAD-201213.

Biel, Davina, Matthias Brendel, Anna Rubinski, Katharina Buerger, Daniel Janowitz, Martin Dichgans, Nicolai Franzmeier, and for the Alzheimer's Disease Neuroimaging Initiative (ADNI). 2021. 'Tau-PET and in Vivo Braak-Staging as Prognostic Markers of Future Cognitive Decline in Cognitively Normal to Demented Individuals'. *Alzheimer's Research & Therapy* 13 (1): 137. https://doi.org/10.1186/s13195-021-00880-x.

Brink, Hilde van den, Anna Kopczak, Tine Arts, Laurien Onkenhout, Jeroen C. W. Siero, Jaco J. M. Zwanenburg, Marco Duering, et al. 2021. 'Zooming in on Cerebral Small Vessel Function in Small Vessel Diseases with 7T MRI: Rationale and Design of the "ZOOM@SVDs" Study'. *Cerebral Circulation - Cognition and Behavior* 2 (January): 100013. https://doi.org/10.1016/j.cccb.2021.100013.

Charidimou, Andreas, Karim Farid, and Jean-Claude Baron. 2017. 'Amyloid-PET in Sporadic Cerebral Amyloid Angiopathy: A Diagnostic Accuracy Meta-Analysis'. *Neurology* 89 (14): 1490–98. https://doi.org/10.1212/WNL.0000000000004539.

Cordero-Grande, Lucilio, Daan Christiaens, Jana Hutter, Anthony N. Price, and Jo V. Hajnal. 2019. 'Complex Diffusion-Weighted Image Estimation via Matrix Recovery under General Noise Models'. *NeuroImage* 200 (October): 391–404. https://doi.org/10.1016/j.neuroimage.2019.06.039.

De Guio, François, Jean-François Mangin, Marco Duering, Stefan Ropele, Hugues Chabriat, and Eric Jouvent. 2015. 'White Matter Edema at the Early Stage of Cerebral Autosomal-Dominant Arteriopathy with Subcortical Infarcts and Leukoencephalopathy'. *Stroke* 46 (1): 258–61. https://doi.org/10.1161/STROKEAHA.114.007018.

Desikan, Rahul S., Florent Ségonne, Bruce Fischl, Brian T. Quinn, Bradford C. Dickerson, Deborah Blacker, Randy L. Buckner, et al. 2006. 'An Automated Labeling System for Subdividing the Human Cerebral Cortex on MRI Scans into Gyral Based Regions of Interest'. *NeuroImage* 31 (3): 968–80. https://doi.org/10.1016/j.neuroimage.2006.01.021.

Dewenter, Anna, Benno Gesierich, Annemieke ter Telgte, Kim Wiegertjes, Mengfei Cai, Mina A Jacob, José P Marques, et al. 2021. 'Systematic Validation of Structural Brain Networks in Cerebral Small Vessel Disease'. *Journal of Cerebral Blood Flow & Metabolism*, 0271678X211069228. https://doi.org/10.1177/0271678X211069228.

Dhollander, Thijs, Adam Clemente, Mervyn Singh, Frederique Boonstra, Oren Civier, Juan Dominguez Duque, Natalia Egorova, et al. 2021. 'Fixel-Based Analysis of Diffusion MRI: Methods, Applications, Challenges and Opportunities'. *NeuroImage* 241 (November): 118417. https://doi.org/10.1016/j.neuroimage.2021.118417.

Dhollander, Thijs, Remika Mito, David Raffelt, and Alan Connelly. 2019. 'Improved White Matter Response Function Estimation for 3-Tissue Constrained Spherical Deconvolution'. In .

Dichgans, Martin, and Didier Leys. 2017. 'Vascular Cognitive Impairment'. *Circulation Research* 120 (3): 573–91. https://doi.org/10.1161/CIRCRESAHA.116.308426.

Duering, Marco, Sofia Finsterwalder, Ebru Baykara, Anil Man Tuladhar, Benno Gesierich, Marek J. Konieczny, Rainer Malik, et al. 2018. 'Free Water Determines Diffusion Alterations and Clinical Status in Cerebral Small Vessel Disease'. *Alzheimer's & Dementia: The Journal of the Alzheimer's Association* 14 (6): 764–74. https://doi.org/10.1016/j.jalz.2017.12.007.

Duering, Marco, Benno Gesierich, Stephan Seiler, Lukas Pirpamer, Mariya Gonik, Edith Hofer, Eric Jouvent, et al. 2014. 'Strategic White Matter Tracts for Processing Speed Deficits in Age-Related Small Vessel Disease'. *Neurology* 82 (22): 1946–50. https://doi.org/10.1212/WNL.0000000000000475.

Duering, Marco, Nikola Zieren, Dominique Hervé, Eric Jouvent, Sonia Reyes, Nils Peters, Chahin Pachai, Christian Opherk, Hugues Chabriat, and Martin Dichgans. 2011. 'Strategic Role of Frontal White Matter Tracts in Vascular Cognitive Impairment: A Voxel-Based Lesion-Symptom Mapping Study in CADASIL'. *Brain: A Journal of Neurology* 134 (Pt 8): 2366–75. https://doi.org/10.1093/brain/awr169.

Finsterwalder, Sofia, Naomi Vlegels, Benno Gesierich, Miguel Á. Araque Caballero, Nick A. Weaver, Nicolai Franzmeier, Marios K. Georgakis, et al. 2020. 'Small Vessel Disease More than Alzheimer's Disease Determines Diffusion MRI Alterations in Memory Clinic Patients'. *Alzheimer's & Dementia* 16 (11): 1504–14. https://doi.org/10.1002/alz.12150.

Flier, Wiesje M. van der, Ingmar Skoog, Julie A. Schneider, Leonardo Pantoni, Vincent Mok, Christopher L. H. Chen, and Philip Scheltens. 2018. 'Vascular Cognitive Impairment'. *Nature Reviews Disease Primers* 4 (1): 1–16. https://doi.org/10.1038/nrdp.2018.3.

Genc, Sila, Chantal M. W. Tax, Erika P. Raven, Maxime Chamberland, Greg D. Parker, and Derek K. Jones. 2020. 'Impact of B-Value on Estimates of Apparent Fibre Density'. *Human Brain Mapping* 41 (10): 2583–95. https://doi.org/10.1002/hbm.24964.

Gurol, M. Edip, J. Alex Becker, Panagiotis Fotiadis, Grace Riley, Kristin Schwab, Keith A. Johnson, and Steven M. Greenberg. 2016. 'Florbetapir-PET to Diagnose Cerebral Amyloid Angiopathy'. *Neurology* 87 (19): 2043–49. https://doi.org/10.1212/WNL.0000000000003197.

Jack, Clifford R., David A. Bennett, Kaj Blennow, Maria C. Carrillo, Billy Dunn, Samantha Budd Haeberlein, David M. Holtzman, et al. 2018. 'NIA-AA Research Framework: Toward a Biological Definition of Alzheimer's Disease'. *Alzheimer's & Dementia* 14 (4): 535–62. https://doi.org/10.1016/j.jalz.2018.02.018.

Jeurissen, Ben, Alexander Leemans, Jacques-Donald Tournier, Derek K. Jones, and Jan Sijbers. 2013. 'Investigating the Prevalence of Complex Fiber Configurations in White Matter Tissue with Diffusion Magnetic Resonance Imaging'. *Human Brain Mapping* 34 (11): 2747–66.

Jeurissen, Ben, Jacques-Donald Tournier, Thijs Dhollander, Alan Connelly, and Jan Sijbers. 2014. 'Multi-Tissue Constrained Spherical Deconvolution for Improved Analysis of Multi-Shell Diffusion MRI Data'. *NeuroImage* 103 (December): 411–26. https://doi.org/10.1016/j.neuroimage.2014.07.061.

Jones, Derek K., Thomas R. Knösche, and Robert Turner. 2013. 'White Matter Integrity, Fiber Count, and Other Fallacies: The Do's and Don'ts of Diffusion MRI'. *NeuroImage* 73 (June): 239–54. https://doi.org/10.1016/j.neuroimage.2012.06.081.

Kapasi, Alifiya, Charles DeCarli, and Julie A. Schneider. 2017. 'Impact of Multiple Pathologies on the Threshold for Clinically Overt Dementia'. *Acta Neuropathologica* 134 (2): 171–86. https://doi.org/10.1007/s00401-017-1717-7.

Kellner, Elias, Bibek Dhital, Valerij G. Kiselev, and Marco Reisert. 2016. 'Gibbs-Ringing Artifact Removal Based on Local Subvoxel-Shifts'. *Magnetic Resonance in Medicine* 76 (5): 1574–81. https://doi.org/10.1002/mrm.26054.

Klunk, William E., Robert A. Koeppe, Julie C. Price, Tammie Benzinger, Michael D. Devous, William Jagust, Keith Johnson, et al. 2015. 'The Centiloid Project: Standardizing Quantitative Amyloid Plaque Estimation by PET'. *Alzheimer's & Dementia : The Journal of the Alzheimer's Association* 11 (1): 1-15.e4. https://doi.org/10.1016/j.jalz.2014.07.003.

Konieczny, Marek J., Anna Dewenter, Annemieke ter Telgte, Benno Gesierich, Kim Wiegertjes, Sofia Finsterwalder, Anna Kopczak, et al. 2021. 'Multi-Shell Diffusion MRI Models for White Matter Characterization in Cerebral Small Vessel Disease'. *Neurology* 96 (5): e698–708. https://doi.org/10.1212/WNL.0000000000011213.

La Joie, Renaud, Adrienne V. Visani, Suzanne L. Baker, Jesse A. Brown, Viktoriya Bourakova, Jungho Cha, Kiran Chaudhary, et al. 2020. 'Prospective Longitudinal Atrophy in Alzheimer's Disease Correlates with the Intensity and Topography of Baseline Tau-PET'. *Science Translational Medicine* 12 (524): eaau5732. https://doi.org/10.1126/scitranslmed.aau5732.

Landau, Susan M., Mark A. Mintun, Abhinay D. Joshi, Robert A. Koeppe, Ronald C. Petersen, Paul S. Aisen, Michael W. Weiner, and William J. Jagust. 2012. 'Amyloid Deposition, Hypometabolism, and Longitudinal Cognitive Decline'. *Annals of Neurology* 72 (4): 578–86. https://doi.org/10.1002/ana.23650.

Leijsen, Esther M. C. van, Frank-Erik de Leeuw, and Anil M. Tuladhar. 2017. 'Disease Progression and Regression in Sporadic Small Vessel Disease-Insights from Neuroimaging'. *Clinical Science (London, England: 1979)* 131 (12): 1191–1206. https://doi.org/10.1042/CS20160384.

McAleese, Kirsty E, Lauren Walker, Sean J Colloby, John-Paul Taylor, Alan J Thomas, Charles DeCarli, and Johannes Attems. 2018. 'Cortical Tau Pathology: A Major Player in Fibre-Specific White Matter Reductions in Alzheimer's Disease?' *Brain* 141 (6): e44–e44. https://doi.org/10.1093/brain/awy084.

Mito, Remika, David Raffelt, Thijs Dhollander, David N Vaughan, J-Donald Tournier, Olivier Salvado, Amy Brodtmann, Christopher C Rowe, Victor L Villemagne, and Alan Connelly. 2018a. 'Fibre-Specific White Matter Reductions in Alzheimer's Disease and

Mild Cognitive Impairment'. *Brain* 141 (3): 888–902. https://doi.org/10.1093/brain/awx355.

Mito, Remika, David Raffelt, Thijs Dhollander, David N Vaughan, J-Donald Tournier, Olivier Salvado, Amy Brodtmann, Christopher C Rowe, Victor L Villemagne, and Alan Connelly. 2018b. 'Reply: Cortical Tau Pathology: A Major Player in Fibre-Specific White Matter Reductions in Alzheimer's Disease?' *Brain* 141 (6): e45–e45. https://doi.org/10.1093/brain/awy086.

Nasrabady, Sara E., Batool Rizvi, James E. Goldman, and Adam M. Brickman. 2018. 'White Matter Changes in Alzheimer's Disease: A Focus on Myelin and Oligodendrocytes'. *Acta Neuropathologica Communications* 6 (1): 22. https://doi.org/10.1186/s40478-018-0515-3.

Norden, Anouk GW van, Karlijn F. de Laat, Rob AR Gons, Inge WM van Uden, Ewoud J. van Dijk, Lucas JB van Oudheusden, Rianne AJ Esselink, et al. 2011. 'Causes and Consequences of Cerebral Small Vessel Disease. The RUN DMC Study: A Prospective Cohort Study. Study Rationale and Protocol'. *BMC Neurology* 11 (1): 29. https://doi.org/10.1186/1471-2377-11-29.

Petersen, Marvin, Benedikt M. Frey, Carola Mayer, Simone Kühn, Jürgen Gallinat, Uta Hanning, Jens Fiehler, et al. 2022. 'Fixel Based Analysis of White Matter Alterations in Early Stage Cerebral Small Vessel Disease'. *Scientific Reports* 12 (1): 1581. https://doi.org/10.1038/s41598-022-05665-2.

Pichet Binette, Alexa, Guillaume Theaud, François Rheault, Maggie Roy, D Louis Collins, Johannes Levin, Hiroshi Mori, et al. 2021. 'Bundle-Specific Associations between White Matter Microstructure and Aβ and Tau Pathology in Preclinical Alzheimer's Disease'. *ELife* 10 (May): e62929. https://doi.org/10.7554/eLife.62929.

Puonti, Oula, Juan Eugenio Iglesias, and Koen Van Leemput. 2016. 'Fast and Sequence-Adaptive Whole-Brain Segmentation Using Parametric Bayesian Modeling'. *NeuroImage* 143 (December): 235–49. https://doi.org/10.1016/j.neuroimage.2016.09.011.

R Core Team. 2016. 'R: A Language and Environment for Statistical Computing'. *Vienna: R Foundations for Statistical Computing*.

Raffelt, David A., J. -Donald Tournier, Robert E. Smith, David N. Vaughan, Graeme Jackson, Gerard R. Ridgway, and Alan Connelly. 2017. 'Investigating White Matter Fibre Density and Morphology Using Fixel-Based Analysis'. *NeuroImage* 144 (January): 58–73. https://doi.org/10.1016/j.neuroimage.2016.09.029.

Raffelt, David, J. -Donald Tournier, Stephen Rose, Gerard R. Ridgway, Robert Henderson, Stuart Crozier, Olivier Salvado, and Alan Connelly. 2012. 'Apparent Fibre Density: A Novel Measure for the Analysis of Diffusion-Weighted Magnetic Resonance Images'. *NeuroImage* 59 (4): 3976–94. https://doi.org/10.1016/j.neuroimage.2011.10.045.

Raghavan, Sheelakumari, Scott A. Przybelski, Robert I. Reid, Timothy G. Lesnick, Vijay K. Ramanan, Hugo Botha, Billie J. Matchett, et al. 2022. 'White Matter Damage Due to Vascular, Tau, and TDP-43 Pathologies and Its Relevance to Cognition'. *Acta Neuropathologica Communications* 10 (1): 16. https://doi.org/10.1186/s40478-022-01319-6.

Raja, Rajikha, Gary Rosenberg, and Arvind Caprihan. 2019. 'Review of Diffusion MRI Studies in Chronic White Matter Diseases'. *Neuroscience Letters* 694 (February): 198–207. https://doi.org/10.1016/j.neulet.2018.12.007.

Schilling, Kurt G., Justin Blaber, Colin Hansen, Leon Cai, Baxter Rogers, Adam W. Anderson, Seth Smith, et al. 2020. 'Distortion Correction of Diffusion Weighted MRI without Reverse Phase-Encoding Scans or Field-Maps'. *PLOS ONE* 15 (7): e0236418. https://doi.org/10.1371/journal.pone.0236418.

Schilling, Kurt G., Justin Blaber, Yuankai Huo, Allen Newton, Colin Hansen, Vishwesh Nath, Andrea T. Shafer, et al. 2019. 'Synthesized B0 for Diffusion Distortion Correction (Synb0-DisCo)'. *Magnetic Resonance Imaging*, Artificial Intelligence in MRI, 64 (December): 62–70. https://doi.org/10.1016/j.mri.2019.05.008.

Schöll, Michael, Samuel N. Lockhart, Daniel R. Schonhaut, James P. O'Neil, Mustafa Janabi, Rik Ossenkoppele, Suzanne L. Baker, et al. 2016. 'PET Imaging of Tau Deposition in the Aging Human Brain'. *Neuron* 89 (5): 971–82. https://doi.org/10.1016/j.neuron.2016.01.028.

Smith, Eric E., Geert Jan Biessels, François De Guio, Frank Erik de Leeuw, Simon Duchesne, Marco Düring, Richard Frayne, et al. 2019. 'Harmonizing Brain Magnetic Resonance Imaging Methods for Vascular Contributions to Neurodegeneration'. *Alzheimer's & Dementia: Diagnosis, Assessment & Disease Monitoring* 11 (December): 191–204. https://doi.org/10.1016/j.dadm.2019.01.002.

Smith, Robert, Thijs Dhollander, and Alan Connelly. 2019. *On the Regression of Intracranial Volume in Fixel-Based Analysis*.

Smith, Stephen M., Mark Jenkinson, Mark W. Woolrich, Christian F. Beckmann, Timothy E.J. Behrens, Heidi Johansen-Berg, Peter R. Bannister, et al. 2004. 'Advances in Functional and Structural MR Image Analysis and Implementation as FSL'. *NeuroImage* 23 (January): S208–19. https://doi.org/10.1016/j.neuroimage.2004.07.051.

Telgte, Annemieke ter, Kim Wiegertjes, Anil M Tuladhar, Marlies P Noz, José P Marques, Benno Gesierich, Mathias Huebner, et al. 2018. 'Investigating the Origin and Evolution of Cerebral Small Vessel Disease: The RUN DMC – InTENse Study'. *European Stroke Journal* 3 (4): 369–78. https://doi.org/10.1177/2396987318776088.

Thomas, Benjamin A., Vesna Cuplov, Alexandre Bousse, Adriana Mendes, Kris Thielemans, Brian F. Hutton, and Kjell Erlandsson. 2016. 'PETPVC: A Toolbox for Performing Partial Volume Correction Techniques in Positron Emission Tomography'. *Physics in Medicine and Biology* 61 (22): 7975–93. https://doi.org/10.1088/0031-9155/61/22/7975.

Tournier, J.-Donald, Fernando Calamante, and Alan Connelly. 2012. 'MRtrix: Diffusion Tractography in Crossing Fiber Regions'. *International Journal of Imaging Systems and Technology* 22 (1): 53–66. https://doi.org/10.1002/ima.22005.

Tournier, J-Donald, Robert Smith, David Raffelt, Rami Tabbara, Thijs Dhollander, Maximilian Pietsch, Daan Christiaens, Ben Jeurissen, Chun-Hung Yeh, and Alan Connelly. 2019. 'MRtrix3: A Fast, Flexible and Open Software Framework for Medical Image Processing and Visualisation'. *NeuroImage* 202 (November): 116137. https://doi.org/10.1016/j.neuroimage.2019.116137.

Tuladhar, Anil M., Ingeborg W.M. van Uden, Loes C.A. Rutten-Jacobs, Andrew Lawrence, Helena van der Holst, Anouk van Norden, Karlijn de Laat, et al. 2016. 'Structural Network Efficiency Predicts Conversion to Dementia'. *Neurology* 86 (12): 1112–19. https://doi.org/10.1212/WNL.0000000000002502.

Tustison, Nicholas J., Philip A. Cook, Arno Klein, Gang Song, Sandhitsu R. Das, Jeffrey T. Duda, Benjamin M. Kandel, et al. 2014. 'Large-Scale Evaluation of ANTs and FreeSurfer Cortical Thickness Measurements'. *NeuroImage* 99: 166–79. https://doi.org/10.1016/j.neuroimage.2014.05.044.

Vemuri, Prashanthi, Timothy G. Lesnick, David S. Knopman, Scott A. Przybelski, Robert I. Reid, Michelle M. Mielke, Jonathan Graff-Radford, et al. 2019. 'Amyloid, Vascular, and Resilience Pathways Associated with Cognitive Aging'. *Annals of Neurology* 86 (6): 866–77. https://doi.org/10.1002/ana.25600.

Veraart, Jelle, Els Fieremans, and Dmitry S. Novikov. 2016. 'Diffusion MRI Noise Mapping Using Random Matrix Theory'. *Magnetic Resonance in Medicine* 76 (5): 1582–93. https://doi.org/10.1002/mrm.26059.

Veraart, Jelle, Dmitry S. Novikov, Daan Christiaens, Benjamin Ades-aron, Jan Sijbers, and Els Fieremans. 2016. 'Denoising of Diffusion MRI Using Random Matrix Theory'. *NeuroImage* 142 (November): 394–406. https://doi.org/10.1016/j.neuroimage.2016.08.016.

Wardlaw, Joanna M, Colin Smith, and Martin Dichgans. 2019. 'Small Vessel Disease: Mechanisms and Clinical Implications'. *The Lancet Neurology* 18 (7): 684–96. https://doi.org/10.1016/S1474-4422(19)30079-1.

Wardlaw, Joanna M, Eric E Smith, Geert J Biessels, Charlotte Cordonnier, Franz Fazekas, Richard Frayne, Richard I Lindley, et al. 2013. 'Neuroimaging Standards for Research into Small Vessel Disease and Its Contribution to Ageing and Neurodegeneration'. *The Lancet Neurology* 12 (8): 822–38. https://doi.org/10.1016/S1474-4422(13)70124-8.

Wasserthal, Jakob, Peter Neher, and Klaus H. Maier-Hein. 2018. 'TractSeg - Fast and Accurate White Matter Tract Segmentation'. *NeuroImage* 183 (December): 239–53. https://doi.org/10.1016/j.neuroimage.2018.07.070.

Weiner, Michael W., Dallas P. Veitch, Paul S. Aisen, Laurel A. Beckett, Nigel J. Cairns, Robert C. Green, Danielle Harvey, et al. 2017. 'The Alzheimer's Disease Neuroimaging Initiative 3: Continued Innovation for Clinical Trial Improvement'. *Alzheimer's & Dementia* 13 (5): 561–71. https://doi.org/10.1016/j.jalz.2016.10.006.

Yu, Xinfeng, Xinzhen Yin, Hui Hong, Shuyue Wang, Yeerfan Jiaerken, Fan Zhang, Ofer Pasternak, et al. 2021. 'Increased Extracellular Fluid Is Associated with White Matter Fiber Degeneration in CADASIL: In Vivo Evidence from Diffusion Magnetic Resonance Imaging'. *Fluids and Barriers of the CNS* 18 (June): 29. https://doi.org/10.1186/s12987-021-00264-1.

2.2.9 Supplementary material

Table e-1: MRI acquisition parameters.

		SVD	**AD**	**Validation**
Sequence	**Feature**	VASCAMY, ZOOM	ADNI-3	RUN DMC
	Scanner	Magnetom Skyra	Magnetom Prisma/PrismaFit	Magnetom Prisma
	Coil channels	64 (head-neck)	20/32/64 (head/head-neck)	32 (head)
3D T1-weighted	Type	MPRAGE	MPRAGE	MP2RAGE
	TR [ms]	2500	2300	5000
	TE [ms]	4.37	2.98	2.98
	TI [ms]	1100	900	732, 2500[a]
	Flip angle [˚]	7	9	4, 5[a]
	Voxel size [mm]	1 isotropic	1 isotropic	0.85 isotropic
3D-FLAIR	TR [ms]	5000	4800	5000
	TE [ms]	398	441	394
	TI [ms]	1800	1650	1800
	Voxel size [mm]	1 isotropic	1.2 x 1 x 1	0.85 isotropic
3D GRE	TR [ms]	35	650	44
	TE [ms]	29.5	20	6.14, 10.1, 14.1, 18.1, 22.1, 26.1, 30.1, 34.1, 38.1
	Flip angle [˚]	15	20	20
	Voxel size [mm]	0.9 x 0.9 x 2	0.86 x 0.86 x 4	0.85 isotropic
MS-DWI	TR [ms]	3800	3400	3220
	TE [ms]	104.8	71	74
	Flip angle [˚]	90	90	90
	In-plane resolution [mm]	2 x 2	2 x 2	1.7 x 1.7
	Slice thickness [mm]	2	2	1.7
	Base resolution (matrix)	120	116	130
	Number of slices	75	81	87
	b-values [s/mm^2]	1000/2000	1000, 2000	1000, 3000
	Directions (per b-value)	30/60	48, 60	30, 60
	b=0 [images]	10	13	10
	Receiver bandwidth [Hz/px]	1894	2270	1924
	Parallel acceleration	2	2	2
	Multi-band acceleration	3	3	3

[a] Double inversion

Abbreviations: FLAIR = fluid-attenuated inversion recovery; GRE = gradient echo; MP(2)RAGE = magnetization prepared (2) rapid acquisition gradient echoes; MS-DWI = multi-shell diffusion-weighted imaging; RUN DMC = Radboud University Nijmegen Diffusion tensor and Magnetic resonance imaging Cohort; TE = echo time; TI = inversion time; TR = repetition time.

Table e-2: Group comparison of fixel metrics in the SVD sample (Cohen's d, $p<0.05$, FDR adj. $p<0.05$ in bold). Please refer to **Figure 3** (main manuscript) for abbreviations of the fiber tracts.

	AF	UF	IFO	MLF	ILF	SLF-I	SLF-II	SLF-III	T-PREF	T-PREM	T-PREC	T-POSTC	T-PAR	T-OCC	ATR	STR	OR	FPT	CST	POPT	CC-I	CC-II	CC-III	CC-IV	CC-V	CC-VI	CC-VII	AC	CG
Fiber density																													
HC>CADASIL	**.49**	**.54**	**.50**	**.50**	**.43**	**.49**	**.50**	**.47**	**.54**	**.55**	**.48**	**.50**	**.51**	**.41**	**.57**	**.45**	**.42**	**.53**	**.44**	**.50**	**.37**	**.53**	**.55**	**.48**	**.46**	**.48**	**.33**	**.50**	**.53**
Fiber-bundle cross-section																													
HC>CADASIL	**.20**	-	-	**.20**	**.23**	**.35**	-	**.25**	-	-	**.30**	**.30**	**.21**	-	**-.33**	**.35**	-	**.20**	**.33**	**.23**	**-.33**	-	-	**.26**	**.32**	**.19**	-	**.24**	-

Table e-3: Group comparison of fixel metrics in the AD sample (Cohen's d, $p<0.05$, FDR adj. $p<0.05$ in bold).

	AF	UF	IFO	MLF	ILF	SLF-I	SLF-II	SLF-III	T-PREF	T-PREM	T-PREC	T-POSTC	T-PAR	T-OCC	ATR	STR	OR	FPT	CST	POPT	CC-I	CC-II	CC-III	CC-IV	CC-V	CC-VI	CC-VII	AC	CG
Fiber density																													
Aβ–T– > Aβ+T–	**.33**	**.34**	**.38**	.33	-	**.36**	**.49**	.28	-	-	-	-	.32	.29	**.33**	-	.27	-	-	-	**.34**	**.46**	**.46**	**.39**	**.43**	**.37**	**.37**	.29	-
Aβ+T– > Aβ+T+	-	**.43**	**.36**	-	.31	-	**.36**	**.35**	.32	.32	-	-	-	-	**.41**	-	-	-	-	-	.30	-	-	-	-	-	.30	**.39**	.32
Aβ–T– > Aβ+T+	-	-	-	-	-	-	-	-	-	-	-	-	-	-	-	-	-	-	-	-	-	-	-	-	-	-	-	-	-
Fiber-bundle cross-section																													
Aβ–T– > Aβ+T–	.35	.29	.27	-	-	.35	-	.34	-	-	**.49**	**.42**	.27	-	-	**.46**	-	.31	**.51**	**.40**	-	-	-	-	.31	-	-	**.37**	-
Aβ+T– > Aβ+T+	.27	.28	.27	-	**.40**	-	-	-	-	.30	.27	-	-	-	-	-	-	.30	.30	-	-	-	-	-	-	-	.30	-	-
Aβ–T– > Aβ+T+	-	-	-	-	-	-	-	-	-	-	-	-	-	-	-	-	-	-	-	-	-	-	-	-	-	-	-	-	-
Sensitivity Analysis: Including WMHV as covariate.																													
Fiber density																													
Aβ–T– > Aβ+T–	.27	.27	-	-	-	.27	.38	-	-	-	-	-	-	-	-	-	-	-	-	-	-	.31	.31	-	.31	-	.26	.31	-
Aβ+T– > Aβ+T+	-	.39	.27	-	-	-	.26	.30	-	-	-	-	-	-	.34	-	-	-	-	-	-	-	-	-	-	-	-	.39	.26
Aβ–T– > Aβ+T+																													
Fiber-bundle cross-section																													
Aβ–T– > Aβ+T–	.32	.28	.28	-	-	.26	-	.30	-	-	.40	.38	-	-	-	.39	-	.30	**.44**	.36	-	-	-	-	.26	-	-	.37	-
Aβ+T– > Aβ+T+	.26	.27	.27	-	.38	-	-	-	-	.32	-	-	-	-	-	-	-	.29	-	-	-	-	-	-	-	-	.30	-	-
Aβ–T– > Aβ+T+	-	-	-	-	-	-	-	-	-	-	-	-	-	-	-	-	-	-	-	-	-	-	-	-	-	-	-	-	-

Table e-4: Simple linear regression models predicting fiber density (top) or fiber-bundle cross-section (bottom) for each fiber tract in the SVD sample (adj. R^2, $p<0.05$, FDR adj. $p<0.05$ in bold). Predictors are represented on the left (age, white matter hyperintensity volume [WMHV], lacunes, microbleeds, brain volume [BrainV]) which were included separately for each model. Please refer to Figure 3 (main manuscript) for abbreviations of the fiber tracts.

	AF	UF	IFOF	MLF	ILF	SLF-I	SLF-II	SLF-III	T-PREF	T-PREM	T-PREC	T-POSTC	T-PAR	T-OCC	ATR	STR	OR	FPT	CST	POPT	CC-I	CC-II	CC-III	CC-IV	CC-V	CC-VI	CC-VII	AC	CG
Fiber density																													
Age	**.04**	**.05**	**.07**	**.07**	**.04**	**.04**	**.05**	**.06**	**.07**	**.04**	**.06**	**.04**	**.08**	**.04**	**.06**	**.05**	-	**.06**	**.07**	**.08**	**.07**	**.09**	**.09**	**.09**	**.13**	**.09**	**.03**	**.06**	**.10**
WMHV	**.70**	**.78**	**.73**	**.65**	**.67**	**.68**	**.67**	**.67**	**.79**	**.68**	**.68**	**.61**	**.62**	**.44**	**.77**	**.62**	**.43**	**.75**	**.62**	**.61**	**.40**	**.75**	**.65**	**.65**	**.60**	**.58**	**.29**	**.70**	**.72**
Lacunes	**.39**	**.28**	**.46**	**.45**	**.24**	**.41**	**.44**	**.35**	**.40**	**.42**	**.31**	**.33**	**.47**	**.48**	**.42**	**.34**	**.47**	**.42**	**.31**	**.46**	**.37**	**.40**	**.39**	**.32**	**.39**	**.47**	**.43**	**.12**	**.43**
Microbleeds	**.33**	**.28**	**.39**	**.38**	**.23**	**.38**	**.37**	**.28**	**.34**	**.36**	**.29**	**.23**	**.37**	**.43**	**.33**	**.24**	**.43**	**.35**	**.30**	**.35**	**.25**	**.33**	**.37**	**.33**	**.33**	**.37**	**.30**	**.16**	**.38**
BrainV	**.05**	-	**.08**	**.09**	-	**.07**	**.08**	**.05**	**.05**	**.06**	**.06**	**.05**	**.12**	**.13**	**.06**	**.08**	**.12**	**.06**	**.08**	**.11**	**.16**	**.08**	**.11**	**.09**	**.16**	**.14**	**.13**	-	**.09**
Fiber-bundle cross-section																													
Age	**.11**	**.07**	**.13**	**.05**	**.11**	**.06**	**.07**	**.09**	**.09**	**.10**	**.08**	**.04**	-	**.08**	-	**.08**	**.08**	**.13**	**.09**	**.04**	-	**.06**	**.06**	**.04**	-	-	-	**.08**	**.12**
WMHV	**.35**	**.29**	**.07**	**.21**	**.28**	**.43**	**.31**	**.39**	**.22**	**.21**	**.37**	**.27**	**.16**	**.06**	-	**.35**	**.07**	**.33**	**.38**	**.18**	-	**.07**	**.13**	**.36**	**.32**	**.11**	-	**.27**	**.23**
Lacunes	**.43**	**.14**	**.16**	**.33**	**.23**	**.42**	**.31**	**.42**	**.26**	**.32**	**.51**	**.40**	**.35**	**.23**	-	**.48**	**.24**	**.44**	**.52**	**.41**	-	**.06**	**.12**	**.39**	**.34**	**.28**	**.07**	**.16**	**.26**
Microbleeds	**.33**	**.07**	**.09**	**.27**	**.17**	**.38**	**.29**	**.30**	**.16**	**.20**	**.30**	**.25**	**.24**	**.16**	-	**.29**	**.18**	**.27**	**.31**	**.26**	-	-	**.07**	**.18**	**.16**	**.16**	-	**.11**	**.26**
BrainV	**.24**	-	**.21**	**.21**	**.10**	**.16**	**.13**	**.22**	**.20**	**.19**	**.22**	**.20**	**.22**	**.18**	**.07**	**.24**	**0.20**	**.29**	**.24**	**.28**	**.06**	**.10**	**.07**	**.09**	**.07**	**.15**	-	**.05**	**.29**

Table e-5: Simple linear regression models predicting fiber density (top) or fiber-bundle cross-section (bottom) for each fiber tract in the AD sample (adj. R^2, $p<0.05$, FDR adj. $p<0.05$ in bold). Predictors are represented on the left (age, white matter hyperintensity volume [WMHV], lacunes, microbleeds, brain volume [BrainV], amyloid, tau: global, tau: regional) which were included separately in each model. Please refer to Figure 3 (main manuscript) for abbreviations of the fiber tracts.

	AF	**UF**	**IFOF**	**MLF**	**ILF**	**SLF-I**	**SLF-II**	**SLF-III**	**T-PREF**	**T-PREM**	**T-PREC**	**T-POSTC**	**T-PAR**	**T-OCC**	**ATR**	**STR**	**OR**	**FPT**	**CST**	**POPT**	**CC-I**	**CC-II**	**CC-III**	**CC-IV**	**CC-V**	**CC-VI**	**CC-VII**	**AC**	**CG**
Fiber density																													
Age	-	-	.07	.06	-	.05	-	-	-	-	-	-	.07	.07	-	-	.06	-	-	-	-	.09	.07	**.14**	**.10**	**.14**	**.17**	-	-
WMHV	-	-	**.16**	**.11**	.05	.06	**.16**	.04	.09	.07	-	-	**.12**	**.11**	**.15**	-	.09	-	-	-	**.12**	**.20**	**.20**	**.20**	**.13**	**.12**	.08	-	-
Lacunes	-	-	-	-	-	-	-	-	-	-	-	-	-	-	-	-	-	-	-	-	-	-	-	-	-	-	-	-	-
Microbleeds	-	-	-	-	-	-	.05	-	.07	-	.08	-	.05	-	-	-	-	-	-	-	-	-	-	.07	-	-	-	.06	-
BrainV	-	-	-	-	-	-	-	-	-	-	-	-	-	-	-	-	-	-	-	-	-	-	-	-	-	-	-	-	-
Amyloid	-	**.11**	.07	-	-	-	**.10**	.06	-	-	-	-	-	-	.07	-	-	-	-	-	.07	.04	-	-	.04	-	.07	.09	-
Tau: global	-	-	-	-	-	-	-	-	-	-	-	-	-	-	-	-	-	-	-	-	-	-	-	-	-	-	-	-	-
Tau: regional	-	-	-	-	-	-	-	-	-	.04	-	-	-	-	-	-	-	-	-	-	.04	-	-	-	-	-	-	-	-
Fiber-bundle cross-section																													
Age	**.09**	.06	**.18**	-	**.11**	.04	-	**.09**	.05	-	**.12**	**.12**	-	**.18**	-	**.12**	**.20**	.07	.07	-	-	-	-	-	.05	-	**.09**	**.08**	.05
WMHV	-	-	-	-	-	.04	-	-	-	-	-	-	-	-	.06	-	-	-	-	-	-	.05	.06	-	-	-	-	-	-
Lacunes	-	-	-	-	-	-	-	-	-	-	-	-	-	-	-	-	-	-	-	-	-	-	-	-	-	-	-	-	-
Microbleeds	-	-	-	-	-	-	-	-	-	-	-	-	-	-	-	-	-	-	-	-	-	-	-	-	-	-	-	-	-
BrainV	**.35**	**.35**	**.32**	**.23**	**.28**	**.19**	**.29**	**.20**	**.31**	**.30**	**.18**	**.19**	**.18**	**.18**	**.22**	**.12**	**.17**	**.34**	**.20**	**.22**	**.18**	**.29**	**.23**	**.19**	.06	**.20**	**.17**	**.25**	**.24**
Amyloid	-	-	-	-	.05	-	-	-	-	-	.04	-	-	-	-	-	-	-	.04	-	-	-	-	-	-	-	.04	-	-
Tau: global	-	-	-	-	.05	-	-	-	-	-	-	-	-	-	-	-	-	-	-	-	-	-	-	-	-	-	-	-	-
Tau: regional	.06	-	-	-	-	-	-	-	-	-	-	-	-	.05	-	-	.05	-	-	-	-	-	-	-	-	-	-	-	-

Table e-6: Simple linear regression models predicting fiber density (top) or fiber-bundle cross-section (bottom) for each fiber tract in the validation sample (adj. R^2, $p<0.05$, FDR adj. $p<0.05$ in bold). Predictors are represented on the left (age, white matter hyperintensity volume [WMHV], lacunes, microbleeds, brain volume [BrainV]) which were included separately for each model. Please refer to Figure 3 (main manuscript) for abbreviations of the fiber tracts.

	AF	UF	IFOF	MLF	ILF	SLF-I	SLF-II	SLF-III	T-PREF	T-PREM	T-PREC	T-POSTC	T-PAR	T-OCC	ATR	STR	OR	FPT	CST	POPT	CC-I	CC-II	CC-III	CC-IV	CC-V	CC-VI	CC-VII	AC	CG
Fiber density																													
Age	**.13**	**.14**	**.18**	**.17**	**.12**	**.08**	**.10**	**.13**	**.13**	**.10**	**.06**	**.09**	**.15**	**.18**	**.17**	**.03**	**.17**	**.07**	**.05**	**.12**	**.12**	**.22**	**.18**	**.17**	**.18**	**.22**	**.23**	**.18**	**.17**
WMHV	**.42**	**.19**	**.38**	**.37**	**.16**	**.40**	**.48**	**.36**	**.47**	**.42**	**.42**	**.33**	**.43**	**.33**	**.39**	**.35**	**.33**	**.39**	**.33**	**.41**	**.12**	**.36**	**.33**	**.36**	**.34**	**.35**	**.26**	**.08**	**.29**
Lacunes	**.23**	**.09**	**.16**	**.15**	**.09**	**.21**	**.26**	**.20**	**.21**	**.26**	**.12**	**.07**	**.15**	**.16**	**.18**	**.07**	**.16**	**.18**	**.08**	**.13**	**.05**	**.17**	**.20**	**.12**	**.09**	**.12**	**.10**	**.03**	**.11**
Microbleeds	**.15**	**.09**	**.12**	**.10**	**.06**	**.10**	**.11**	**.15**	**.11**	**.11**	**.08**	**.07**	**.10**	**.09**	**.11**	**.05**	**.10**	**.08**	**.04**	**.09**	**.06**	**.10**	**.08**	**.07**	**.06**	**.08**	**.05**	**.04**	**.10**
BrainV	**.12**	**.14**	**.15**	**.12**	**.09**	**.08**	**.09**	**.14**	**.11**	**.10**	**.02**	**.03**	**.10**	**.13**	**.18**	**-**	**.13**	**.07**	**.01**	**.07**	**.12**	**.19**	**.16**	**.11**	**.14**	**.15**	**.13**	**.16**	**.12**
Fiber-bundle cross-section																													
Age	**.14**	**.20**	**.09**	**.10**	**.12**	**.10**	**.05**	**.11**	**.06**	**.04**	**.13**	**.08**	**.06**	**.06**	**-**	**.11**	**.06**	**.09**	**.10**	**.08**	**.05**	**-**	**-**	**.02**	**.03**	**.04**	**-**	**.26**	**.13**
WMHV	**-**	**-**	**.02**	**-**	**-**	**.09**	**-**	**-**	**-**	**-**	**.09**	**.03**	**-**	**-**	**.09**	**.09**	**-**	**-**	**.09**	**.03**	**.03**	**.08**	**.02**	**.03**	**.04**	**-**	**-**	**.02**	**-**
Lacunes	**.05**	**-**	**-**	**.08**	**.02**	**.12**	**.06**	**.05**	**-**	**-**	**.13**	**.10**	**.09**	**-**	**-**	**.12**	**-**	**.04**	**.12**	**.10**	**-**	**-**	**-**	**.06**	**.07**	**.03**	**-**	**-**	**.05**
Microbleeds	**.06**	**-**	**-**	**.04**	**.02**	**.09**	**.05**	**.03**	**-**	**.02**	**.05**	**.05**	**.03**	**-**	**-**	**.03**	**-**	**.02**	**.04**	**.03**	**-**	**-**	**-**	**.05**	**.05**	**.03**	**-**	**-**	**.03**
BrainV	**.35**	**.32**	**.29**	**.27**	**.20**	**.27**	**.23**	**.31**	**.31**	**.24**	**.34**	**.29**	**.25**	**.14**	**.11**	**.34**	**.15**	**.42**	**.35**	**.33**	**.12**	**.13**	**.06**	**.12**	**.16**	**.19**	**.08**	**.33**	**.36**

Figure-e1

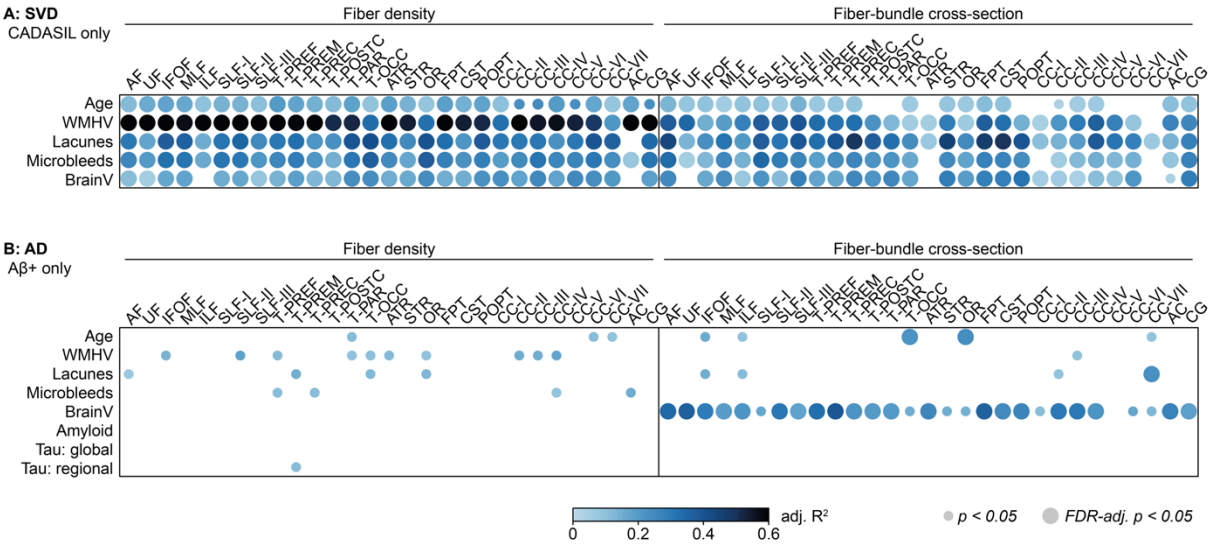

Sensitivity analysis for associations with disease markers. Effect sizes (adj. R^2) obtained from simple linear regression analyses are represented by color. Associations between fixel metrics of white matter fiber tracts and disease markers were assessed in (**A**) only CADASIL patients from the SVD sample, and (**B**) only Aβ+ study participants from the AD sample. Circle size depicts statistical significance level. Please refer to **Figure 3** (main manuscript) for abbreviations of the fiber tracts. BrainV = brain volume, FDR = false discovery rate, WMHV = white matter hyperintensity volume.

Figure-e2

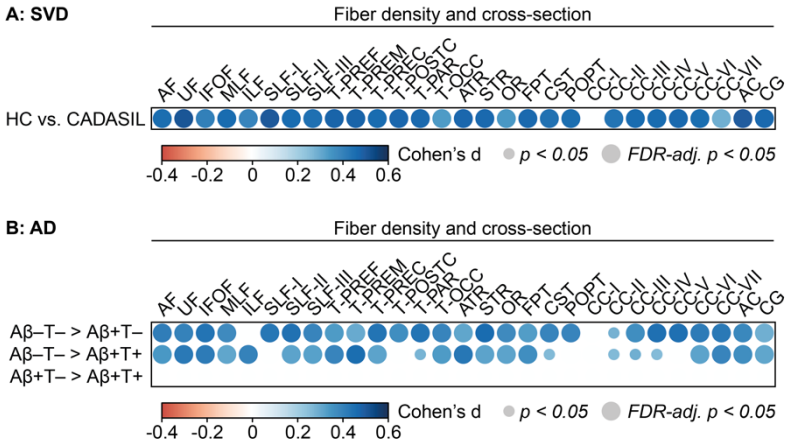

Group comparisons for the combined fixel metric fiber density and cross-section. (**A**) Difference in fiber density and cross-section between age-matched healthy controls (HC) and CADASIL patients in the SVD sample quantified with Cohen's d represented by color. (**B**) Difference in fiber density and cross-section between age-matched Aβ–T– and Aβ+T–; Aβ–T– and Aβ+T+; Aβ+T– and Aβ+T+ quantified with Cohen's d represented by color. Circle size depicts statistical significance level. Please refer to **Figure 3** (main manuscript) for abbreviations of the fiber tracts. FDR = false discovery rate.

Figure-e3

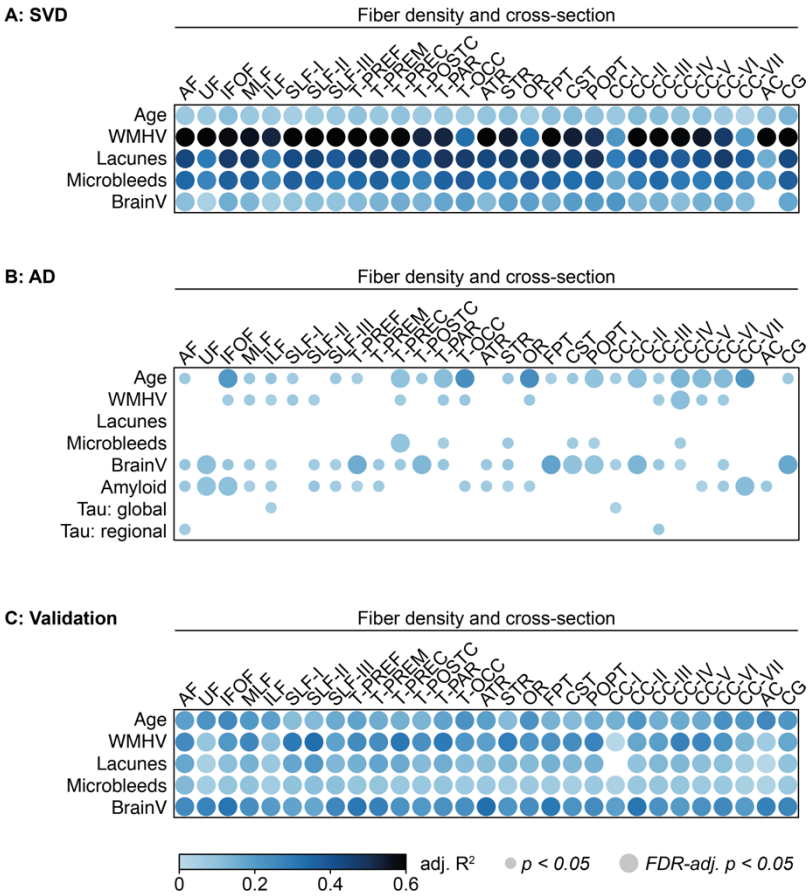

Associations with the combined fixel metric fiber density and cross-section. Effect sizes (adj. R^2) obtained from simple linear regression analyses are represented by color. Associations between fixel metrics of white matter fiber tracts and disease markers were assessed in (**A**) the SVD sample, (**B**) the AD sample – including in addition amyloid-PET and tau-PET markers – and (**C**) the validation sample. Circle size depicts statistical significance level. Please refer to **Figure 3** (main manuscript) for abbreviations of the fiber tracts. BrainV = brain volume, FDR = false discovery rate, WMHV = white matter hyperintensity volume.

Figure-e4

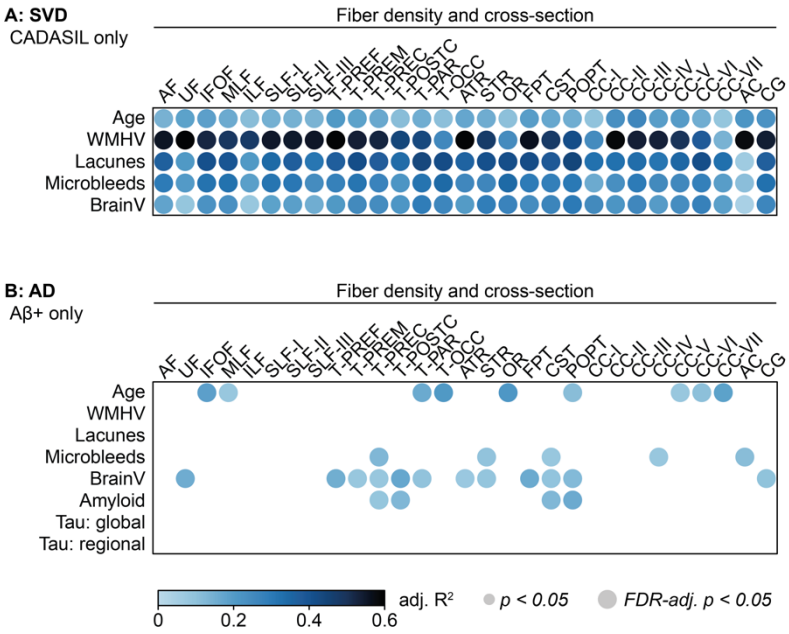

Sensitivity analysis for associations with the combined fixel metric fiber density and cross-section. Associations between disease markers in (**A**) only CADASIL patients from the SVD sample, and (**B**) only Aβ+ study participants from the AD sample. Effect sizes (adj. R^2) obtained from simple linear regression analyses are represented by color. Circle size depicts statistical significance level. Please refer to **Figure 3** for abbreviations of the fiber tracts. BrainV = brain volume, FDR = false discovery rate, WMHV = white matter hyperintensity volume.

Figure-e5

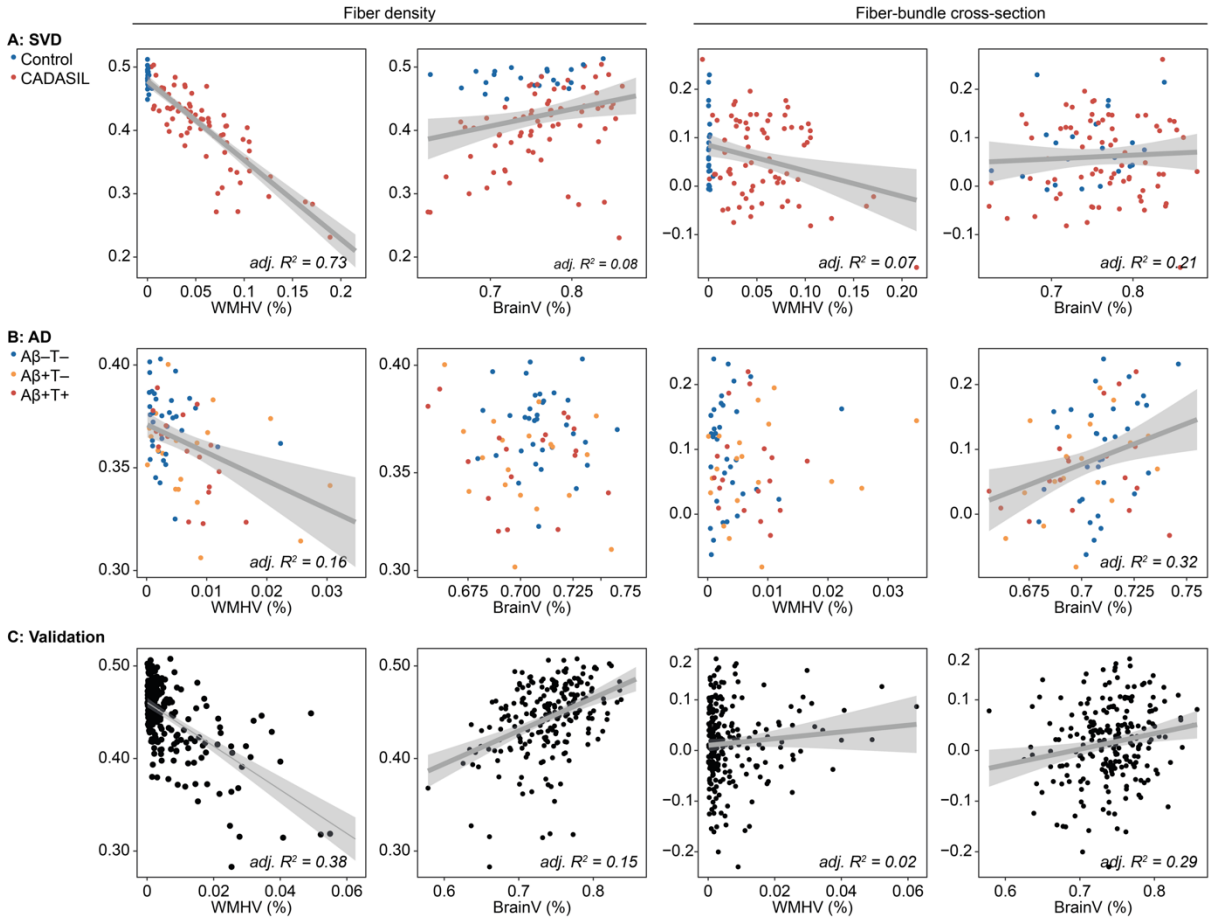

Scatterplots illustrating the key findings in a representative fiber tract (inferior fronto-occipital fasciculus). Associations between fixel metrics and white matter hyperintensity volume (WMHV) and brain volume (BrainV) in (**A**) SVD sample, (**B**) AD sample and (**C**) validation sample.

Supplementary Analysis: Scanner effects

To investigate scanner effects on fixel-based analysis (FBA), we analyzed an inter-site dataset of 10 CADASIL patients with multi-shell diffusion MRI acquired on two different scanners (Siemens Magnetom Prisma and Siemens Magnetom Skyra; see http://intersite.isd-muc.de). After performing FBA for each scanner separately following the pipeline in this study, we assessed the inter-site reproducibility with the intraclass correlation coefficient, ICC (2,1).

Reproducibility was excellent for both fiber density (ICC median=0.981; range[0.901; 0.998]) and fiber-bundle cross-section (ICC median=0.989; range[0.843; 0.999], suggesting that scanner differences play only a minor role in FBA when using the tract-average approach.

3. GENERAL DISCUSSION

In the following sections, main findings of Study I and II, their key implications, limitations and future directions are discussed.

3.1. Main findings

3.1.1. Study I

Our main finding of Study I was that structural brain network analysis does not show a meaningful benefit over simpler, skeleton-based white matter diffusion markers in explaining processing speed deficits in sporadic SVD. Furthermore, while almost all structural brain networks showed excellent test-retest reliability, they did not capture short-term disease progression in the high-frequency longitudinal dataset, in contrast to skeleton-based metrics. Opposed to our hypothesis, structural brain networks derived from multi-shell diffusion MRI did not perform better than those derived from a simpler tractography pipeline albeit modelling crossing fibers and enhancing anatomical precision through anatomical constraints (Tournier, Calamante, and Connelly 2012; Smith et al. 2012). Given that analysis steps are simpler and less prone to arbitrary design choices for skeleton-based markers compared to network analysis, these simpler diffusion markers remain the method of choice for SVD research, and potentially clinical routine. Our results demonstrate that tractography algorithm, node and edge definition have a substantial effect on brain network analysis, which highlights the need for standardization to facilitate comparisons between research studies.

3.1.2. Study II

Study II found that metrics derived from fixel-based analysis allow to disentangle effects of SVD and neurodegeneration on white matter fiber tracts. Specifically, fiber density of all white matter fiber tracts was strongly reduced in genetically defined SVD and highly associated with SVD imaging markers. Fiber-bundle cross-section was associated with brain volume, a marker of neurodegeneration. Both fiber density and fiber-bundle cross-section were reduced upon amyloid deposition in the Alzheimer's disease sample. However, concomitant SVD was highest in the Aβ positive group and after controlling for global WMH volume, the reductions in fiber density were attenuated, suggesting that the effect of amyloid on fiber density can at least partly be explained by concomitant SVD, e.g., due to CAA which is highly prevalent in Alzheimer's

disease (Attems and Jellinger 2014) and also captured by amyloid-PET (Charidimou, Farid, and Baron 2017). Notably, neither fiber density nor fiber-bundle cross-section were associated with tau deposition in the Alzheimer's disease sample.

With decreasing fiber density, fiber-bundle cross-section of the anterior thalamic radiation and the rostrum harboring the forceps minor increased when comparing patients with CADASIL to matched controls. Interestingly, these two key regions were previously found to be associated with processing speed deficits in SVD (Duering et al. 2014; Biesbroek, Weaver, and Biessels 2017). This finding might seem counter-intuitive at first, but might be explained by blood-brain barrier breakdown leading to vasogenic cerebral edema, i.e. an increase in intracellular water leading to expansion of the extracellular space and ultimately fiber tract swelling (Dhollander et al. 2021). Supporting the concept of vasogenic cerebral edema in SVD, increased white matter volume has previously been observed at the early stage of CADASIL (François De Guio et al. 2015), while increased brain tissue volumes with subtle blood-brain barrier leaking were found in sporadic SVD (Zhang et al. 2017). Yet, this post-hoc hypothesis explaining the increase in fiber-bundle cross-section observed in CADASIL requires validation in future studies.

3.2. Key implications

3.2.1. The need for standardizing network analysis to facilitate comparisons between research studies

Study I demonstrated that performance of network-based diffusion markers is highly dependent on tractography algorithm, node, and edge definition. Previous work already indicated that these design choices play a major role in determining network topology (Fornito, Zalesky, and Breakspear 2013; Zalesky et al. 2010), but the best approach for a network-based marker for SVD was not yet investigated. In Study I, networks derived from the deterministic, tensor-based tractography pipeline combined with the FA-edge and automated anatomical labeling (AAL)-node definition showed the highest clinical validity among network-based markers and excellent technical validity. Thus, future research might focus on this pipeline with FA-edge and AAL-node combination. It also became apparent that pre-defining edge and node definition is essential to keep the number of comparisons low if relying on statistical probabilities to draw conclusions. In our study, we obtained in total 26 measures of global efficiency of different

brain networks (i.e., 13 different edge definitions x 2 different node definitions). If we would have also assessed different graph measures, this number would have rapidly multiplied. Examining different edge and node definitions to reconstruct networks and only reporting those which are significant, i.e., *p*-hacking, is easy, yet, as evident in our study, the best node and edge combination in one sample might not translate to an independent sample and might even be a false positive after many statistical tests. To not fall into these pitfalls, it is essential to pre-define analysis concepts in network-based analysis. Pre-registering analysis concepts and planned statistical analyses via Open Science platforms (e.g., AsPredicted.org or the Open Science Framework) before carrying out any analysis is an ideal way to increase reproducibility and transparency in research (Simmons, Nelson, and Simonsohn 2021). Since biomedical research forms the basis for clinical trials, reproducible research findings are indispensable to facilitate the development of new therapies for SVD (Ioannidis 2005; Hillary and Medaglia 2020). In addition, consensus guidelines as proposed by expert panels are required to expand on previous STRIVE criteria (Wardlaw et al. 2013) towards latest MRI markers of SVD including network analysis to facilitate standardization and comparability across research studies.

3.2.2. Fixel metrics disentangle effects of SVD and neurodegeneration

Study II showed that metrics from fixel-based analysis allow to disentangle effects of SVD and neurodegeneration on white matter. Fixel-based diffusion markers thus offer the possibility to better understand the extent to which SVD and neurodegeneration contribute to cognitive impairment and other clinical manifestations in mixed disease. This furthermore facilitates disease-specific interventions targeting e.g., AD- or SVD-related brain alterations rather than managing disease-shared risk factors. Similarly, fixel metrics might be used to pre-select patients with high SVD burden and likely higher rate of progression to clinical end points as potential study participants for SVD-focused clinical trials. Enriching target populations and reducing the heterogeneity of underlying pathologies in clinical trials may allow the required sample size to be reduced, ultimately improving the methodology of clinical trials (Markus et al. 2022). Yet, in mixed disease, other age-related pathologies might play an additional role (Kapasi, DeCarli, and Schneider 2017) and it remains to be determined how these reflect in fixel metrics. Most studies employing fixel-based analysis in disease did not examine disease-specific effects on either of the fixel metrics, but instead focused on the combined fiber density and cross-section metric to confirm previous voxel-based findings of diffusion alterations by more advanced fiber-specific analyses (Dhollander et al. 2021).

Results of Study II further confirm previous work showing that SVD is a main contributor to alterations in tissue microstructure, as recently shown for diffusion tensor and free water imaging (Finsterwalder et al. 2020). Thus, SVD should always be accounted for in research studies investigating elderly participants. Even when neurodegenerative pathology is in focus, comorbid SVD is highly prevalent and thus at least a major confounder in research studies investigating elderly participants (Kapasi, DeCarli, and Schneider 2017; Arvanitakis et al. 2016). Ensuring that results are not driven by comorbid SVD (e.g. by controlling statistical analyses for SVD burden through quantification of conventional markers – WMH volumes, lacune and microbleed count – or inclusion of the SVD summary score (Staals et al. 2014)), is of utmost importance to provide a better understanding of underlying pathologies contributing to the observed effects.

3.4. Limitations

Several caveats of the work presented in this thesis need to be considered.

3.4.1. Study I

One limitation of the network analysis approach employed in Study I might be that we did not normalize the brain networks against null-models. Consequently, global efficiency values might be heavily influenced by the density of the structural network. However, white matter tissue alterations of SVD are likely to affect the density of the network as well (Boot et al. 2020) and thus, normalizing against null models might lead to unwanted overcorrection of disease effects. In addition, previous work on network analysis in SVD (Tuladhar et al. 2016; 2020; Boot et al. 2020) did not normalize against null models either and thus, to facilitate comparison with previous studies, we a priori decided against this normalization.

Another limitation might be the lack of biomarker characterization in the included samples and hence, comorbid Alzheimer's disease and other age-related diseases might have contributed to the results. While Study I might have benefitted from the inclusion of a sample with pure SVD, accurate segmentation of T1-weighted images of CADASIL patients is challenging, since the severe SVD lesions appearing hypointense on T1-weighted images are often misclassified as grey matter due to a reduced grey-white matter contrast in CADASIL patients (De Guio et al. 2014). Given that the anatomical constraints in the multi-shell pipeline rely on high-quality segmentations of T1-weighted images (Smith et al. 2012), these effects might have altered the

results in CADASIL or would have required postprocessing to an extent that it is no longer feasible as imaging marker for SVD in clinical trials or clinical routine.

3.4.2. Study II

The lack of biomarker characterization of the RUN DMC study also limited Study II. Hence, we can only assume that subjects of the validation sample are affected by mixed pathology. It would have been tempting to pool subjects across all samples into one large sample and predict the underlying pathology of each subject given observations in both fiber density and fiber-bundle cross-section. However, fixel-based analysis largely depends on (a set of) response functions and the scanner used for data acquisition and thus, the heterogeneity in diffusion protocols and scanners of the individual samples did not allow us to pool subjects.

Some of these limitations might be addressed in future studies (see next paragraph).

3.5. Future directions

3.5.1. Network based analysis to capture secondary neurodegeneration

Contrary to our hypotheses of Study I, network-based analysis did not capture short-term disease progression. One reason might be the rather short follow-up time of ten months in the high-frequency longitudinal dataset. While tracking short-term disease progression is of great interest for clinical trials with typically limited study duration considering costs and patient burden, network analysis might still be valuable to gain pathophysiological insights. SVD is considered a global brain disease, with focal lesions also having an impact on remote tissue structures leading to secondary degeneration (Duering et al. 2012; 2015). One might speculate that secondary degeneration leads to network alterations which can be assessed with brain network analysis, as shown in stroke (Crofts et al. 2011; Veldsman et al. 2020), rendering the network approach more suitable to assess long-term effects of the disease. Still, whether network markers are in this regard superior to the simpler, skeleton-based diffusion markers remains to be determined. Nonetheless, network-based analysis has provided pathological insight into the disease. Specifically, especially connections between rich club hubs, i.e. nodes that are highly interconnected, as well as central network connections have shown to be disrupted in SVD (Tuladhar et al. 2017; Reijmer et al. 2016).

3.5.2. Fiber density as surrogate marker for SVD

While blood-based biomarkers sensitive to the underlying pathology are on the rise in the Alzheimer's disease field (Teunissen et al. 2022), truly disease-specific markers for SVD are lacking. One reason might be that SVD is a complex cerebrovascular disease with likely many underlying disease pathways which are still incompletely understood (Wardlaw, Smith, and Dichgans 2019). Diffusion MRI markers are strongly associated with clinical deficits and very sensitive to disease progression (Konieczny et al. 2021), however, they are not disease-*specific*. Given findings of Study II, one might speculate fiber density to be a more specific marker for SVD than typical DTI metrics which simply reflect the magnitude and directionality of main water diffusion per voxel.

Future work is required to validate fiber density as a disease-specific marker for SVD, e.g. in animal models. A previous histology study found (apparent) fiber density obtained from high-resolution *ex vivo* diffusion MRI to be highly associated with axonal density in a rat model with induced unilateral retinal ischemia (Rojas-Vite et al. 2019). Importantly, apparent fiber density in crossing fibers complied with histopathological axonal density of crossing fibers in the chiasm. Yet, these findings do not easily translate to dementia patients and thus, future histology studies are needed to validate fiber density as SVD marker in mixed disease models. Animal models would furthermore allow to confirm the specificity of fixel metrics in a controlled environment, using transgenic animal models for pure Alzheimer's disease, pure SVD or models for mixed disease, e.g. by crossing the pure transgenic models.

Fiber density might be a promising candidate as surrogate marker in clinical trials facilitating the development of new therapies for SVD. Skeleton-based diffusion MRI markers have shown to reduce required sample sizes for clinical trials by approx. 60% compared to conventional MRI markers due to their high sensitivity in detecting subtle tissue alterations and their excellent test-retest reliability (Baykara et al. 2016; Benjamin et al. 2016; Konieczny et al. 2021). Yet, future work is needed to systematically assess the value of fiber density as surrogate marker for clinical trials. In this regard, longitudinal studies are needed to examine the sensitivity of fiber density to change upon disease progression. Given previous suggestions of lesion regression in SVD (van Leijsen, de Leeuw, and Tuladhar 2017; Leijsen et al. 2019), longitudinal studies will also inform us about the temporal dynamics of the observed reductions in fiber density as found in Study II. In addition, technical validation studies assessing the test-retest reliability and inter-site reproducibility of fiber density on different scanners will be essential to advance fiber density as surrogate marker of the disease for clinical trials.

3.5.3. Fiber-bundle cross-section as imaging marker for neurodegeneration

Neurodegeneration is characterized by neuronal loss and often caused by Alzheimer's disease, but also many other age-related diseases including SVD (Kovacs et al. 2013). As shown in Study II, fiber-bundle cross-section is highly sensitive towards neurodegeneration. Given that advanced fixel metrics capture fiber-specific tissue alterations and operate on the *sub*-voxel level, one might speculate fiber-bundle cross-section to be sensitive towards earliest neurodegenerative tissue alterations. As shown in multiple studies, local SVD lesions lead to remote tissue effects and secondary neurodegeneration (Duering et al. 2015; 2012). Thus, the fiber-bundle cross-section metric might also be used to examine remote effects of secondary neurodegeneration in SVD and their time course thereby expanding previous results to the fixel level.

Serum neurofilament light chain (NfL) is a blood marker of neuroaxonal injury reflecting axonal damage and has been applied in various neurological conditions, including multiple sclerosis, SVD and neurodegenerative diseases (Disanto et al. 2017; Duering, Konieczny, et al. 2018; Preische et al. 2019). To better understand the fundamentals of alterations in fiber-bundle cross-section, future work might assess associations between fiber-bundle cross-section and NfL levels. One might speculate that NfL is highly associated with fiber-bundle cross-section since both measure some degree of axonal damage but might follow different time courses.

3.5.4. Biophysical models

In contrast to voxel-averaged signal representations (e.g. diffusion tensor or kurtosis imaging), biophysical models aim to sketch the underlying white matter microstructure (Jelescu et al. 2020). Fixel-based analysis might also be considered a biophysical model. One disadvantage of the fixel-based analysis approach employed in Study II is the necessity of a group template based on which the fiber-bundle cross-section metric is derived (Raffelt et al. 2017). In addition, the current implementation relies on (averaged) response functions – in this case the average was computed over a subset of representative study participants. Thus, the proposed implementation as performed in Study II is ideal for group studies but does not translate to the individual patient yet and implementation in clinical routine involving monitoring of disease progression is challenging due to the dependency on response functions.

Other biophysical models have been proposed which might model similar tissue properties as fixel metrics in our study. We previously investigated the multicompartment model neurite

orientation dispersion and density imaging (NODDI) (Zhang et al. 2012). In two samples covering sporadic SVD and CADASIL, NODDI metrics were less sensitive to processing speed deficits and showed poorer test-retest reliability compared to metrics of DTI and DKI (Konieczny et al. 2021). One reason of the latter finding might be that in NODDI, the tissue compartments are not independent but additive. Thus, upon smallest tissue alterations due to e.g., measurement error, all tissue compartments are affected. New biophysical models are constantly emerging, and their potential as SVD markers has yet to be investigated. The applied analytical approach in Study I, i.e. pre-specifying hypotheses via pre-registration, the inclusion of an independent sample and systematic clinical and technical validation, offers an unbiased and transparent strategy to validate diffusion markers for clinical trials and eventually clinical routine.

3.6. Conclusion

Tractography-based diffusion MRI markers are appealing in SVD research since they allow to approach the disease as disconnection syndrome through structural brain network analysis and enable to derive fiber-specific properties of white matter fiber tracts through fixel-based analysis. As demonstrated in this thesis, albeit excellent test-retest reliability, structural brain network analysis does not show an added benefit over well-established diffusion markers in explaining cognitive deficits in SVD or monitoring disease progression and thus, skeleton-based markers of diffusion tensor imaging remain the preferred choice for these purposes. Fixel-based analysis of white matter fiber tracts yields promise to disentangle effects of SVD and neurodegeneration in mixed disease. As shown in Study II, fiber density is highly sensitive towards SVD-related brain alterations while neurodegeneration is captured by fiber-bundle cross-section. Future research should address gaps in technical validation and apply fixel-based analysis in longitudinal datasets in order to facilitate widespread clinical use and the development of a surrogate endpoint for clinical trials.

4. REFERENCES OF INTRODUCTION AND GENERAL DISCUSSION

Araque Caballero, Miguel Ángel, Marc Suárez-Calvet, Marco Duering, Nicolai Franzmeier, Tammie Benzinger, Anne M Fagan, Randall J Bateman, et al. 2018. 'White Matter Diffusion Alterations Precede Symptom Onset in Autosomal Dominant Alzheimer's Disease'. *Brain* 141 (10): 3065–80. https://doi.org/10.1093/brain/awy229.

Arvanitakis, Zoe, Ana W. Capuano, Sue E. Leurgans, David A. Bennett, and Julie A. Schneider. 2016. 'Relation of Cerebral Vessel Disease to Alzheimer's Disease Dementia and Cognitive Function in Older Persons: A Cross-Sectional Study'. *The Lancet. Neurology* 15 (9): 934–43. https://doi.org/10.1016/S1474-4422(16)30029-1.

Attems, Johannes, and Kurt A. Jellinger. 2014. 'The Overlap between Vascular Disease and Alzheimer's Disease - Lessons from Pathology'. *BMC Medicine* 12 (1): 206. https://doi.org/10.1186/s12916-014-0206-2.

Baykara, Ebru, Benno Gesierich, Ruth Adam, Anil Man Tuladhar, J. Matthijs Biesbroek, Huiberdina L. Koek, Stefan Ropele, et al. 2016. 'A Novel Imaging Marker for Small Vessel Disease Based on Skeletonization of White Matter Tracts and Diffusion Histograms'. *Annals of Neurology* 80 (4): 581–92. https://doi.org/10.1002/ana.24758.

Benjamin, Philip, Eva Zeestraten, Christian Lambert, Irina Chis Ster, Owen A. Williams, Andrew J. Lawrence, Bhavini Patel, Andrew D. MacKinnon, Thomas R. Barrick, and Hugh S. Markus. 2016. 'Progression of MRI Markers in Cerebral Small Vessel Disease: Sample Size Considerations for Clinical Trials'. *Journal of Cerebral Blood Flow and Metabolism: Official Journal of the International Society of Cerebral Blood Flow and Metabolism* 36 (1): 228–40. https://doi.org/10.1038/jcbfm.2015.113.

Biesbroek, J. Matthijs, Nick A. Weaver, and Geert Jan Biessels. 2017. 'Lesion Location and Cognitive Impact of Cerebral Small Vessel Disease'. *Clinical Science* 131 (8): 715–28. https://doi.org/10.1042/CS20160452.

Biffi, Alessandro, and Steven M. Greenberg. 2011. 'Cerebral Amyloid Angiopathy: A Systematic Review'. *Journal of Clinical Neurology (Seoul, Korea)* 7 (1): 1–9. https://doi.org/10.3988/jcn.2011.7.1.1.

Boot, Esther M., Esther MC van Leijsen, Mayra I. Bergkamp, Roy P. C. Kessels, David G. Norris, Frank-Erik de Leeuw, and Anil M. Tuladhar. 2020. 'Structural Network Efficiency Predicts Cognitive Decline in Cerebral Small Vessel Disease'. *NeuroImage: Clinical* 27 (January): 102325. https://doi.org/10.1016/j.nicl.2020.102325.

Brink, Hilde van den, Fergus N Doubal, and Marco Duering. 2022. 'Advanced MRI in Cerebral Small Vessel Disease'. *International Journal of Stroke*, March, 17474930221091880. https://doi.org/10.1177/17474930221091879.

Chabriat, Hugues, Anne Joutel, Martin Dichgans, Elizabeth Tournier-Lasserve, and Marie-Germaine Bousser. 2009. 'CADASIL'. *The Lancet Neurology* 8 (7): 643–53. https://doi.org/10.1016/S1474-4422(09)70127-9.

Charidimou, Andreas, Gregoire Boulouis, Matthew P Frosch, Jean-Claude Baron, Marco Pasi, Jean Francois Albucher, Gargi Banerjee, et al. 2022. 'The Boston Criteria Version 2.0 for Cerebral Amyloid Angiopathy: A Multicentre, Retrospective, MRI–Neuropathology Diagnostic Accuracy Study'. *The Lancet Neurology* 21 (8): 714–25. https://doi.org/10.1016/S1474-4422(22)00208-3.

Charidimou, Andreas, Karim Farid, and Jean-Claude Baron. 2017. 'Amyloid-PET in Sporadic Cerebral Amyloid Angiopathy: A Diagnostic Accuracy Meta-Analysis'. *Neurology* 89 (14): 1490–98. https://doi.org/10.1212/WNL.0000000000004539.

Charlton, R. A., R. G. Morris, A. Nitkunan, and H. S. Markus. 2006. 'The Cognitive Profiles of CADASIL and Sporadic Small Vessel Disease'. *Neurology* 66 (10): 1523–26. https://doi.org/10.1212/01.wnl.0000216270.02610.7e.

Crofts, J.J., D.J. Higham, R. Bosnell, S. Jbabdi, P.M. Matthews, T.E.J. Behrens, and H. Johansen-Berg. 2011. 'Network Analysis Detects Changes in the Contralesional Hemisphere Following Stroke'. *NeuroImage* 54 (1): 161–69. https://doi.org/10.1016/j.neuroimage.2010.08.032.

De Guio, F., S. Reyes, M. Duering, L. Pirpamer, H. Chabriat, and E. Jouvent. 2014. 'Decreased T1 Contrast between Gray Matter and Normal-Appearing White Matter in CADASIL'. *AJNR. American Journal of Neuroradiology* 35 (1): 72–76. https://doi.org/10.3174/ajnr.A3639.

De Guio, François, Jean-François Mangin, Marco Duering, Stefan Ropele, Hugues Chabriat, and Eric Jouvent. 2015. 'White Matter Edema at the Early Stage of Cerebral Autosomal-Dominant Arteriopathy with Subcortical Infarcts and Leukoencephalopathy'. *Stroke* 46 (1): 258–61. https://doi.org/10.1161/STROKEAHA.114.007018.

Dhollander, Thijs, Adam Clemente, Mervyn Singh, Frederique Boonstra, Oren Civier, Juan Dominguez Duque, Natalia Egorova, et al. 2021. 'Fixel-Based Analysis of Diffusion MRI: Methods, Applications, Challenges and Opportunities'. *NeuroImage* 241 (November): 118417. https://doi.org/10.1016/j.neuroimage.2021.118417.

Dichgans, Martin, and Didier Leys. 2017. 'Vascular Cognitive Impairment'. *Circulation Research* 120 (3): 573–91. https://doi.org/10.1161/CIRCRESAHA.116.308426.

Disanto, Giulio, Christian Barro, Pascal Benkert, Yvonne Naegelin, Sabine Schädelin, Antonella Giardiello, Chiara Zecca, et al. 2017. 'Serum Neurofilament Light: A Biomarker of Neuronal Damage in Multiple Sclerosis'. *Annals of Neurology* 81 (6): 857–70. https://doi.org/10.1002/ana.24954.

Duchesnay, Edouard, Fouad Hadj Selem, François De Guio, Mathieu Dubois, Jean-François Mangin, Marco Duering, Stefan Ropele, et al. 2018. 'Different Types of White Matter Hyperintensities in CADASIL'. *Frontiers in Neurology* 9. https://www.frontiersin.org/article/10.3389/fneur.2018.00526.

Duering, Marco, Sofia Finsterwalder, Ebru Baykara, Anil Man Tuladhar, Benno Gesierich, Marek J. Konieczny, Rainer Malik, et al. 2018. 'Free Water Determines Diffusion Alterations and Clinical Status in Cerebral Small Vessel Disease'. *Alzheimer's & Dementia : The Journal of the Alzheimer's Association* 14 (6): 764–74. https://doi.org/10.1016/j.jalz.2017.12.007.

Duering, Marco, Benno Gesierich, Stephan Seiler, Lukas Pirpamer, Mariya Gonik, Edith Hofer, Eric Jouvent, et al. 2014. 'Strategic White Matter Tracts for Processing Speed Deficits in Age-Related Small Vessel Disease'. *Neurology* 82 (22): 1946–50. https://doi.org/10.1212/WNL.0000000000000475.

Duering, Marco, Marek J. Konieczny, Steffen Tiedt, Ebru Baykara, Anil Man Tuladhar, Esther van Leijsen, Philippe Lyrer, et al. 2018. 'Serum Neurofilament Light Chain Levels Are Related to Small Vessel Disease Burden'. *Journal of Stroke* 20 (2): 228–38. https://doi.org/10.5853/jos.2017.02565.

Duering, Marco, Ruthger Righart, Endy Csanadi, Eric Jouvent, Dominique Hervé, Hugues Chabriat, and Martin Dichgans. 2012. 'Incident Subcortical Infarcts Induce Focal Thinning in Connected Cortical Regions'. *Neurology* 79 (20): 2025–28. https://doi.org/10.1212/WNL.0b013e3182749f39.

Duering, Marco, Ruthger Righart, Frank Arne Wollenweber, Vera Zietemann, Benno Gesierich, and Martin Dichgans. 2015. 'Acute Infarcts Cause Focal Thinning in Remote Cortex via Degeneration of Connecting Fiber Tracts'. *Neurology* 84 (16): 1685–92. https://doi.org/10.1212/WNL.0000000000001502.

Finsterwalder, Sofia, Naomi Vlegels, Benno Gesierich, Miguel Á. Araque Caballero, Nick A. Weaver, Nicolai Franzmeier, Marios K. Georgakis, et al. 2020. 'Small Vessel Disease More than Alzheimer's Disease Determines Diffusion MRI Alterations in Memory

Clinic Patients'. *Alzheimer's & Dementia* 16 (11): 1504–14. https://doi.org/10.1002/alz.12150.

Flier, Wiesje M. van der, Ingmar Skoog, Julie A. Schneider, Leonardo Pantoni, Vincent Mok, Christopher L. H. Chen, and Philip Scheltens. 2018. 'Vascular Cognitive Impairment'. *Nature Reviews Disease Primers* 4 (1): 1–16. https://doi.org/10.1038/nrdp.2018.3.

Fornito, Alex, Andrew Zalesky, and Michael Breakspear. 2013. 'Graph Analysis of the Human Connectome: Promise, Progress, and Pitfalls'. *NeuroImage*, Mapping the Connectome, 80 (October): 426–44. https://doi.org/10.1016/j.neuroimage.2013.04.087.

Greenberg, Steven M., Brian J. Bacskai, Mar Hernandez-Guillamon, Jeremy Pruzin, Reisa Sperling, and Susanne J. van Veluw. 2020. 'Cerebral Amyloid Angiopathy and Alzheimer Disease — One Peptide, Two Pathways'. *Nature Reviews. Neurology* 16 (1): 30–42. https://doi.org/10.1038/s41582-019-0281-2.

Greenberg, Steven M., and Andreas Charidimou. 2018. 'Diagnosis of Cerebral Amyloid Angiopathy'. *Stroke* 49 (2): 491–97. https://doi.org/10.1161/STROKEAHA.117.016990.

Hamilton, Olivia K. L., Ellen V. Backhouse, Esther Janssen, Angela C. C. Jochems, Caragh Maher, Tuula E. Ritakari, Anna J. Stevenson, Lihua Xia, Ian J. Deary, and Joanna M. Wardlaw. 2021. 'Cognitive Impairment in Sporadic Cerebral Small Vessel Disease: A Systematic Review and Meta-Analysis'. *Alzheimer's & Dementia* 17 (4): 665–85. https://doi.org/10.1002/alz.12221.

Hillary, Frank G., and John D. Medaglia. 2020. 'What the Replication Crisis Means for Intervention Science'. *International Journal of Psychophysiology : Official Journal of the International Organization of Psychophysiology* 154 (August): 3–5. https://doi.org/10.1016/j.ijpsycho.2019.05.006.

Iadecola, Costantino, Marco Duering, Vladimir Hachinski, Anne Joutel, Sarah T. Pendlebury, Julie A. Schneider, and Martin Dichgans. 2019. 'Vascular Cognitive Impairment and Dementia'. *Journal of the American College of Cardiology* 73 (25): 3326–44. https://doi.org/10.1016/j.jacc.2019.04.034.

Ioannidis, John P. A. 2005. 'Why Most Published Research Findings Are False'. *PLOS Medicine* 2 (8): e124. https://doi.org/10.1371/journal.pmed.0020124.

Jack, Clifford R., David A. Bennett, Kaj Blennow, Maria C. Carrillo, Billy Dunn, Samantha Budd Haeberlein, David M. Holtzman, et al. 2018. 'NIA-AA Research Framework: Toward a Biological Definition of Alzheimer's Disease'. *Alzheimer's & Dementia* 14 (4): 535–62. https://doi.org/10.1016/j.jalz.2018.02.018.

Jelescu, Ileana O., Marco Palombo, Francesca Bagnato, and Kurt G. Schilling. 2020. 'Challenges for Biophysical Modeling of Microstructure'. *Journal of Neuroscience Methods* 344 (October): 108861. https://doi.org/10.1016/j.jneumeth.2020.108861.

Jensen, Jens H., Joseph A. Helpern, Anita Ramani, Hanzhang Lu, and Kyle Kaczynski. 2005. 'Diffusional Kurtosis Imaging: The Quantification of Non-Gaussian Water Diffusion by Means of Magnetic Resonance Imaging'. *Magnetic Resonance in Medicine* 53 (6): 1432–40. https://doi.org/10.1002/mrm.20508.

Jeurissen, Ben, Alexander Leemans, Jacques-Donald Tournier, Derek K. Jones, and Jan Sijbers. 2013. 'Investigating the Prevalence of Complex Fiber Configurations in White Matter Tissue with Diffusion Magnetic Resonance Imaging'. *Human Brain Mapping* 34 (11): 2747–66.

Jiang, Hangyi, Peter C. M. van Zijl, Jinsuh Kim, Godfrey D. Pearlson, and Susumu Mori. 2006. 'DtiStudio: Resource Program for Diffusion Tensor Computation and Fiber Bundle Tracking'. *Computer Methods and Programs in Biomedicine* 81 (2): 106–16. https://doi.org/10.1016/j.cmpb.2005.08.004.

Jones, Derek K., Thomas R. Knösche, and Robert Turner. 2013. 'White Matter Integrity, Fiber Count, and Other Fallacies: The Do's and Don'ts of Diffusion MRI'. *NeuroImage* 73 (June): 239–54. https://doi.org/10.1016/j.neuroimage.2012.06.081.

Kalaria, Raj N. 2016. 'Neuropathological Diagnosis of Vascular Cognitive Impairment and Vascular Dementia with Implications for Alzheimer's Disease'. *Acta Neuropathologica* 131 (5): 659–85. https://doi.org/10.1007/s00401-016-1571-z.

Kapasi, Alifiya, Charles DeCarli, and Julie A. Schneider. 2017. 'Impact of Multiple Pathologies on the Threshold for Clinically Overt Dementia'. *Acta Neuropathologica* 134 (2): 171–86. https://doi.org/10.1007/s00401-017-1717-7.

Konieczny, Marek J., Anna Dewenter, Annemieke ter Telgte, Benno Gesierich, Kim Wiegertjes, Sofia Finsterwalder, Anna Kopczak, et al. 2021. 'Multi-Shell Diffusion MRI Models for White Matter Characterization in Cerebral Small Vessel Disease'. *Neurology* 96 (5): e698–708. https://doi.org/10.1212/WNL.0000000000011213.

Kovacs, Gabor G., Ivan Milenkovic, Adelheid Wöhrer, Romana Höftberger, Ellen Gelpi, Christine Haberler, Selma Hönigschnabl, et al. 2013. 'Non-Alzheimer Neurodegenerative Pathologies and Their Combinations Are More Frequent than Commonly Believed in the Elderly Brain: A Community-Based Autopsy Series'. *Acta Neuropathologica* 126 (3): 365–84. https://doi.org/10.1007/s00401-013-1157-y.

Leeuw, F.-E. de, J. C. de Groot, E. Achten, M. Oudkerk, L. M. P. Ramos, R. Heijboer, A. Hofman, J. Jolles, J. van Gijn, and M. M. B. Breteler. 2001. 'Prevalence of Cerebral White Matter Lesions in Elderly People: A Population Based Magnetic Resonance Imaging Study. The Rotterdam Scan Study'. *Journal of Neurology, Neurosurgery & Psychiatry* 70 (1): 9–14. https://doi.org/10.1136/jnnp.70.1.9.

Leijsen, Esther M. C. van, Frank-Erik de Leeuw, and Anil M. Tuladhar. 2017. 'Disease Progression and Regression in Sporadic Small Vessel Disease-Insights from Neuroimaging'. *Clinical Science (London, England: 1979)* 131 (12): 1191–1206. https://doi.org/10.1042/CS20160384.

Leijsen, Esther MC van, Mayra I Bergkamp, Ingeborg WM van Uden, Sjacky Cooijmans, Mohsen Ghafoorian, Helena M van der Holst, David G Norris, et al. 2019. 'Cognitive Consequences of Regression of Cerebral Small Vessel Disease'. *European Stroke Journal* 4 (1): 85–89. https://doi.org/10.1177/2396987318820790.

Maillard, Pauline, Evan Fletcher, Samuel N. Lockhart, Alexandra E. Roach, Bruce Reed, Dan Mungas, Charles DeCarli, and Owen T. Carmichael. 2014. 'White Matter Hyperintensities and Their Penumbra Lie Along a Continuum of Injury in the Aging Brain'. *Stroke* 45 (6): 1721–26. https://doi.org/10.1161/STROKEAHA.113.004084.

Markus, H. S., R. J. Martin, M. A. Simpson, Y. B. Dong, N. Ali, A. H. Crosby, and J. F. Powell. 2002. 'Diagnostic Strategies in CADASIL'. *Neurology* 59 (8): 1134–38. https://doi.org/10.1212/WNL.59.8.1134.

Markus, Hugh S., Wiesje M. van Der Flier, Eric E. Smith, Philip Bath, Geert Jan Biessels, Emily Briceno, Amy Brodtman, et al. 2022. 'Framework for Clinical Trials in Cerebral Small Vessel Disease (FINESSE): A Review'. *JAMA Neurology*, August. https://doi.org/10.1001/jamaneurol.2022.2262.

Nasrabady, Sara E., Batool Rizvi, James E. Goldman, and Adam M. Brickman. 2018. 'White Matter Changes in Alzheimer's Disease: A Focus on Myelin and Oligodendrocytes'. *Acta Neuropathologica Communications* 6 (1): 22. https://doi.org/10.1186/s40478-018-0515-3.

Nucifora, Paolo G. P., Ragini Verma, Seung-Koo Lee, and Elias R. Melhem. 2007. 'Diffusion-Tensor MR Imaging and Tractography: Exploring Brain Microstructure and Connectivity'. *Radiology* 245 (2): 367–84. https://doi.org/10.1148/radiol.2452060445.

P. Simmons, Joseph, Leif D. Nelson, and Uri Simonsohn. 2021. 'Pre-Registration: Why and How'. *Journal of Consumer Psychology* 31 (1): 151–62. https://doi.org/10.1002/jcpy.1208.

Pantoni, Leonardo. 2010. 'Cerebral Small Vessel Disease: From Pathogenesis and Clinical Characteristics to Therapeutic Challenges'. *The Lancet Neurology* 9 (7): 689–701. https://doi.org/10.1016/S1474-4422(10)70104-6.

Pichet Binette, Alexa, Guillaume Theaud, François Rheault, Maggie Roy, D Louis Collins, Johannes Levin, Hiroshi Mori, et al. 2021. 'Bundle-Specific Associations between White Matter Microstructure and Aβ and Tau Pathology in Preclinical Alzheimer's Disease'. Edited by Tamar R Makin, Morgan Barense, Arun Bokde, Alfie Wearn, and Hakon Grydeland. *ELife* 10: e62929. https://doi.org/10.7554/eLife.62929.

Preische, Oliver, Stephanie A. Schultz, Anja Apel, Jens Kuhle, Stephan A. Kaeser, Christian Barro, Susanne Gräber, et al. 2019. 'Serum Neurofilament Dynamics Predicts Neurodegeneration and Clinical Progression in Presymptomatic Alzheimer's Disease'. *Nature Medicine* 25 (2): 277–83. https://doi.org/10.1038/s41591-018-0304-3.

Raffelt, David A., J. -Donald Tournier, Robert E. Smith, David N. Vaughan, Graeme Jackson, Gerard R. Ridgway, and Alan Connelly. 2017. 'Investigating White Matter Fibre Density and Morphology Using Fixel-Based Analysis'. *NeuroImage* 144 (January): 58–73. https://doi.org/10.1016/j.neuroimage.2016.09.029.

Raffelt, David, J. -Donald Tournier, Stephen Rose, Gerard R. Ridgway, Robert Henderson, Stuart Crozier, Olivier Salvado, and Alan Connelly. 2012. 'Apparent Fibre Density: A Novel Measure for the Analysis of Diffusion-Weighted Magnetic Resonance Images'. *NeuroImage* 59 (4): 3976–94. https://doi.org/10.1016/j.neuroimage.2011.10.045.

Raghavan, Sheelakumari, Scott A. Przybelski, Robert I. Reid, Timothy G. Lesnick, Vijay K. Ramanan, Hugo Botha, Billie J. Matchett, et al. 2022. 'White Matter Damage Due to Vascular, Tau, and TDP-43 Pathologies and Its Relevance to Cognition'. *Acta Neuropathologica Communications* 10 (1): 16. https://doi.org/10.1186/s40478-022-01319-6.

Raja, Rajikha, Gary Rosenberg, and Arvind Caprihan. 2019. 'Review of Diffusion MRI Studies in Chronic White Matter Diseases'. *Neuroscience Letters* 694 (February): 198–207. https://doi.org/10.1016/j.neulet.2018.12.007.

Reijmer, Yael D., Panagiotis Fotiadis, Giovanni Piantoni, Gregoire Boulouis, Kathleen E. Kelly, Mahmut E. Gurol, Alexander Leemans, Michael J. O'Sullivan, Steven M. Greenberg, and Anand Viswanathan. 2016. 'Small Vessel Disease and Cognitive Impairment: The Relevance of Central Network Connections'. *Human Brain Mapping* 37 (7): 2446–54. https://doi.org/10.1002/hbm.23186.

Rojas-Vite, Gilberto, Ricardo Coronado-Leija, Omar Narvaez-Delgado, Alonso Ramírez-Manzanares, José Luis Marroquín, Ramsés Noguez-Imm, Marcos L. Aranda, Benoit Scherrer, Jorge Larriva-Sahd, and Luis Concha. 2019. 'Histological Validation of Per-Bundle Water Diffusion Metrics within a Region of Fiber Crossing Following Axonal Degeneration'. *NeuroImage* 201 (November): 116013. https://doi.org/10.1016/j.neuroimage.2019.116013.

Rubinov, Mikail, and Olaf Sporns. 2010. 'Complex Network Measures of Brain Connectivity: Uses and Interpretations'. *NeuroImage*, Computational Models of the Brain, 52 (3): 1059–69. https://doi.org/10.1016/j.neuroimage.2009.10.003.

Salvadori, Emilia, Michela Brambilla, Giorgia Maestri, Alessia Nicotra, Ilaria Cova, Simone Pomati, and Leonardo Pantoni. 2022. 'The Clinical Profile of Cerebral Small Vessel Disease: Toward an Evidence-Based Identification of Cognitive Markers'. *Alzheimer's & Dementia: The Journal of the Alzheimer's Association*, March. https://doi.org/10.1002/alz.12650.

Schilling, Kurt G., François Rheault, Laurent Petit, Colin B. Hansen, Vishwesh Nath, Fang-Cheng Yeh, Gabriel Girard, et al. 2021. 'Tractography Dissection Variability: What Happens When 42 Groups Dissect 14 White Matter Bundles on the Same Dataset?' *NeuroImage* 243 (November): 118502. https://doi.org/10.1016/j.neuroimage.2021.118502.

Singhal, Sumeet, Philip Rich, and Hugh S. Markus. 2005. 'The Spatial Distribution of MR Imaging Abnormalities in Cerebral Autosomal Dominant Arteriopathy with Subcortical Infarcts and Leukoencephalopathy and Their Relationship to Age and Clinical Features'. *American Journal of Neuroradiology* 26 (10): 2481–87. http://www.ajnr.org/content/26/10/2481.

Smith, Robert E., Jacques-Donald Tournier, Fernando Calamante, and Alan Connelly. 2012. 'Anatomically-Constrained Tractography: Improved Diffusion MRI Streamlines Tractography through Effective Use of Anatomical Information'. *NeuroImage* 62 (3): 1924–38. https://doi.org/10.1016/j.neuroimage.2012.06.005.

Smith, Stephen M., Mark Jenkinson, Heidi Johansen-Berg, Daniel Rueckert, Thomas E. Nichols, Clare E. Mackay, Kate E. Watkins, et al. 2006. 'Tract-Based Spatial Statistics: Voxelwise Analysis of Multi-Subject Diffusion Data'. *NeuroImage* 31 (4): 1487–1505. https://doi.org/10.1016/j.neuroimage.2006.02.024.

Staals, Julie, Stephen D. J. Makin, Fergus N. Doubal, Martin S. Dennis, and Joanna M. Wardlaw. 2014. 'Stroke Subtype, Vascular Risk Factors, and Total MRI Brain Small-Vessel Disease Burden'. *Neurology* 83 (14): 1228–34. https://doi.org/10.1212/WNL.0000000000000837.

Tabesh, Ali, Jens H. Jensen, Babak A. Ardekani, and Joseph A. Helpern. 2011. 'Estimation of Tensors and Tensor-Derived Measures in Diffusional Kurtosis Imaging'. *Magnetic Resonance in Medicine* 65 (3): 823–36. https://doi.org/10.1002/mrm.22655.

Tax, Chantal M. W., Matteo Bastiani, Jelle Veraart, Eleftherios Garyfallidis, and M. Okan Irfanoglu. 2022. 'What's New and What's next in Diffusion MRI Preprocessing'. *NeuroImage* 249 (April): 118830. https://doi.org/10.1016/j.neuroimage.2021.118830.

Telgte, Annemieke ter, Esther M. C. van Leijsen, Kim Wiegertjes, Catharina J. M. Klijn, Anil M. Tuladhar, and Frank-Erik de Leeuw. 2018. 'Cerebral Small Vessel Disease: From a Focal to a Global Perspective'. *Nature Reviews Neurology* 14 (7): 387–98. https://doi.org/10.1038/s41582-018-0014-y.

Teunissen, Charlotte E, Inge M W Verberk, Elisabeth H Thijssen, Lisa Vermunt, Oskar Hansson, Henrik Zetterberg, Wiesje M van der Flier, Michelle M Mielke, and Marta del Campo. 2022. 'Blood-Based Biomarkers for Alzheimer's Disease: Towards Clinical Implementation'. *The Lancet Neurology* 21 (1): 66–77. https://doi.org/10.1016/S1474-4422(21)00361-6.

Tournier, J-Donald, Fernando Calamante, and Alan Connelly. 2012. 'MRtrix: Diffusion Tractography in Crossing Fiber Regions'. *International Journal of Imaging Systems and Technology* 22 (1): 53–66. https://doi.org/10.1002/ima.22005.

Tournier, J-Donald, Robert Smith, David Raffelt, Rami Tabbara, Thijs Dhollander, Maximilian Pietsch, Daan Christiaens, Ben Jeurissen, Chun-Hung Yeh, and Alan Connelly. 2019. 'MRtrix3: A Fast, Flexible and Open Software Framework for Medical Image Processing and Visualisation'. *NeuroImage* 202 (November): 116137. https://doi.org/10.1016/j.neuroimage.2019.116137.

Tuladhar, Anil M., Andrew Lawrence, David G. Norris, Thomas R. Barrick, Hugh S. Markus, and Frank-Erik de Leeuw. 2017. 'Disruption of Rich Club Organisation in Cerebral Small Vessel Disease'. *Human Brain Mapping* 38 (4): 1751–66. https://doi.org/10.1002/hbm.23479.

Tuladhar, Anil M., Jonathan Tay, Esther van Leijsen, Andrew J. Lawrence, Ingeborg Wilhelmina Maria van Uden, Mayra Bergkamp, Ellen van der Holst, et al. 2020.

'Structural Network Changes in Cerebral Small Vessel Disease'. *Journal of Neurology, Neurosurgery & Psychiatry* 91 (2): 196–203. https://doi.org/10.1136/jnnp-2019-321767.

Tuladhar, Anil M., Ingeborg W.M. van Uden, Loes C.A. Rutten-Jacobs, Andrew Lawrence, Helena van der Holst, Anouk van Norden, Karlijn de Laat, et al. 2016. 'Structural Network Efficiency Predicts Conversion to Dementia'. *Neurology* 86 (12): 1112–19. https://doi.org/10.1212/WNL.0000000000002502.

Veldsman, Michele, Hsiao-Ju Cheng, Fang Ji, Emilio Werden, Mohamed Salah Khlif, Kwun Kei Ng, Joseph K W Lim, et al. 2020. 'Degeneration of Structural Brain Networks Is Associated with Cognitive Decline after Ischaemic Stroke'. *Brain Communications* 2 (2): fcaa155. https://doi.org/10.1093/braincomms/fcaa155.

Vemuri, Prashanthi, Charles Decarli, and Marco Duering. 2022. 'Imaging Markers of Vascular Brain Health: Quantification, Clinical Implications, and Future Directions'. *Stroke* 53 (2): 416–26. https://doi.org/10.1161/STROKEAHA.120.032611.

Viswanathan, Anand, and Steven M. Greenberg. 2011. 'Cerebral Amyloid Angiopathy in the Elderly'. *Annals of Neurology* 70 (6): 871–80. https://doi.org/10.1002/ana.22516.

Walsh, Jessica, Dan J Tozer, Hasan Sari, Young T Hong, Anna Drazyk, Guy Williams, N Jon Shah, et al. 2021. 'Microglial Activation and Blood–Brain Barrier Permeability in Cerebral Small Vessel Disease'. *Brain*, May, awab003. https://doi.org/10.1093/brain/awab003.

Wardlaw, JM, C Smith, and M Dichgans. 2013. 'Mechanisms Underlying Sporadic Cerebral Small Vessel Disease: Insights from Neuroimaging'. *Lancet Neurology* 12 (5): 10.1016/S1474-4422(13)70060-7. https://doi.org/10.1016/S1474-4422(13)70060-7.

Wardlaw, Joanna M, Colin Smith, and Martin Dichgans. 2019. 'Small Vessel Disease: Mechanisms and Clinical Implications'. *The Lancet Neurology* 18 (7): 684–96. https://doi.org/10.1016/S1474-4422(19)30079-1.

Wardlaw, Joanna M, Eric E Smith, Geert J Biessels, Charlotte Cordonnier, Franz Fazekas, Richard Frayne, Richard I Lindley, et al. 2013. 'Neuroimaging Standards for Research into Small Vessel Disease and Its Contribution to Ageing and Neurodegeneration'. *The Lancet Neurology* 12 (8): 822–38. https://doi.org/10.1016/S1474-4422(13)70124-8.

Warrington, Shaun, Katherine L. Bryant, Alexandr A. Khrapitchev, Jerome Sallet, Marina Charquero-Ballester, Gwenaëlle Douaud, Saad Jbabdi, Rogier B. Mars, and Stamatios N. Sotiropoulos. 2020. 'XTRACT - Standardised Protocols for Automated Tractography in the Human and Macaque Brain'. *NeuroImage* 217 (August): 116923. https://doi.org/10.1016/j.neuroimage.2020.116923.

Wasserthal, Jakob, Peter Neher, and Klaus H. Maier-Hein. 2018. 'TractSeg - Fast and Accurate White Matter Tract Segmentation'. *NeuroImage* 183 (December): 239–53. https://doi.org/10.1016/j.neuroimage.2018.07.070.

Wollenweber, Frank Arne, Ebru Baykara, Marialuisa Zedde, Benno Gesierich, Melanie Achmüller, Eric Jouvent, Anand Viswanathan, et al. 2017. 'Cortical Superficial Siderosis in Different Types of Cerebral Small Vessel Disease'. *Stroke* 48 (5): 1404–7. https://doi.org/10.1161/STROKEAHA.117.016833.

Zalesky, Andrew, Alex Fornito, Ian H. Harding, Luca Cocchi, Murat Yücel, Christos Pantelis, and Edward T. Bullmore. 2010. 'Whole-Brain Anatomical Networks: Does the Choice of Nodes Matter?' *NeuroImage* 50 (3): 970–83. https://doi.org/10.1016/j.neuroimage.2009.12.027.

Zhang, C. Eleana, Sau May Wong, Harm J. van de Haar, Julie Staals, Jacobus F. A. Jansen, Cécile R. L. P. N. Jeukens, Paul A. M. Hofman, Robert J. van Oostenbrugge, and Walter H. Backes. 2017. 'Blood–Brain Barrier Leakage Is More Widespread in Patients with Cerebral Small Vessel Disease'. *Neurology* 88 (5): 426–32. https://doi.org/10.1212/WNL.0000000000003556.

Zhang, Hui, Torben Schneider, Claudia A. Wheeler-Kingshott, and Daniel C. Alexander. 2012. 'NODDI: Practical in Vivo Neurite Orientation Dispersion and Density Imaging of the Human Brain'. *NeuroImage* 61 (4): 1000–1016. https://doi.org/10.1016/j.neuroimage.2012.03.072.

ACKNOWLEDGEMENTS

First of all, I would like to thank Marco Düring for taking me on as a PhD student in the first place and his guidance and mentorship over the last three years.

Secondly, I would like to thank Nicolai Franzmeier for welcoming me in his new research group at the ISD and his support and guidance.

Next, I would like to thank my wonderful colleagues, some of whom have also become good friends: Davina Biel, Anna Rubinski, Sofia Finsterwalder, Benno Gesierich, Rong Fang, Anna Steward, Lukai Zheng and Sebastian Römer – for making my PhD time more enjoyable during retreats, conferences, NeuroLunch and actual lunch breaks. I also would like to sincerely thank my collaborators for their valuable contributions: Anil M. Tuladhar, Frank-Erik de Leeuw, Annemieke ter Telgte, Mengfei Cai, Mina Jacob and Anna Kopczak.

I would like to thank Martin Dichgans for his support and guidance as well my TAC members Michael Ewers and Virginia Flanagin for their valuable input.

Ganz besonders danke ich meinen Eltern, meiner Oma und meiner großen Schwester Caterina für ihre bedingungslose Liebe und ihre Unterstützung. Meiner besten Freundin Isabell danke ich für ihre treue Freundschaft. Zu guter Letzt danke ich meinem Partner Valentin für seine Hilfsbereitschaft und seine Liebe – angefangen vom Bachelor in Osna bis zum PhD in München.

CURRICULUM VITAE

Education

Since 10/2019	PhD candidate Graduate School of Systemic Neurosciences, Ludwig-Maximilians-University, Munich, Germany
09/2017 – 08/2019	Cognitive Neuroscience, MSc Radboud University, Nijmegen, The Netherlands
10/2014 – 08/2017	Cognitive Science, BSc Osnabrück University, Osnabrück, Germany
09/2016 – 12/2016	Semester abroad University of York, York, United Kingdom

Research experience

Since 10/2019	Research associate Institute for Stroke and Dementia research, Munich, Germany
09/2018 – 08/2019	Trainee Language function and dysfunction lab, Donders Institute for Cognition, Radboud University, Nijmegen, The Netherlands
10/2018 – 01/2019	Research assistant Sensorimotor lab, Donders Institute for Cognition, Radboud University, Nijmegen, The Netherlands
09/2016 – 12/2016	Trainee Social Language Lab, Department of Psychology, University of York, York, United Kingdom

LIST OF PUBLICATIONS

Accepted for publication

Franzmeier, N., **Dewenter, A.,** Frontzkowski, L., Dichgans, M., Rubinski, A., Neitzel, J., ... & Ewers, M. (2020). Patient-centered connectivity-based prediction of tau pathology spread in Alzheimer's disease. *Science Advances*, 6(48), eabd1327.

Konieczny, M. J.*, **Dewenter, A.*,** ter Telgte, A., Gesierich, B., Wiegertjes, K., Finsterwalder, S., … & Duering, M. (2021). Multi-shell diffusion MRI models for white matter characterization in cerebral small vessel disease. *Neurology*, 96(5), e698-e708.

Dewenter, A., Gesierich, B., ter Telgte, A., Wiegertjes, K., Cai, M., Jacob, M. A., Marques, J.P., Norris, D.G., Franzmeier, N., de Leeuw, F.E., Tuladhar, A.M., Duering, M. (2022). Systematic validation of structural brain networks in cerebral small vessel disease. *Journal of Cerebral Blood Flow & Metabolism*, *42*(6), 1020-1032. PMID: 34929104.

de Brito Robalo, B. M., Biessels, G. J., Chen, C., **Dewenter, A.**, Duering, M., Hilal, S., …, de Luca, A. (2021). Diffusion MRI harmonization enables joint-analysis of multicentre data of patients with cerebral small vessel disease. *Neuroimage Clin.* 2021;32:102886. doi: 10.1016/j.nicl.2021.102886. PMID: 34911192; PMCID: PMC8609094.

Georgakis, M.K., Fang, R., Duering, M., Wollenweber, F. A., Bode, F. J., Stösser, S., …, **Dewenter, A.**, …, Dichgans, M., on behalf of the DEMDAS Investigators. (2022). Cerebral small vessel disease burden and cognitive and functional outcomes after stroke: a multicenter prospective cohort study. *Alzheimers Dement*, accepted for publication June 2022.

Dewenter, A., Jacob, M. A., Cai, M., Gesierich, B., Hager, P. Kopczak, A., Biel, D., Ewers, M., Tuladhar, A.M., de Leeuw, F.E., Dichgans, M., Franzmeier, N., Duering, M. (2022). Disentangling the effects of Alzheimer's and small vessel disease on white matter fibre tracts. *Brain*, accepted for publication June 2022.

Chupina, I., Sierpowska, J., Zheng, X., **Dewenter, A.,** Piastra, M.C., Piai, V. (2022). Time-course of right-hemisphere recruitment during word production following left-hemisphere damage: A single case of young stroke. *European Journal of Neuroscience*, accepted for publication August 2022.

*shared first authorship

Frontzkowski, L., Ewers, M., Brendel, M., Biel, D., Ossenkoppele, R., Hager, P., Steward, A., Dewenter, A., Römer, S., Rubinski, A., Buerger, K., Janowitz, D., Binette, A.P., Smith, R., Strandberg, O., Carlgren, N.M., Dichgans, M., Hansson, O., Franzmeier, N. (2022). Earlier Alzheimer's disease onset is associated with tau pathology in brain hub regions and facilitated tau spreading. *Nat Commun*, accepted for publication August 2022.

Rubinski, A., Franzmeier, N., **Dewenter, A.,** Luan, Y., Smith, R., Strandberg, O., Ossenkopele, R., Dichgans, M., Hansson, O., Ewers, M. (2022). Higher levels of myelin are associated with higher resistance against tau pathology in Alzheimer's disease. *Alz Research Therapy*, accepted for publication August 2022.

Submitted for publication

Steward, A., Biel, D., Brendel, M., **Dewenter, A.,** Roemer, S., Rubinski, A., Luan, Y., Dichgans, M., Ewers, M., Franzmeier, N. (2022). Functional Network Segregation is associated with attenuated tau spreading in Alzheimer's disease.

Biel, D., Luan, Y., Brendel, M., Hager, P., **Dewenter, A.,** Moscoso, A., Otero Svaldi, D., Higgins, I. A., Pontecorvo, M., Roemer, S., Steward, A., Rubinski, A., Zheng, L., Schöll, M., Shcherbinin, S., Ewers, M., Franzmeier, N. (2022). Combining tau-PET and fMRI meta-analyses for patient-centered prediction of cognitive decline in Alzheimer's disease.

Franzmeier, N., Brendel, M., Luan, Y., Biel., Frontzkowski, L., **Dewenter, A.,** Rubinski, A., Duering, M., Dichgans, M., Ewers, M. (2021). Functional brain networks mediate the spread of metabolic decline in Alzheimer's disease.

Katzdobler, S., Nitschmann, A., Barthel, H., Bischof, G., Beyer, L., Marek, K., …, **Dewenter, A.,** …, Levin, J., Brendel, M. (2022). Additive value of [18F]PI-2620 perfusion imaging in four-repeat tauopathies.

Coenen, M., Kuijf, H. J., Huenges Wajer, I. M. C., Duering, M., Wolters, F.J., Fletcher, E.F., …, **Dewenter, A.,** …, Biesbroek, J. M. (2022). Strategic white matter hyperintensity locations for cognitive impairment: a multicenter lesion-symptom mapping study in 3525 memory clinic patients.

AFFIDAVIT

I hereby confirm that the dissertation “Tractography-based Diffusion MRI Markers of Cerebral Small Vessel Disease” is the result of my own work and that I have only used sources or materials listed and specified in the dissertation.

Hiermit versichere ich an Eides statt, dass ich die vorliegende Dissertation “Tractography-based Diffusion MRI Markers of Cerebral Small Vessel Disease” selbstständig angefertigt habe, mich außer der angegebenen keiner weiteren Hilfsmittel bedient und alle Erkenntnisse, die aus dem Schrifttum ganz oder annähernd übernommen sind, als solche kenntlich gemacht und nach ihrer Herkunft unter Bezeichnung der Fundstelle einzeln nachgewiesen habe.

Munich, September 13, 2022 Anna Dewenter

DECLARATION OF AUTHOR CONTRIBUTIONS

Study I: (Dewenter et al., 2022, Journal of Cerebral Blood Flow and Metabolism) "Systematic validation of structural brain networks in cerebral small vessel disease"

Authors: *Anna Dewenter, Benno Gesierich, Annemieke ter Telgte, Kim Wiegertjes, Mengfei Cai, Mina A. Jacob, José P. Marques, David G. Norris, Nicolai Franzmeier, Frank-Erik de Leeuw, Anil M. Tuladhar and Marco Duering*

Contribution of co-authors: B.G. performed part of the analysis, interpreted data and revised the manuscript. A.t.T. contributed to the study design, acquisition and interpretation of data and revised the manuscript. K.W., M.C. and M.A.J. acquired and interpreted data and revised the manuscript. J.P.M designed the MRI protocol, acquired and interpreted data and revised the manuscript. D.G.N. designed the MRI protocol, interpreted the data and revised the manuscript. N.F. interpreted the results and revised the manuscript. F.E.d.L. designed and supervised the study, interpreted the data and revised the manuscript. M.D. designed and supervised the study, analyzed and interpreted the data, drafted and revised the manuscript.

My contribution to this publication detail: together with my first supervisor, I designed and preregistered the study. I processed the diffusion MRI data including quality control of the 3rd follow-up visit of the RUN DMC main study, fitting DTI and DKI maps, reconstruction of brain networks and calculation of graph metrics. I performed all statistical analyses, interpreted the results, drafted and revised the manuscript.

Munich, September 13, 2022

Anna Dewenter (1st author)

Marco Düring (1st supervisor)

Study II: (Dewenter et al., 2022, Brain) "Disentangling the effects of Alzheimer's and small vessel disease on white matter fiber tracts"

Authors: *Anna Dewenter, Mina A. Jacob, Mengfei Cai, Benno Gesierich, Paul Hager, Anna Kopczak, Davina Biel, Michael Ewers, Anil M. Tuladhar, Frank-Erik de Leeuw, Martin Dichgans, Nicolai Franzmeier and Marco Duering*

Contribution of co-authors: M.A.J., M.C., B.G. and A.K. acquired and interpreted data and revised the manuscript. P.H. and D.B. analyzed and interpreted data and revised the manuscript. M.E., A.M.T., F.E.d.L. and M. Dichgans designed and supervised the study, interpreted data and revised the manuscript. N.F. and M. Duering designed and supervised the study, analyzed and interpreted data, drafted and revised the manuscript.

My contribution to this publication detail: together with M. Duering and N.F., I designed the study. I processed the diffusion MRI data, including preprocessing of the 3rd follow-up visit of the RUN DMC main study and ADNI study. I conducted group-wise fixel-based analyses, reconstructed white matter fiber tracts, performed all statistical analyses, interpreted results, drafted and revised the manuscript.

Munich, September 13, 2022

Anna Dewenter (1st author)

Marco Düring (1st supervisor)